Seismic Ratcheting of Steel Low-Damage Buildings

Ali Abdolahi Rad

A thesis presented for the degree of

Doctor of philosophy

in

Structural Engineering

at the

University of Canterbury

Christchurch, New Zealand.

December 2017

Abstract

During earthquake shaking some structures tend to deform and yield more in one direction than in the other. This phenomenon is sometimes termed “ratcheting” and the displacement demands may become significantly larger than for structures without a ratcheting tendency. This thesis explores the numerical and experimental studies on performance of steel low damage buildings with ratcheting tendency under seismic demands.

Numerical studies are used to develop simple methods to estimate the displacement demands of such structures with different periods (T) and force design reduction factors (R). Shake table studies of two storeys half-scale steel moment frame with asymmetric friction connections (AFCs) at the column bases and at the beam ends were carried out. A tested structure with residual displacements due to earthquakes was strengthened/stiffened using several methods to minimize the possibility of increase in peak/residual displacements in the residual displacement direction due to aftershocks. Experimental tests were conducted with i) no brace, ii) a buckling brace with slackness, (iii) a ratcheting brace, and (iv) gapping braces, which had a ratcheting brace in conjunction with a buckling brace with a displacement gap.

Time history analysis of steel structures with initial out-of-plumb showed that buildings with greater initial out-of-plumb and force design reduction factor tended to have larger residual and peak inter-story drifts. It also showed that for

high out-of-plumb, the ratio of residual-to-maximum possible peak drift tends to unity, indicating that the buildings are yielding predominantly in one direction.

Nonlinear time history analysis of steel structures also showed that a sequence of realistic shakes from actual earthquake recording tended to increase the median peak and residual drift response of the structures. The structures tended to experience ratcheting in predominantly one direction. The tendency for ratcheting increased with increasing force reduction factor (R) and design drift.

Time history analysis of the single degree of freedom elastic structures with different stiffness in each direction showed that greater displacements generally occurred in the direction of lower stiffness for elastic structures. Peak drift in the stiffer direction was able to be predicted by the spectral displacement associated with the period in that direction and the peak drift in the flexible direction estimated from the displacement in the opposite direction using energy considerations.

For yielding structures with different stiffness/strengths in opposite horizontal directions, when strength proportional to stiffness, the inelastic displacement in each direction could be estimated from the elastic response in that direction using standard modifications for inelasticity. For long period structures peak inelastic displacements were similar to the peak elastic displacements considering the stiffness difference.

Shaking table testing of a half-scale two-story steel moment frame with asymmetric friction connections (AFCs) at the column bases and at the beam ends showed that, when beam ends and the base-column joints were modelled by

appropriate trilinear and bilinear hysteresis loops respectively, the response with time matched the numerical simulations well. Residual drifts were less than 0.2% for peak inter-storey drifts up to 3%, and less than 0.7% for peak inter-storey drifts of 6.0% indicating desirable seismic performance. It was also found that it was possible to obtain repeatable peak and residual displacements with a variation of less than 2.0% for straight structures subject to same record. Since there was no significant member damage, these friction structures may be considered to be low-damage.

Shake table study of strengthening/stiffening of a two storey low damage half scale steel structure using tension braces showed that adding a buckling brace (BB) reduced the residual drift by 75% and did not push the frame in the opposite direction. The ratcheting brace (RB) was very effective of straightening the structure with a residual displacement change of -260% implies that it caused a 60% greater residual displacement in the opposite direction. The gapping brace (GB) also changed the residual displacement by -150%. Both the buckling brace (BB) and gapping/buckling brace (GB/BB) combination had the desirable characteristic of limiting further drift in the residual displacement direction without pushing the frame in the opposite direction.

Acknowledgements

I would like to begin this thesis by acknowledging all the people that helped make it possible. Without their continuing support and contribution this research would not have been completed.

I wish to thank and acknowledge my supervisor, Associate Prof. Gregory MacRae for the patient guidance, encouragement and advice they have provided throughout this research. I have been extremely lucky to have a supervisor who cared so much about my work and accepted nothing less than excellence from me. And a special thanks to Dr. Trevor Yeow who is always there for me whenever I ran into a trouble or had a question about my research. I would like also acknowledge Associate Prof. Geoff Rodgers for his support and help during experimental tests.

The financial support provided by the New Zealand Earthquake Commission (EQC) is gratefully acknowledged.

Besides my advisor, I would like to express my deepest gratitude to my colleague, best friend, love and wife Nikoo Hazaveh for his unwavering love, support and understanding especially during the challenging times of conducting experimental tests at UoA.

My acknowledgment is also extended to the technicians and staff of the Department of Civil Engineering at the University of Auckland who helped me during this project. In particular, I would like to acknowledge Dr. Quincy Ma from UoA who helped us carry out shake table tests in UoA, Shane Smith and

Mark Byrami from UoA for their support during experimental testing. I wish to thank Elizabeth Ackermann for her support and help with administrative tasks during my PhD study. In particular, I would like to Thanks Professor Mark Davidson from UoC for his support especially during the challenging times of conducting experimental tests at UoA. Without his support, my PhD experimental tests would not have been possible.

Finally, but foremost, I would like to extend my thanks to my family: my parents, Rahim Abdolahi Rad and Niloufar Faridi, who were always there for me and provided unwavering life-long love and understanding throughout what were sometimes tough times.

Contents

List of Figures

List of Tables

ACRONYMS

Acronyms used in this thesis are listed below.

OOP = Out of plumb

CISDR = Constant inter-story drift ratio

PISDR = Peak inter-story drift ratio

RISDR = Residual inter-story drift ratio

NPISDR = Peak inter-story drift ratio

RPR = Residual-peak ratio

PPD = Peak positive displacement

PND = Peak negative displacement

PE_P = Positive potential energy

PE_N = Negative potential energy

NPPD = Normalized peak positive displacement

PNR = Positive-to-negative displacement ratio

$\Delta_{e,f}$ = Elastic more flexible direction displacement

$\Delta_{e,s}$ = Elastic stiffer direction displacement

$\Delta_{u,f}$ = Ultimate more flexible direction displacement

$\Delta_{u,s}$ = Ultimate stiffer direction displacement

DCF = Drift concentration factor

AFC = Asymmetric friction connection

BB = Buckling bracing

RB = Ratcheting bracing

GB = Gapping bracing

Chapter 1: Introduction

1.1. Background

During earthquake shaking some structures tend to deform and yield more in one direction than in the other. This phenomenon, termed “ratcheting”, can be caused by (i) the ground motion effect, where the earthquake can excite the structure in one direction more than the other, (ii) the dynamic stability effect, where the structures with negative dynamic stability, due to effects such as P-delta, have a tendency to deform predominantly in the direction of first yielding or damage (MacRae, 1994), (iii) building out-of-plumb, which induces eccentric moments at the base of structures, changes the effective lateral strength of the structure making it yield more easily in the direction of out-of-plumb, and (iv) Structural form effect, where the structure has different stiffness or strengths’s in the forward and reverse directions.

Recently, a number of techniques have been developed around the world in order to minimize the possibility of structural damage. One of these methods uses friction connections. The hysteretic behaviour of the connections can be approximated as a bilinear hysteresis loop similar to traditional steel connections that are not flag shaped. In friction connections, before sliding occurs, the connections behave as fixed connections. Then, when sliding starts the hysteretic behaviour is similar to bilinear behaviour. Because of that, the design methodology and mathematical model for this system are similar to that of fixed based steel structures.

These connections minimize the possibility of structural damage. However, as this system does not have significant self-centring behaviour, there may be out-of-plumb because of post-earthquake residual deformation. If out of plumb is very large, then the structure will keep moving in the same direction and collapse. For design we need to know what effect different amounts of OOP have on structures so we can assess the demands (which may be significantly greater than that if there is no OOP). This issue may detrimentally affect structure performance in subsequent seismic events. There is relatively little information in the literature about how the level of out-of-plumb affects the displacement demands of such structures on the likely future earthquake events.

Moreover, recent events has shown that strong shaking at a particular site may be subsequently followed by several other considerably large aftershocks over a period of minutes, days, or months. Because of the potentially short time between events, there may be insufficient time for structure to be repaired, which may lead to further damage or the possibility of building collapse during aftershocks. Even if the building is being repaired, workers in the building performing repairs may be at risk during aftershocks.

Structures with residual displacements due to earthquakes may be strengthened/stiffened in the residual displacement direction to mitigate increase in peak or residual displacement on that direction due to aftershocks. This mitigation can act as a permanent measure, or as an interim measure until the building is manually straightened and fixed, or until it is deconstructed. The added stiffness/strength causes a change in response in each direction during future

ground shaking or aftershocks. While the concept regarding such mitigation measures is clear, simple methods to estimate the displacement demands of such structures with different strength/stiffness in the different directions are not available.

1.2. Specific Need

Based on this summary introduction there is a need to know how a building with a specified initial out-of-plumb may behave in an earthquake or series of shaking event, (ii) how different mitigation techniques are likely to influence the response so that better engineer decision can be made.

1.3. Objective and Scope

This thesis seeks to address the need above by answering the following questions:

1) How can the peak and residual displacement response of the structure with initial out-of-plumb be estimated?
2) How does earthquake sequence affect the peak and residual displacement response of the structure?
3) How can the peak displacement response of the elastic structure with unbalanced stiffness be estimated?
4) How can the peak and residual displacement response of the yielding structure with unbalanced stiffness/strengths be estimated?
5) What is the performance of the steel low damage frame during shake table testing?

6) How effective are different interventions in a frame with residual displacements during shake table testing?

1.4. Thesis Outline

Chapter 2 presents a design procedure to show how peak and residual inter-story drift of the structures with initial out-of-plumb can be estimated. The displacements of buildings are quantified in subsequent seismic events by means of inelastic dynamic time history analysis. Structures considered have different structural heights, force design reduction factors (R), and target inter-story drifts. In particular, this chapter seeks to answer Question 1.

Chapter 3 presents the effect of the 2010-2011 Canterbury earthquake sequence on the potential for ratcheting of steel buildings by means of inelastic dynamic time history analysis. It shows how earthquake sequence change the peak and residual drifts of the structures with different structural heights, design force reduction factors (R), and target inter-story drifts. In particular, this chapter seeks to answer Question 2.

Chapter 4 presents the seismic response of elastic single degree of freedom structures with unbalanced stiffness. Here, peak displacements of the structures in each direction were obtained using response history analysis. Finally, a simple energy approach is developed to show how peak displacements can be estimated for unbalanced stiffness structures. In particular, this chapter seeks to answer Question 3.

Chapter 5 presents the seismic response of yielding single degree of freedom steel structures with unbalanced stiffness/strength. Peak and residual drift response of the structures with different stiffness/strengths in each direction were quantified by means of dynamic time history analysis. Finally, a simple design approach is developed to show how peak displacements can be estimated for yielding structures with unbalanced stiffness/strengths. In particular, this chapter seeks to answer Question 4.

Chapter 6 presents the shaking table performance of a half-scale two-story steel moment frame with asymmetric friction connections (AFCs) at the column bases and at the beam ends. The hysteretic behaviour of the connections and peak and residual displacement response of the tested frame have been described and validated by numerical simulation. In particular, this chapter seeks to answer Question 5.

Chapter 7 presents structural strengthening of a tested frame having residual drifts by shake table testing. Several tension braces were applied to the structure to ensure that there is no increase in peak or residual displacement response of the structure on the residual direction due to aftershocks. Numerical models are also developed to represent the structure behaviour and they were able to capture the responses well.

Chapters 8 presents the overall conclusions to the research, and discusses possible extensions and future work.

Chapter 2: Seismic Behaviour of Steel Buildings with Out-of-Plumb

2.1. Introduction

Buildings are never truly vertical or plumb. The out-of-plumb (OOP) can be caused by a number of reasons including construction errors, unbalanced gravity loads, foundation settlement, or permanent deformation after an earthquake. The construction allowable maximum OOP is 0.2% (AISC, 2010), but earthquake can cause higher permanent drifts. The OOP may affect building behaviour under both non-seismic and seismic loading.

Previous research (Surrovek-Maleck and White 2004a; Surrovek-Maleck and White 2004b; White et al. 2005) has shown that geometric imperfections can have an appreciable impact on stability behaviour in design scenarios considering non-seismic cases. In non-seismic design, Direct Analysis Method (DM) can be used to consider OOP in the 2010 American Institute of Steel Construction (AISC) Specification (AISC, 2010). DM requires Second-Order analysis to consider OOP. In second-order analysis, OOP can be modelled either using a notional load or alternatively by directly modelling the structure as being OOP.

Currently, there are no methods to consider the effect of OOP in seismic design. However, a few studies have been conducted to evaluate the effect of building OOP or effects of eccentric loading on the seismic response of structures (MacRae and Kawashima, 1993; Masuno et al. 2011; Yeow et al. 2013)

A study by MacRae and Kawashima (1993) and Yeow et al. (2013) looked at the seismic behaviour of cantilever bridge columns subjected to eccentric gravity loads before earthquake shaking occurred. They showed that during earthquake shaking the bridge tended to predominantly deform in the direction in which the moment was applied. Since OOP building structures also have additional moment at the base caused by the eccentric loads it would also be expected that these structures also have a tendency for larger displacements in the direction in which they are leaning.

A preliminary study on the effect of OOP on the response of shear structures with continuous columns, as shown in Figure 2-1(a), was undertaken by Masuno et al. (2011). Two shear-type structure stiffness distributions were considered: (i) constant stiffness over the height (CS); and (ii) stiffness decreasing with increasing height to obtain a constant inter-story drift ratio (CISDR) as shown in Figure 2-1(b). Bilinear hysteresis loops were used to represent of steel structures (MacRae and Kawashima, 1997).

Masuno et al. (2011) found that greater out-of-plumb generally caused greater displacement response increases relative to structures with no out-of-plumb. In addition, structures with greater design ductility also tend to have greater response. The CISDR model in Figure 2-1(b) gave the largest increases in response. Masuno et al. found that structures designed to the same peak drift level tend to experience increasing peak drifts response with increasing height. The reason for this was not explained. This preliminary study was limited in that it only considered frames with one design drift ratio of 1.8%. Also, the moment-

axial force interaction curve was not realistic, and the *P-Delta* effects were not appropriately considered.

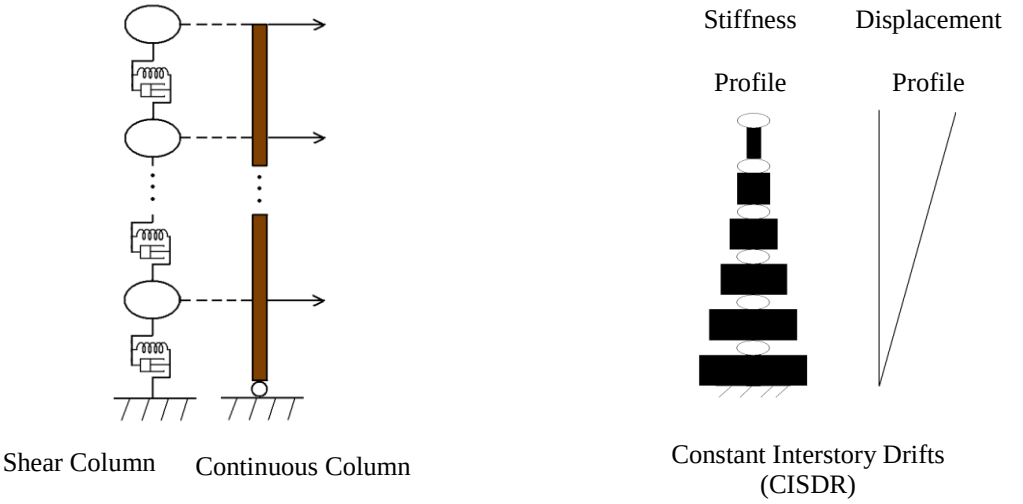

(a): Shear building model (b): Structure stiffness distribution

Figure 2-1 Shear type structure (Masuno et al. (2011))

It may be seen from the above discussion that there is a need to quantify the effect of OOP on the seismic response of buildings. In this study inelastic dynamic time history analyses of simple shear-type buildings are conducted using a suite of ground motion records. The building's force design reduction factor (ratio of elastic demand to provided capacity), structural height, and target inter-story drifts were varied. This study seeks to address this need by answering to the following questions:

1) What factors affect peak inter-story drift?

2) What factors affect residual inter-story drift?

3) Can peak and residual drift be predicted for design?

2.2. Modelling and Evaluation Approach

In this study, the simplified model consists of shear, continuous and P-Delta columns is used as shown in Figure 2-2 following Tagawa (2005). This simplified analytical model was verified by comparison with full 2-D moment frame models 3, 9 and 20 story structures with beams-columns. This study was conducted by Tagawa (2005) and found to match the drifts well. This approach has been used in a number of publications (e.g. Tagawa et al. 2004, MacRae et al. 2004, Sadashiva et al. 2009, Tagawa et al. 2010 and MacRae 2011). Earlier studies (Tagawa et al. 2005, Tagawa et al. 2004, MacRae et al. 2004, Sadashiva et al. 2009, Tagawa et al. 2010 and MacRae 2011) on structural modelling have shown that the frames modelled as a combination of vertical shear column and a vertical continuous column (flexural column) can represent the behaviour of real structures well. The flexural column represents all continuous columns throughout the whole structure. If the continuous column is not considered, unrealistically high drift concentrations may occur (sadashiva et al. 2009). The shear structure was modeled as a single shear column. A rigid link between shear column and continuous column make the horizontal displacement of the joined nodes the same at each level. The continuous column was pinned at the bottom (with a perfect pin). A continuous column stiffness ratio α_{cci} (Tagawa et al. 2005, Tagawa et al. 2004, MacRae et al. 2004, Sadashiva et al. 2009, Tagawa et al. 2010 and MacRae 2011) defines the continuous column stiffness relative to the shear column stiffness at the i_{th} floor. It is computed using Eq. 2-1 where E is the material Elastic Modulus; H_i is the story height of the i_{th} floor level; I_i is the moment of

inertia of the continuous column between the floor levels; and K_{oi} is the initial lateral stiffness of the i_{th} floor level.

$$\alpha_{cci} = \frac{EI_i}{H_i^3 K_{oi}} \tag{2-1}$$

A continuous column stiffness ratio α_{cci} (Eq. 2-1) of 0.2 is assumed following Tagawa (2005). This is a lower bound on realistic values in moment frame structures based on Tagawa (2005). Here the shear column only has in-plane translational degrees of freedom. The continuous column has both rotational and in-plane translational degrees of freedom over its height and the P-delta column consists of rigid props with pinned ends. Bi-linear hysteresis loop with strain hardening stiffness of 4% was used for the shear column. The continuous column was assumed to remain elastic during an earthquake. Critical initial stiffness proportional damping of 5% is assumed for all modes (Caughey, 1960). A constant mass of 20 Tons, *m*, was lumped at each floor. The structure is also assumed to have constant story height, *h*, of 4m.

In this study, the OOP is defined as the constant inter-story drift before the earthquake shaking starts. This is assumed to be constant over all stories as shown in Figure 2. It is shown by θ in Figure 2-2, and the values of OOP considered were 0.3%, 0.6%, 0.9%, 1.2%, 1.5%, 1.8% and 2.1%. OOP is modelled by directly assigning deformed horizontal coordinates (Δx_i) to the nodes as shown in Figure 2-2. These structures are modelled with their deformed configuration before the seismic analysis is performed as shown in Figure 2-3. The nodal shifts

are calculated by equation below where *i* is the floor level and *h* is the inter-story height:

$$\Delta x_i = i \times h \times \theta \tag{2-2}$$

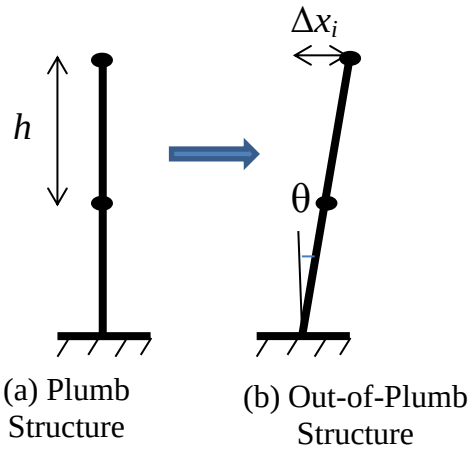

Figure 2-2: Application of Out-Of-Plumb

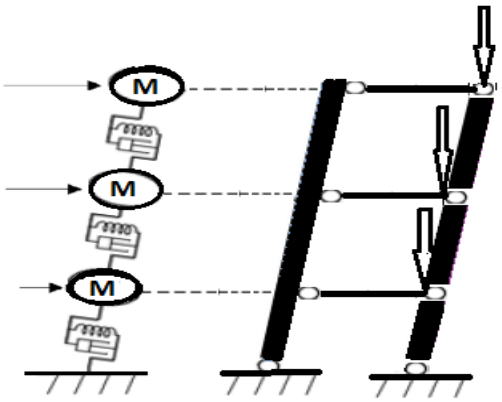

Figure 2-3: Simplified model with out-of-plumb

In order to further show that the shear-type model described above represented the behaviour of OOP building well, analyses were conducted for the shear type model, as well as for a beam-column frame structure of 9 stories with R of 2 and

OOP of 1.2%. The difference in response of those models was generally less than 3% showing that the shear type model represented the beam-column model response well.

The design parameters and analysis process are illustrated in Figure 2-4. The basic structure was designed as an ordinary building in Wellington on site class C. Structures were designed with target maximum allowable inter-story drifts of 1.0%, 1.5%, 2%, and 2.5% and force design reduction factor (R) of 1 to 6 in steps of 1 according to the Equivalent Static Method in NZS1170.5 (NZS 1170.5, 2004). The number of stories (*N*) considered in this study are 3, 6, 9 and 15. The fundamental period of each structure is obtained as part of the design process and the total period range of the structures is 0.7 to 4.8 seconds. The structure stiffness distribution is designed with the constant inter-story drift ratio (CISDR) because it allows for conservative approximation (Masuno et al. 2011). The iteration steps to obtain design of the structure are shown in the Figure 2-4 flow chart.

The SAC (SEAOC-ATC-CUREE) (SAC, 2000) suite of twenty earthquake ground motion records for Los Angeles with probability of exceedance of 10% in 50 years were used. All earthquake records are scaled to the elastic design spectral acceleration at the fundamental period of the structures considered. To eliminate the directional trends in displacement from ground motion records, each structure was analysed in both directions.

The dynamic inelastic time history computer program RUAUMOKO-2D (Carr and Ruamoko, 2004) was used in this project to run the analysis. Input files for

RUAUMOKO-2D (Carr and Ruamoko, 2004) are generated using MATLAB (The MathWork, 2008a). The two programs were automated to run and extract desired output values.

By assuming that the distributions of the maximum peak and residual inter-story drift ratio over all levels for the different records (*PISDR* and *RISDR*) are lognormal (Cornell et al. 2002), the median and dispersion are found using Eq. 2-3 and 4 where x_i = *PISDR* or *RISDR* of structures due to i_{th} record and *n* is the total number of earthquake records considered.

$$\hat{x} = e^{\left(\frac{1}{n}\sum_{i=1}^{n} ln(x_i)\right)} \tag{2-3}$$

$$STDEV = std(l\,n(x_i)) \tag{2-4}$$

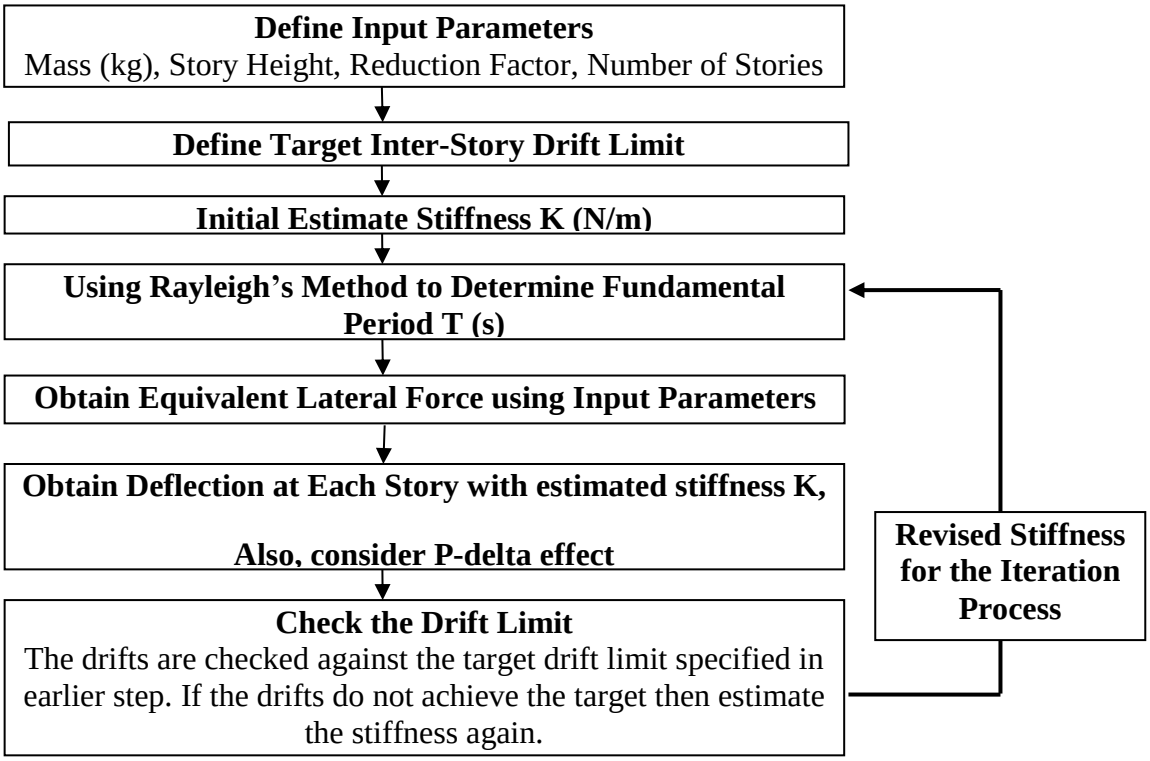

Figure 2-4: Flow Chart for Structural Design

The PISDR considering out-of-plumb, [*PISDR* (*OOP*)] is divided by the PISDR from initially plumb models, [*PISDR* (*plumb*)] for each record to obtain the normalized PISDR, *NPISDR*, as follows:

$$NPISDR = \frac{[PISDR\ (OOP)]}{[PISDR\ (plumb)]} \tag{2-5}$$

Also, the *RISDR* was divided by the *PISDR* for each record to obtain the ratio of residual-to-peak drift, known as the residual-peak ratio (*RPR*):

$$RPR = \frac{RISDR}{PISDR} \tag{2-6}$$

The median absolute value of N*PISDR* and *RPR* was obtained for all records.

2.3. Peak Inter-story Drift Response

2.3.1. *Effect of Force Design Reduction Factor*

Figure 2-5 compares the NPISDR of buildings with changing force design reduction factor (R). It shows that NPISDR increases with increasing force design reduction factor (R) and OOP.

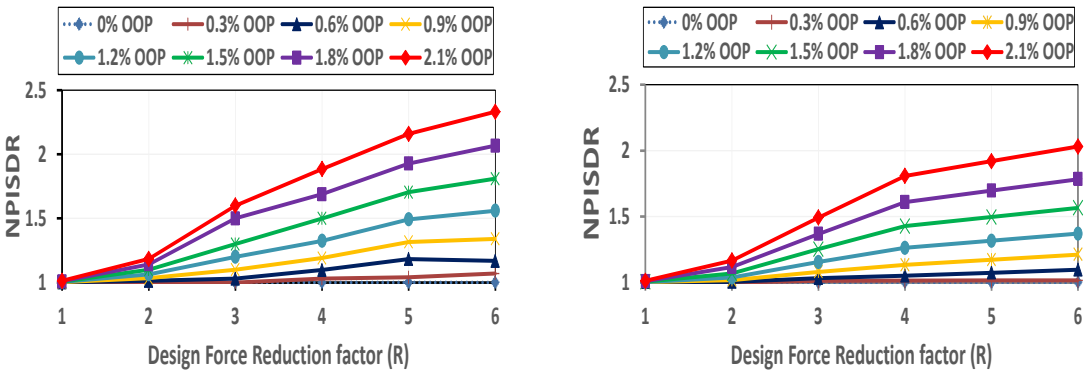

(a) 6 story, Design Drift = 1% (b) 12 story, Design Drift = 1%

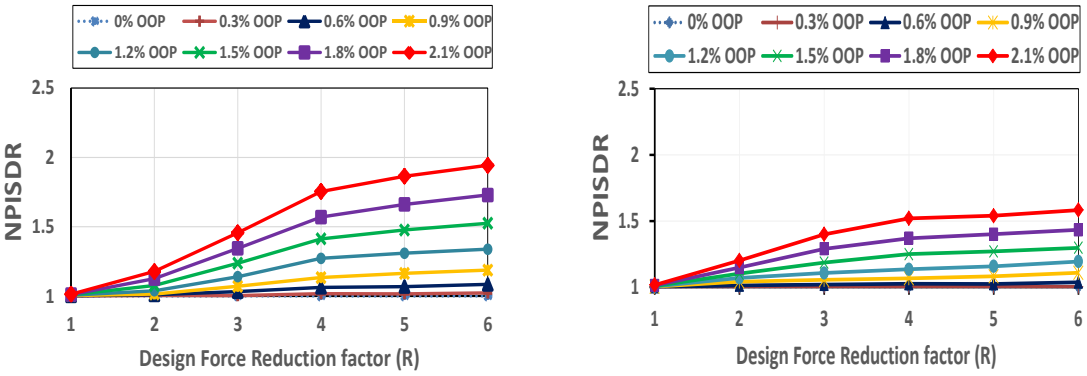

(c) 6 story, Design Drift = 2% (d) 12 story, Design Drift = 2%

Figure 2-5: Effect of R on median NPISDR

This can be explained based on the dynamic stability studies of MacRae (1994) and Yeow et al. (2013). Here, if F_y^+ is the yield strength in the positive direction, F_y^- is absolute value of the yield strength in negative direction and F_i is initial force causing deformation in the positive direction as shown in Figure 2-6, then the building will have a tendency to yield in the positive direction if the ratio of $\frac{F_y^+ - F_i}{F_y^- + F_i}$ is less than 1, and in the negative direction if $\frac{F_y^+ - F_i}{F_y^- + F_i}$ is greater than 1. In this study F_y^+ and F_y^- are equal so yielding structures tend to predominantly deform in the positive direction. Moreover, with increasing of R, the strength F_y decreases, so the ratio also decreases. For example, if F_i is assumed to be $0.1F_y$ $(R = 1)$, for R=2, this ratio equals to 0.67. For R=4 it equals to 0.43. Therefore, OOP building structures with increasing of R have a tendency for larger displacements in the direction in which they are leaning.

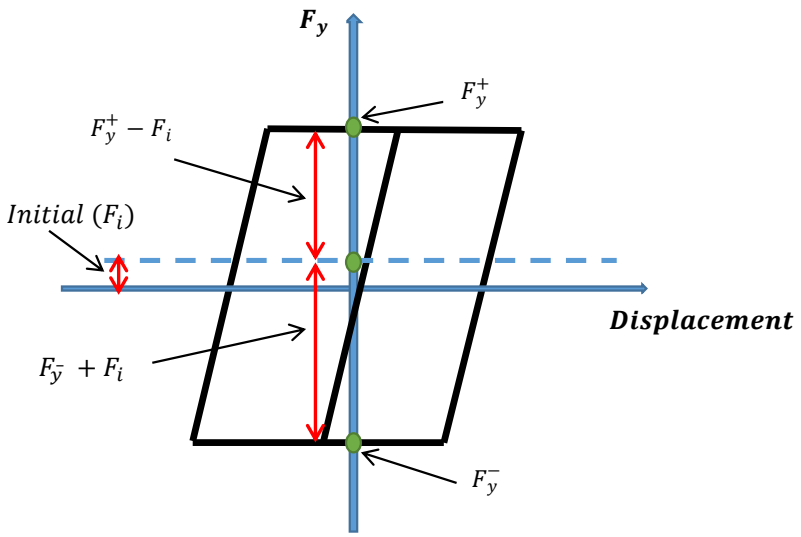

Figure 2-6: Hysteresis loop of the structure.

2.3.2. Effect of Structural Height

Figure 2-7 shows that the number of stories does not have much effect on the NPISDR. This is because all buildings were designed for the same design drift.

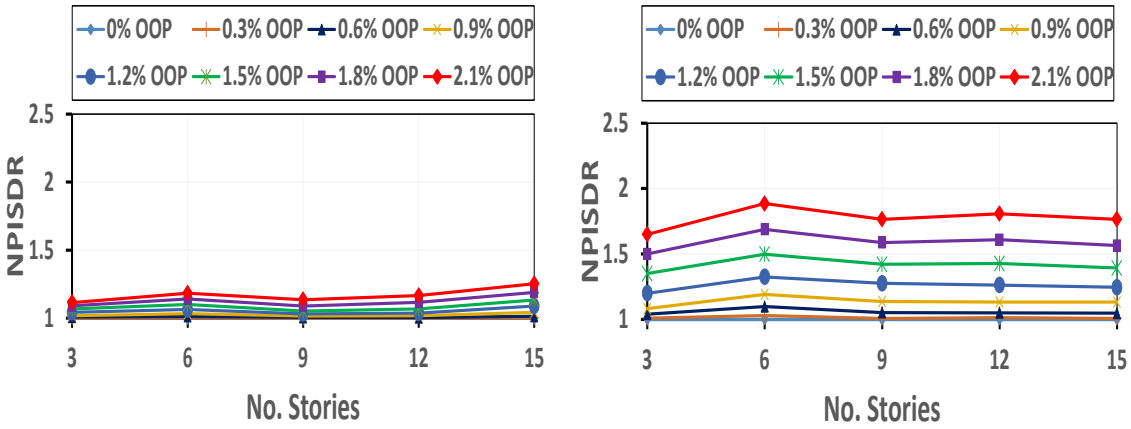

(a) R = 2, Design Drift = 1%

(b) R = 4, Design Drift = 1%

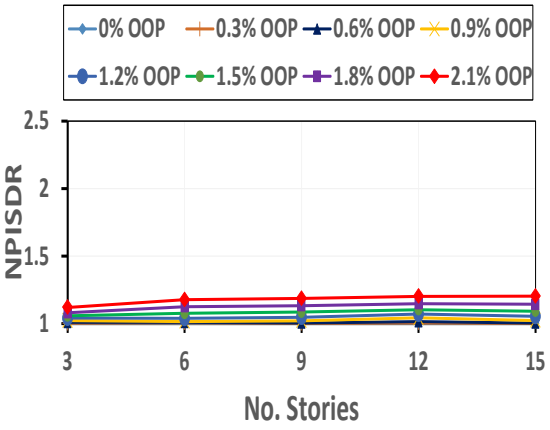

(c) R = 2, Design Drift = 2%

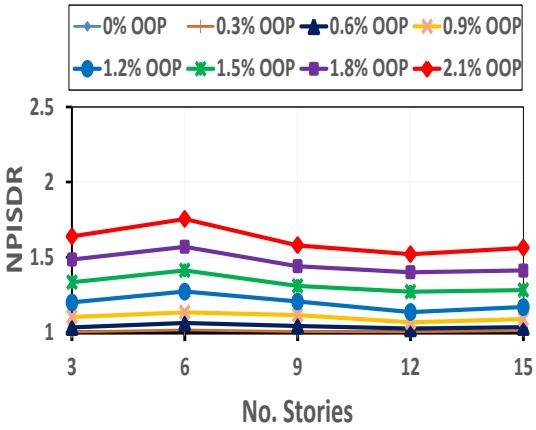

(d) R = 4, Design Drift = 2%

Figure 2-7: Effect of number of stories on median NPISDR

2.3.3. Effect of Design Drift

With increasing design drift, NPISDR tends to decrease in Figure 2-8 for the 12 story building with *R* of 2 and 4. This is because the OOP tends to make a close to constant increase in drift as shown in Figure 2-9. Therefore, when this is divided by the increasing drift of the plumb structure, the NPISDR decreases.

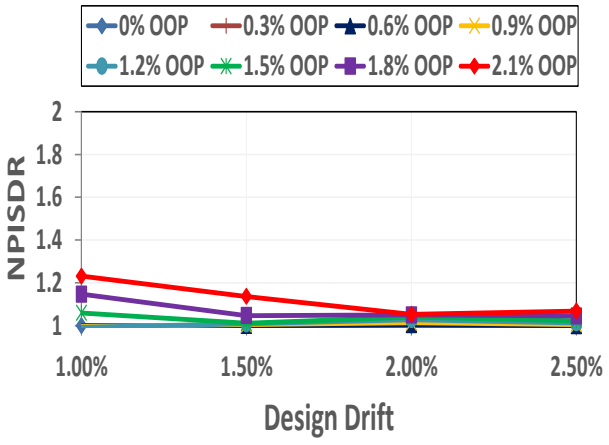

(a) R= 2, 12 story

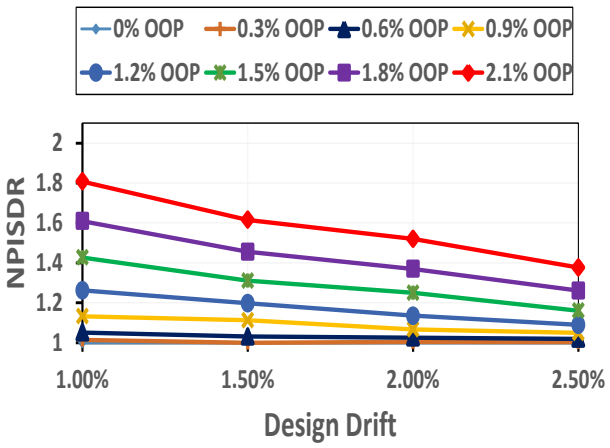

(b) R= 4, 12 story

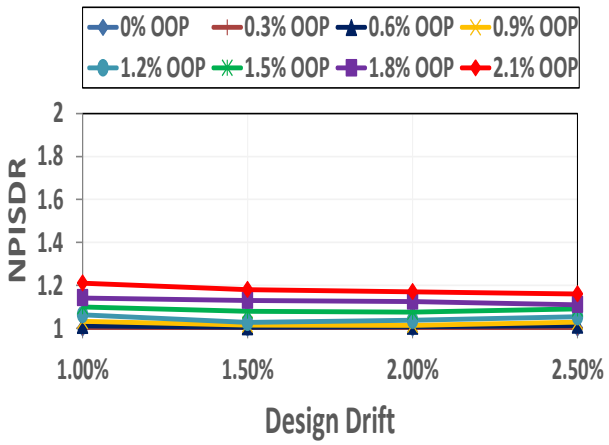

(a) R= 2, 6 story

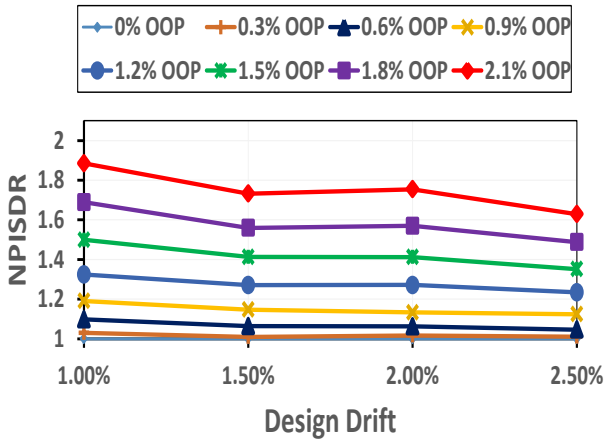

(a) R= 4, 6 story

Figure 2-8: Effect of design drift on median NPISDR

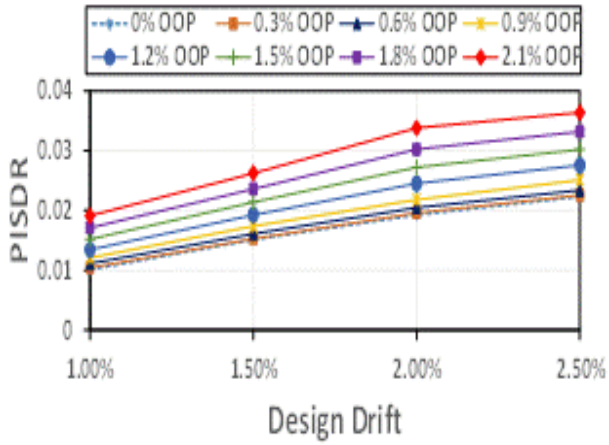

(a) 6 story, R = 4

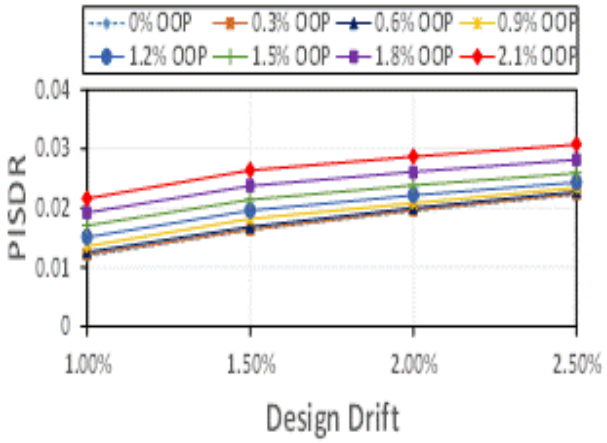

(b) 12 story, R = 4

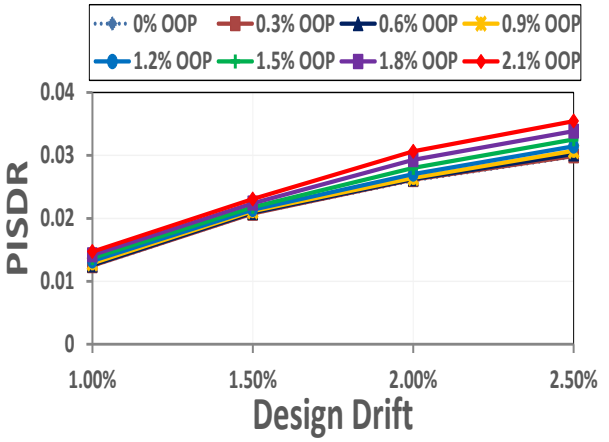

(c) 6 story, R = 2

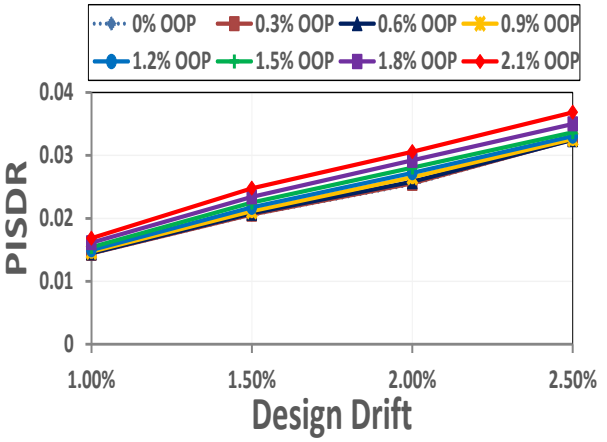

(d) 12 story, R = 2

Figure 2-9: Effect of design drift on median PISDR.

2.4. Residual Inter-story Drift Response

2.4.1. Effect of Force Design Reduction Factor(R)

Figure 2-10 shows that the RPR of buildings increases with increasing force design reduction factor (R) and OOP. When R = 1 the RPR is expected to be zero for elastic response. It is about 0.1 because after ground motion scaling to the elastic design spectral acceleration at the fundamental period of the structures, high spectral accelerations at shorter periods can cause yielding and residual displacements. The response of the straight structure is about one half of the peak value. At high OOP, the RPR tends to value of one, indicating that the buildings are yielding only in one direction and not in the other direction.

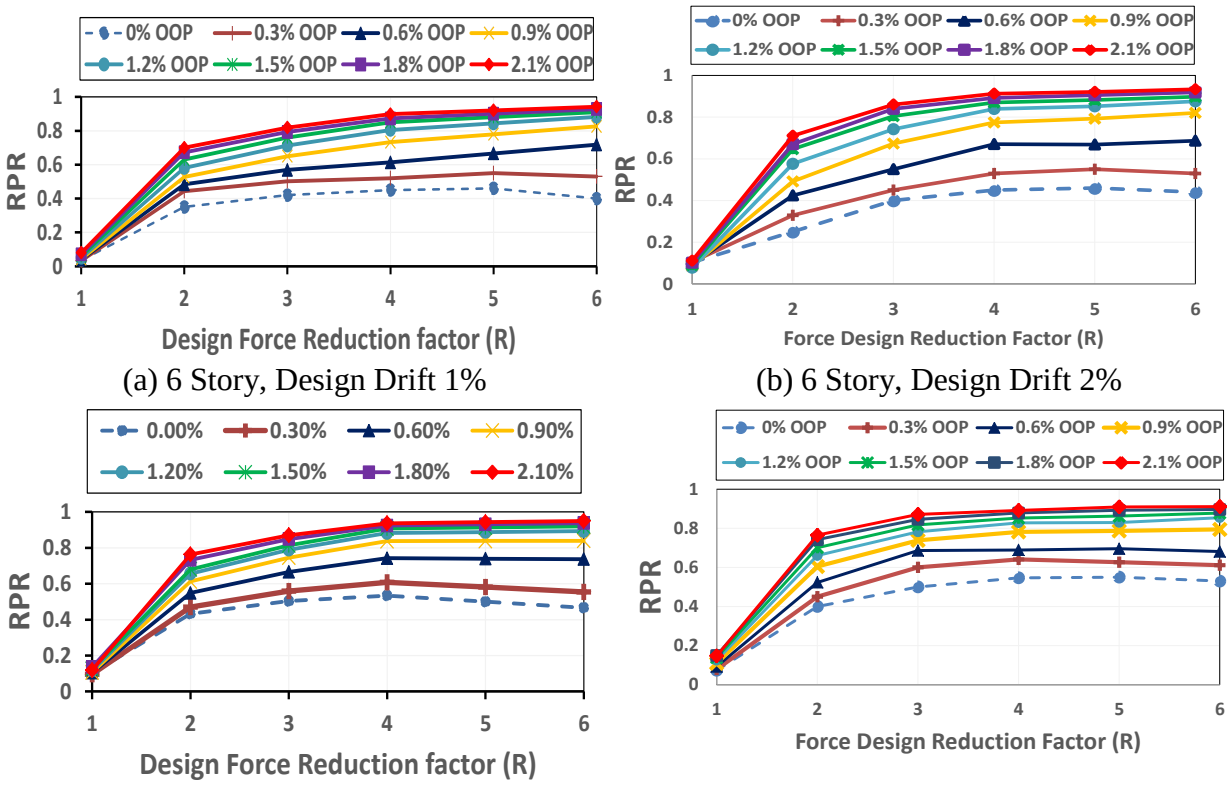

(a) 6 Story, Design Drift 1%

(b) 6 Story, Design Drift 2%

(c) 12 Story, Design Drift 1%

(d) 12 Story, Design Drift 2%

Figure 2-10: Effect of R on median RPR

2.4.2. Effect of Structural Height

Figure 2-11 shows that the buildings with different structural height have similar RPR with 1% and 2% design drifts because they have the same design drift and similar peak responses. Also, since they were designed for same *R*, they have equal residual responses. The sight tendency for larger RPR with a greater number of stories is due to the higher mode effects which become more significant in taller structures.

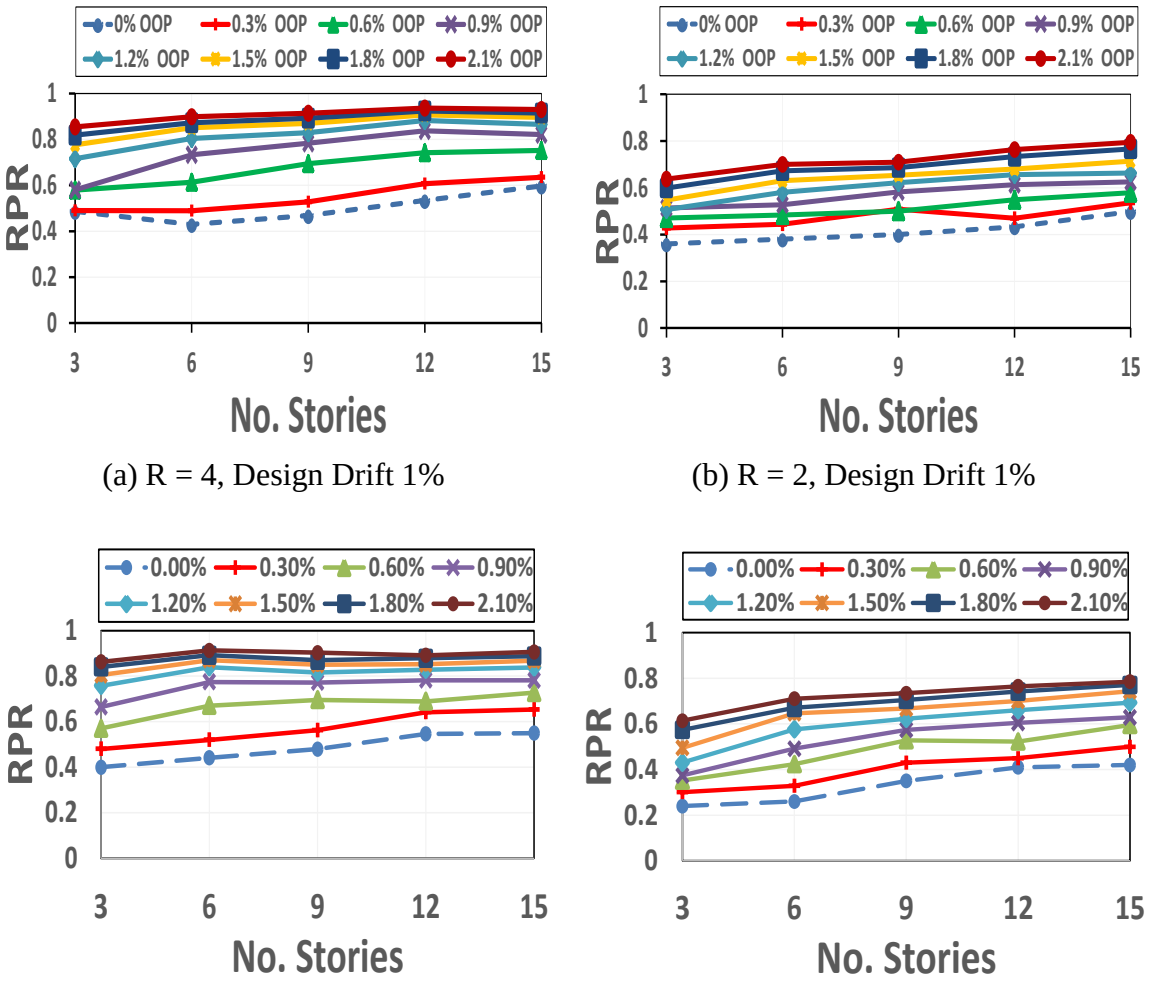

(a) R = 4, Design Drift 1%

(b) R = 2, Design Drift 1%

(c) R = 4, Design Drift 2%

(d) R = 2, Design Drift 2%

Figure 2-11: Effect of Structural Height on median RPR

2.4.3. Effect of Design Drift

Figure 2-12 shows that buildings with different design drifts have similar RPR. Moreover, it shows that RPR increases with higher OOP due to reduction on structural dynamic stability for all design drifts.

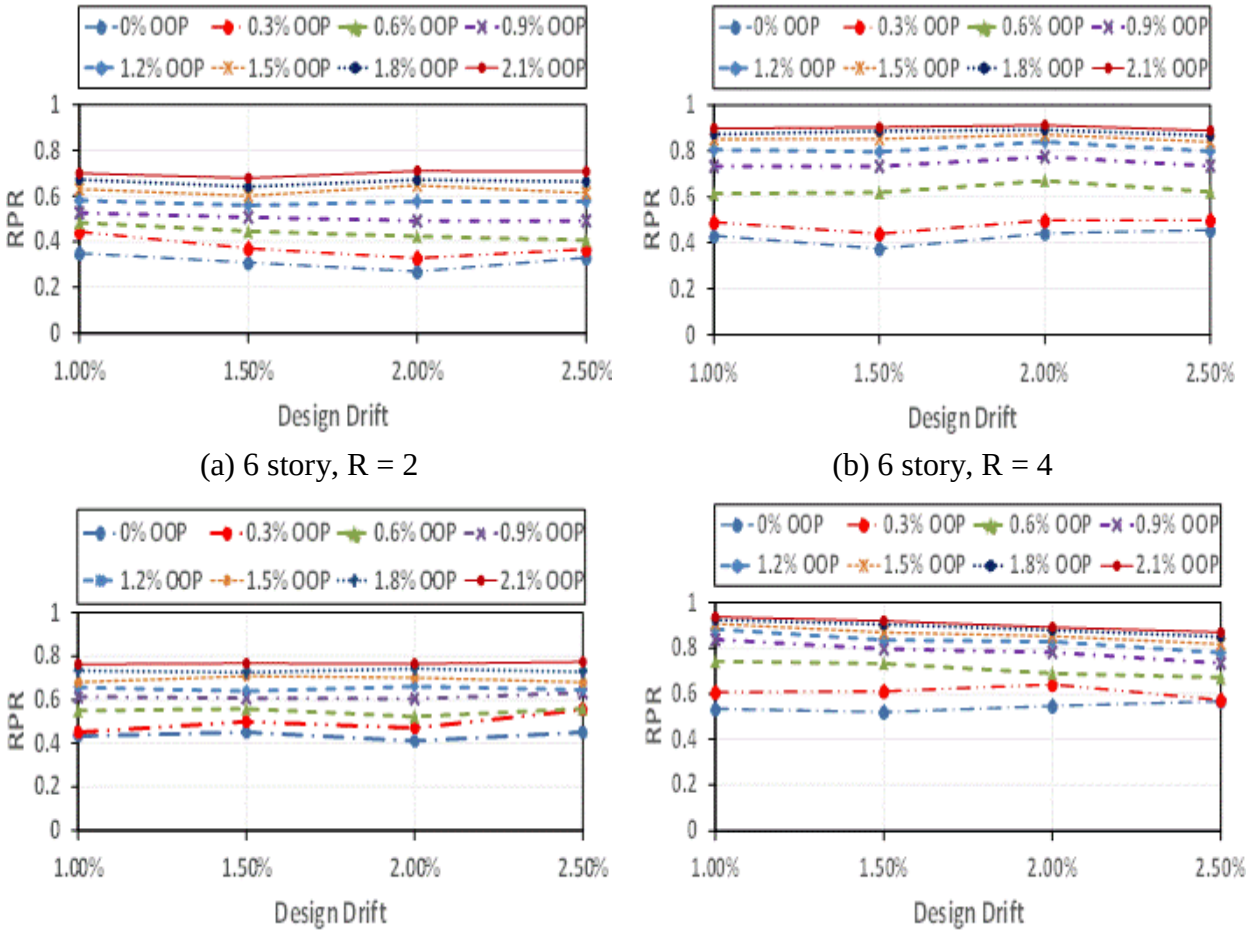

(a) 6 story, R = 2

(b) 6 story, R = 4

(c) 12 story, R = 2

(d) 12 story, R = 4

Figure 2-12: Effect of Design Drift on median RPR

2.5. Design Considerations

2.5.1. Estimation of Peak Inter-story Drift

A simple PISDR prediction procedure is developed here for buildings with out-of-plumb. Since structural height does not have much effect on structural behaviour with changing OOP as shown in Figure 2-6, the median NPISDR for structures with all numbers of stories is used. The NPISDR increases approximately parabolically with OOP as shown in Figure 2-13. Eq. 2-7 is fit to the actual responses for specific R values and design drifts, but it needs to be calibrated for design drift and R.

$$NPISDR = function(R,\ Design\ Drift) * (OOP(\%))\text{^}2 + 1 \qquad (2\text{-}7)$$

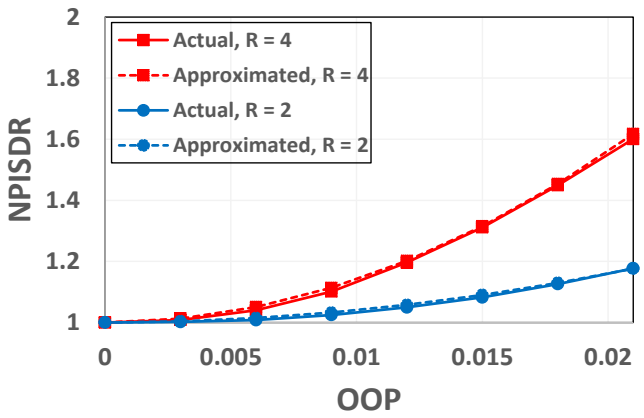

Figure 2-13: Calibration of NPISDR with OOP and R, Design drift = 2%.

A linear approximation is used to fit the NPISDR as a function of *R* for buildings with design drift of 1% and 2% as shown in Figure 2-14.

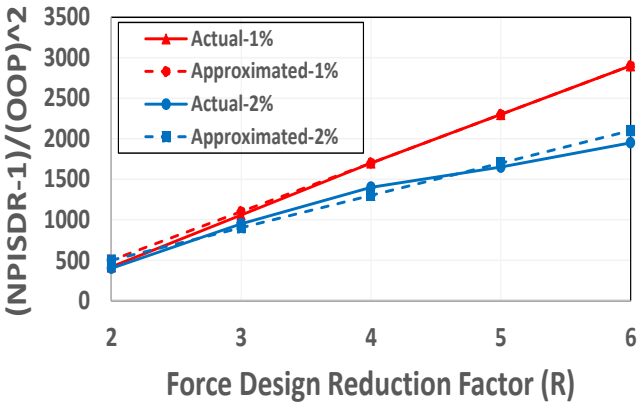

Figure 2-14: Calibration of NPISDR with design drift and R.

Finally, a relationship between NPISDR, OOP, *R* and design drift is produced as shown in Eq. 2-8.

$$NPISDR_{50\%} = ((-16000 \times Drift + 755) \times R - (-20000 * Drift + 900)) \times OOP^2 + 1 \quad (2\text{-}8)$$

This general equation can be used to approximate the increase in PISDR due to given OOP compare to the same building with no OOP by considering R and design drift.

Also, the 84% percentile of NPISDR was obtained for different OOP, *R*, and design drift and following relationship is produced to fit the actual response.

$$NPISDR_{84\%} = exp((-(-4600 \times Drift + 283) \times exp(-R) + (-720 * Drift + 58)) \times (OOP)) \quad (2\text{-}9)$$

Figure 2-15 compared the actual and approximated 84% percentile and 50% percentile (median) of NPISDR. It shows that the developed prediction equations can estimate the NPISDR.

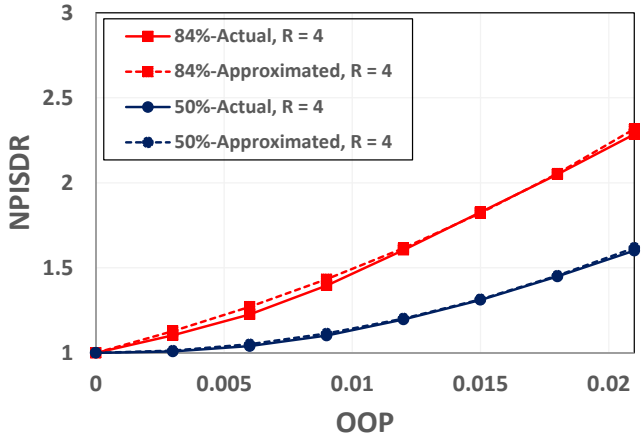

Figure 2-15: Comparing the actual and approximated 84% and 50% (median) of NPISDR for building with 2% design drift.

2.5.2. Estimation of Residual Inter-story Drift

A simple RPR prediction procedure is developed here for buildings with out-of-plumb. Since structural height and design drift do not significantly affect structural behaviour with changing OOP, the median RPR for all numbers of stories and design drifts was used.

Based on the equal displacement assumption, d_u, the peak displacement of structure, equals to $R \times d_y$(yield displacement) and d_r, the maximum possible residual displacement for a SDOF structure with zero OOP, a elastically perfectly plastic hysteresis loop and no p-delta effects is $d_u - d_y$. Therefore, the maximum possible RPR is given in Eq.2-10.

$$Maximum\ possible\ RPR = \frac{d_r}{d_u} = \frac{R-1}{R} \tag{2-10}$$

Hence, here the relationship between force design reduction factor (R), OOP and RPR is proportion of maximum RPR and can be expressed by Eq.2-11 where 0.085 shows that there is some residual displacements for design building with R

of 1 which is explained in section 4.1 and the coefficient of 0.5, obtained from empirical fit, shows self-centering characteristics (MacRae and Kawashima, 1997) in the building structure which decreases the value of RPR for this particular hysteresis loop:

$$RPR_{OOP}^{Median} = 0.085 + (\frac{R-1}{R}) \times (0.5 + 0.5 \times (1 - \exp(-20000 \times OOP^2))) \quad (2\text{-}11)$$

At high OOP (infinity), the RPR tends to $0.085 + (\frac{R-1}{R})$ and at OOP of zero, the RPR equals to $0.085 + 0.5 \times (\frac{R-1}{R})$. Also, as R tends to the infinity, the RPR become a constant value which is greater with greater OOPs. This general equation can be used to approximate the RPR due to given OOP and R is compared with actual experimental behaviour in Figure 2-16.

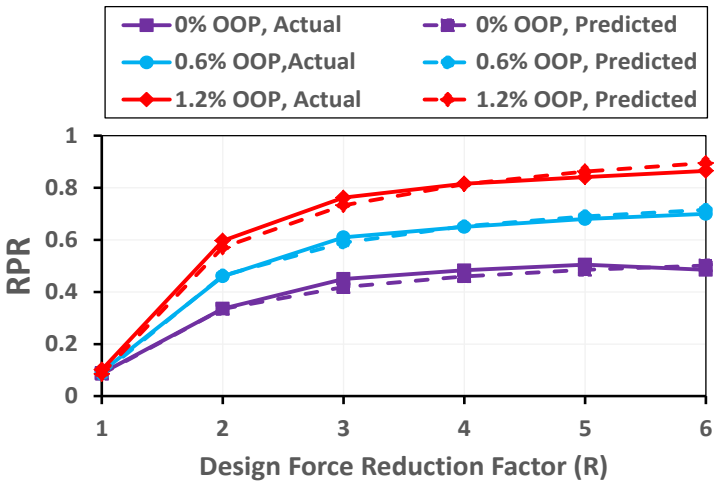

Figure 2-16: Comparison between median of actual and predicted RPR

Also, the 84% percentile of RPR was obtained for plumb building with different *R* and it is compared with the values of 50% (median) as shown in Figure 2-17. It shows that the 50% and 84% percentile of RPR increased with *R* and were less than 0.5 and 0.7 respectively.

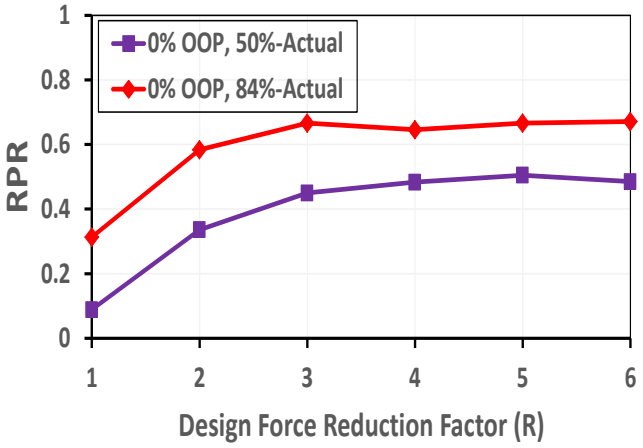

Figure 2-17: Comparison between 84% (median + STDEV) and median of RPR.

The 84th percentile RPR of an out-of-plumb structure is given by Equation 12 with the match given in Figure 2-18.

$$RPR_{oop}^{84\%} = 0.3 + \left(\frac{R-1}{R}\right) \times (0.5 + 0.275 \times (1 - \exp(-20000 \times OOP^2))) \qquad (2\text{-}12)$$

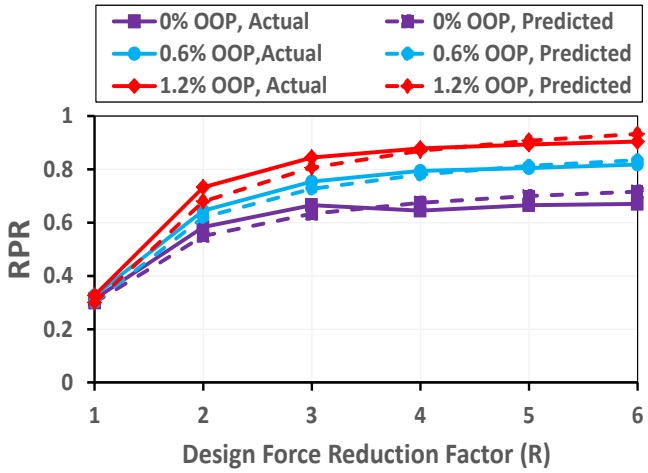

Figure 2-18: Comparison between 84% of actual and predicted RPR

2.5.3. Design Application

A RISDR and PISDR prediction procedure is developed here to estimate the likely (median) increase in response for buildings with OOP. Also, 84 percentile

equations may be used for a more conservative estimate of either the peak, or residual displacement demand. The applicability of the peak and residual ISDR prediction method given in the steps below:

Step 1: Find the PISDR of the building if it were plumb using standard methods.

Step 2: The normalized peak inter-story drift ratio (NPISDR) is obtained from Equation 8 using the design force reduction factor (*R*), design drift and OOP;

Step 3: Compute the relative PISDR of the OOP building by multiplying the NPISDR by the PISDR of the plumb building;

Step 4: Compute total PISDR of OOP building from summation of relative PISDR of OOP building with OOP;

Step 5: The RPR is obtained from Equation 11;

Step 6: Compute relative residual ISDR of OOP building from multiplying RPR and relative PISDR of plumb building;

Step 7: Compute total residual ISDR from summation of relative RISDR of OOP building with the OOP;

For example, if the 9 story building with story height of 4 m was designed with R of 3 and design drift of 2%, what is the likely maximum peak and residual ISDR for structure with OOP of 1.2%:

Step 1: The peak inter-story drift ratio (PISDR) of the plumb structure is likely to be similar to the design drift of 2%;

Step 2: The NPISDR from Equation 8, is 1.12 using R of 3, design drift of 2% and OOP of 1.2%;

Step 3: The change in PISDR of the OOP building is 1.12*2% = 2.24%;

Step 4: The total PISDR of OOP building: 2.24%+1.2%= 3.44%

Step 5: The RPR from Equation 11, is about 0.73;

Step 6: The total RISDR: 0.73*2.24% +1.2%=2.83%

For this example the actual maximum median total PISDR of OOP building from analysis using the records described previously is 3.3% and the maximum median total RISDR is 2.77%. This is consistent with the calculation above showing that the developed prediction procedure can estimate the peak and residual drifts.

2.6. Conclusion

Time history analyses were conducted of shear-type structures with continuous columns, bilinear hysteresis loops and post elastic stiffness factor of 1%, force design reduction factors, *R*, of 1, 2, 3, 4, 5, and 6, number of stories, *N*, of 3, 6, 9, 12, and 15, and design drifts of 1, 1.5, 2, and 2.5, in order to evaluate peak and residual inter-story drift ratio considering building out-of-plumb. The main findings are:

1) The normalized peak inter-story drift ratio (NPISDR) was found to increase most strongly with increasing out-of-plumb and with lateral force reduction factor. The response was less sensitive to design drift and not

sensitive to number of stories. Reasons for trends observed were described and empirical relationships were developed for NPISDR depending on OOP, R and design drift. For OOP less than 0.3% the increase in peak displacement is less than 5%.

2) The ratio of residual-to-peak inter-story drift response was strongly dependent on the OOP and force design reduction factor. Empirical relationships to estimate the maximum residual inter-story drift for those structures were obtained. For OOP less than 0.3%, the increase in residual displacement is less than 15%. Thus, residual displacement is much more sensitive to OOP and adds to initial OOP. Residual displacement may well determine the acceptable OOP without explicit consideration in realistic structures.

3) A design procedure to estimate likely peak and residual drifts in multistory structures similar to those analysed was developed using the relationships obtained. A design example is also provided.

2.7. References

American Institute of Steel Construction (AISC), Specification for Structural Steel Buildings, ANSI/AISC Standard, Chicago, Illinois, 2010; 360-10.

Caughey T. K. Classical normal modes in damped linear dynamic systems. Transactions of ASME, Journal of Applied Mechanics, 1960; 27, 269-271.

Carr A.J. Ruaumoko 2D, Inelastic dynamic time-history analysis program, Department of Civil Engineering, University of Canterbury, Christchurch, 2004.

Cornell, C. A., Fatemeh, J. F., Hamburger, R. O. and Foutch, D. A. Probabilistic basis for 2000 SAC FEMA steel moment frame guidelines, Journals of Structural Engineering, 2002; 128 (4): 526-533.

MacRae G. A. and Kawashima K. The Seismic Response of Bilinear Oscillators Using Japanese Earthquake Records, Journal of Research of the Public Works Research Institute, Ministry of Construction, Japan, 1993; 30.

MacRae G. A. P-Δ effects on single-degree-of-freedom structures in earthquakes, Journal of Earthquake Spectra, 1994; 10 (3): 539-568.

MacRae G. A. and Kawashima K. Post-earthquake residual displacements bilinear oscillators, Earthquake Engineering and Structural Dynamics, 1997; 26, 701-716.

MacRae G. A., Kimura Y. and Rodgers C. W. Effect of column stiffness on braces frame seismic behaviour, Journal of Structural Engineering, American Society of Civil Engineers, 2004; 130 (3): 381-391.

MacRae, G. A., The Continuous Column Concept - Development and Use, Ninth Pacific Conference on Earthquake Engineering, Auckland, New Zealand, 2011.

Masuno T., MacRae G. A., and Sadashiva V. K. Response of Out-of-Plumb Structures in Earthquake, Ninth Pacific Conference on Earthquake Engineering, Auckland, New Zealand, 2011.

NZS 1170.5:2004. Structural Design Actions Part 5: Earthquake actions New Zealand, Standards New Zealand, Wellington, New Zealand, 2004.

Tagawa H., Towards an Understanding of Seismic Response of 3D Structures – Stability & Reliability, Doctoral Thesis, University of Washington, Seattle, 2005.

Tagawa H., MacRae G. A. and Lowes, L. Evaluations of 1D Simple Structural Models for 2D Steel Frame Structures, Thirteen World Conference of Earthquake Engineering, Vancouver, Canada, 2004.

Tagawa H., MacRae, G.A. & Lowes, L. Continuous column effects of gravity columns in U.S. steel moment-resisting frame structures- continuous column effects in steel moment frames in perspective of dynamic stability (Part 2) Journal of Structural and Constructional Engineering, Transactions of the Architectural Institute of Japan, AIJ, 2010; 75(650): 761-770.

The MathWork, Inc., Matlab R2008a.

SAC (SEAOC-ATC-CUREE). The SAC Steel Project. Berkeley, Ca, 2000.

Sadashiva V. K, MacRae G. A, Deam B. L. Determination of Structural Irregularity Limits- Mass Irregularity Example, Bulletin of The New Zealand Society for Earthquake Engineering, 2009; 42(4).

Surovek-Maleck A.E. and White, D.W. Alternative Approaches for Elastic Analysis and Design of Steel Frames, I: Overview. Journal of Structural Engineering, ASCE, 2004a; 130(8): 1186-1196.

Surovek-Maleck, A.E. and White, D.W. Alternative Approaches for Elastic Analysis and Design of Steel Frames, II: Verification Studies. Journal of Structural Engineering, ASCE, 2004b; 130(8): 1197-1205.

White D.W., Surovek A.E., Alemdar B.N., Chang C.J., Kim Y.D., and Kuchenbecker G.H. Stability analysis and design of steel building frames using the 2005 AISC Specification. International Journal of Steel Structures, Korean Society of Steel Construction, 2006; 6, 71-91.

Yeow T. Z., MacRae G. A., Sadashiva V. K., and Kawashima K. Dynamic Stability and Design of C-Bent Columns. Journal of Earthquake Engineering, 2013; 17:5,750-768.

Chapter 3: Potential for Ratcheting of Steel Buildings with Balanced Lateral Stiffness and Strength under the 2010-2011 Canterbury Earthquake Sequence

3.1. Introduction

Recent events has shown that strong shaking at a particular site may be subsequently followed by several other considerably large aftershocks over a period of minutes, days, or months. Because of the potentially short time between events, there may be insufficient time for structure to be repaired, which may lead to further damage or the possibility of building collapse during aftershocks. Even if the building is being repaired, workers in the building performing repairs may be at risk during aftershocks.

Because of the potential effect of an entire earthquake sequence on the response of buildings, a number of numerical studies have been conducted on this topic. These indicate that in cases when each record being run multiple times with different scale factors to mimic aftershock effects peak and residual structural drift demands may be increased following aftershocks. However, many of these studies have not considered actual sequence records. Furthermore, many studies were conducted on single-degree-of-freedom models or a limited range of multistory structures. These findings were also contradictory to observations from the Christchurch earthquakes, where it was found that the residual displacements of some steel buildings decreased with subsequent shaking; such as the Pacific

Tower which residual roof displacement decreased from 60mm to 30mm after the 2011 February event (MacRae et al., 2015).

It may be seen from the above discussion that there is a need to understand the likely effect of a realistic earthquake sequence effects considering shaking orientation on the performance of the ductile steel buildings of different strength and stiffness. In order to address this need, response history analyses are conducted on a range of multi-storey steel frame structures using records obtained from the 2010-2011 Canterbury earthquake sequence to seek answers to the following questions:

1) How does the 2010-11 Canterbury earthquake sequence affect the peak drift response?

2) How does the 2010-11 Canterbury earthquake sequence affect the residual drift response?

3) What building properties have the greatest effect on its ratcheting response under the 2010-2011 Canterbury earthquake sequence?

3.2. Literature Review

3.2.1. Previous Work on Aftershocks Effects on Structures

Several research studies have been conducted on the nonlinear seismic response of the structures subjected to a suite of ground motion records, with each record being run multiple times with different scale factors to mimic aftershock effects.

Examples include Amadio et al. (2003), Fragiacomo et al. (2004), Li and Ellingwood (2007), Hatzigeorgiou and Beskos (2009), Hatzigeorgiou (2010) and Erochko et al. (2011). A common conclusion reached in these studies is that a sequence of earthquakes tends to increase the displacement demands of the structures in comparison with single seismic events. However, Ruiz-Garcia (2012) highlighted that this method gives unrealistic results since the main-shock and the largest aftershock generally have different frequency content due to varying rupture location and magnitude.

Goda and Taylor (2012) had performed two sets of analyses; one by using an unrealistic aftershock sequence, and the other using recorded data available from the Pacific Earthquake Engineering Research Centre - Next Generation Attenuation (PEER-NGA) database. It was shown that use of the unrealistic aftershocks can lead to greater demands on the structure during aftershocks. In contrast, the findings using real sequences showed that the increase in peak displacement demands on some SDOF structures due to real aftershock ground motions was less than 10%.

An additional study using realistic ground motion sequence from the 1994 Northridge earthquake was performed by Ruiz-García and Negrete-Manriquez (2011) for steel frame buildings. They showed that as-recorded aftershocks did not significantly increase peak and residual drift demands in the cases considered.

Wilson and Bradley (2012) studied the cumulative ground motions effects using the Canterbury earthquake sequence on SDOF structures without modelling P-delta effects. They found that the 4th of September 2010 earthquake increased the

resulting peak displacement demands from the 22nd of February 2011 event by less than 5% for the majority of concrete structures considered in Christchurch.

Abdelnaby and Elnashai (2014) applied Tohoku and Christchurch earthquake sequences to degrading reinforced concrete frame systems designed with (i) gravity considerations only, (ii) gravity considerations and the direct lateral force design method, and (iii) the method used in (ii) plus capacity design concepts. For the cases considered they found that inter-story drifts were smaller in the capacity designed frame compared to gravity and direct lateral force design frames under multiple earthquake shakes.

3.2.2. Previous Work on Dynamic Stability

Another factor which strongly dictates the residual displacement response for structures subjected to a series of earthquake motions is the characteristics of the building's hysteretic behaviour. MacRae and Kawashima (1993), MacRae (1994), and Yeow et al. (2013) showed that for a hysteresis loop where force-displacement bilinear factors including P-delta effects, $r_{P\text{-}\Delta}$, is positive as shown in Figure 3-1a, the structure would require a larger shear force in the positive direction to cause yielding compared to the negative direction if it starts at position A. Thus, yielding is more likely to occur in the negative direction, which would bring the position of the oscillator back towards the zero displacement position. Such a hysteresis loop is said to be dynamically stable.

However, for a hysteresis loop where $r_{P\text{-}\Delta}$ is negative as shown in Figure 3-1a, it can be seen that yielding is more likely to occur in the positive direction and away

from the zero displacement position. Therefore, yielding will then predominantly occur in one direction only, resulting in larger residual and maximum displacements in subsequent shaking. This effect is known as ratcheting, and buildings which exhibit this behaviour are dynamically unstable.

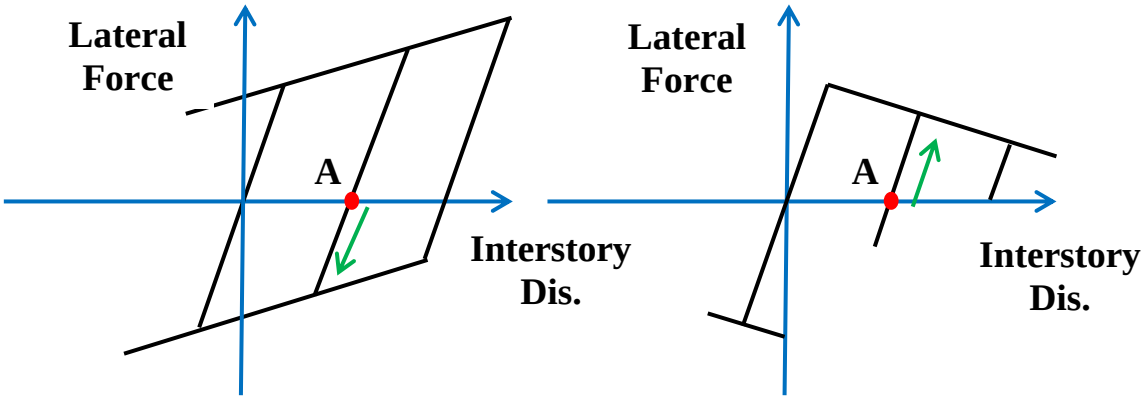

(a) Positive Bilinear Hysteresis Loop ***(b) Negative Bilinear Hysteresis Loop***

Figure 3-1: Dynamic stability effect

In addition to unbalanced provided strength, an initial eccentric moment applied to the building may cause ratcheting. For example, Rad et al. (2015) showed that buildings with greater initial out-of-plumb and force design reduction factor, *R*, generally exhibited larger peak inter-story drifts and residual-to-peak drift ratios in subsequent seismic events. This study also showed that at high out-of-plumb, the ratio of residual-to-maximum possible residual drift tends to unity, indicating that the buildings are yielding predominantly in one direction.

3.3. Modelling and Evaluation Approach

The simple structural model for shear type frames proposed by Tagawa (2005, 2010) shown in Figure 3-2 was implemented. This consists of three different types of columns per floor, with all horizontal degrees-of-freedom on each floor being slaved together. The first is a shear-type column with lateral but no rotational degrees of freedom at each level providing the elastic stiffness of the seismic frames and the hysteretic energy dissipation. The second is a continuous column, which represents the stiffness of all columns in the structure which provide continuity over the building height to mitigate drift concentration. The continuous column has a perfect pin at its base and both rotational and in-plane translational degrees of freedom at all other levels. The final type are *P*-delta columns, consisting of rigid props with pinned ends, and are used to consider the effect of gravity loads on gravity columns being displaced. This model has been shown to represent the behaviour of full 2-D moment frames well, and has been implemented in numerous studies, e.g. Tagawa (2005, 2010), Sadashiva et al. (2009), and Rad et al. (2015).

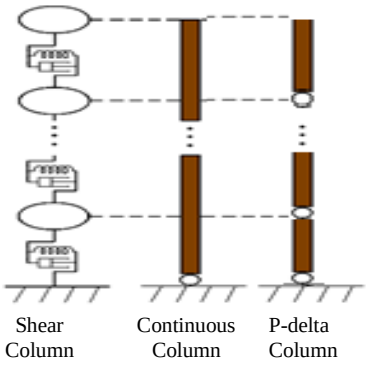

Figure 3-2: Simplified model with Shear, Continuous and P-delta columns

A continuous column stiffness ratio α_{cci} (MacRae et al., 2004), which defines the continuous column stiffness relative to the shear column stiffness at the i^{th} floor, was computed using Eq.3-1. Here, E is the material Elastic Modulus; H_i is the story height of the i^{th} floor level; I_i is the moment of inertia of the continuous column between the floor levels; and K_{oi} is the initial lateral stiffness of the i^{th} floor level. A continuous column stiffness ratio α_{cci} of 0.2 is assumed at each level following Tagawa (2005) and MacRae (2011). This is on the lower end of the realistic scale of continuous column stiffness for actual structures, and is thus more likely to give conservative results.

$$\alpha_{cci} = \frac{EI_i}{H_i^3 K_{oi}} \tag{3-1}$$

The iterative steps used to design the structure are shown in Figure 3-3. The basic structure was designed as an ordinary building in Christchurch (Hazard factor (Z) = 0.3) on site class C post-2011. A constant mass of 20 Tons, m, was lumped at each floor. The number of stories (N) considered in this study are 3, 6, 9, and 12, with constant story heights, h, of 4m. Structures were designed with target peak inter-story drifts of 1%, 1.5%, 2% and 2.5% and force design reduction factors (R) of 1 to 6 in steps of 1 according to the Equivalent Static Method in NZS1170.5 (2004) using a structural performance factor, S_p, of 1.0. The structure's stiffness distribution is designed so that it exhibits a constant inter-story drift ratio over its height when subjected to the equivalent lateral forces from NZS1170.5 (2004) because this results in greater displacements on all floors compared to other

stiffness distribution approaches (i.e. constant stiffness) as shown by Masuno et al. (2011).

Earthquake ground motions from five Christchurch stations close to the central business district listed in Table 3-1 were used. At each station, both the north-south and east-west orientations from the 2010-2011 Canterbury earthquakes were considered individually, giving a total of 10 record sequences. Each record sequence contained the 4 major shakes; 4th of September 2010 at 4:35am (with a magnitude, Mw, of 7.1), 22nd of February 2011 at 12:51pm (Mw 6.2) earthquake record, 13th of June 2011 at 3:20pm (Mw 6.0) at and 23rd of December 2011 at 3:18pm (Mw 6.0). Further details of these records can be found in Bradley and Cubrinovski (2011) and Bradley (2012). The ground acceleration time history of the earthquake sequence from the Christchurch Botanic Gardens (CBGS) in the north-south direction is shown in Figure 3-4. The 1 in 500 year spectral acceleration response spectrum for design based on recommendations from NZS1170.5 (2004) is shown in Figure 3-5. In this study, since the spectral acceleration of the February event is larger than the other events as shown in Figure 3-5, the February event is considered as the main shock.

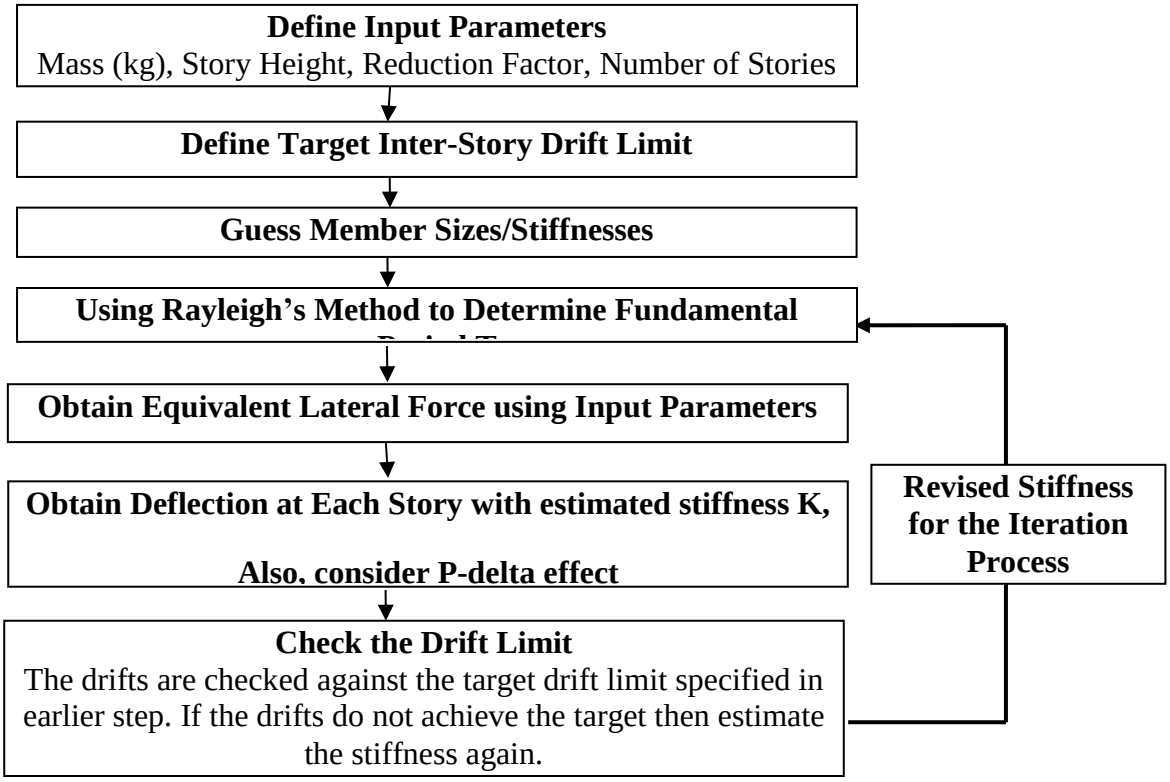

Figure 3-3: Flow Chart for Structural Design

Table 3-1. Stations of Canterbury Earthquake

Station	Location	Site Code
1	Botanic Gardens	CBGS
2	Christchurch Hospital	CHHC
3	Resthaven	REHS
4	Papanui High School	PPHS
5	Riccarton High School	RHSC

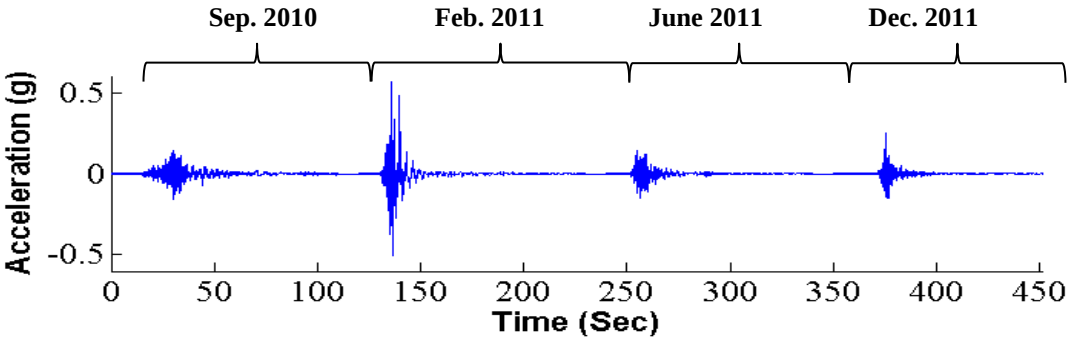

Figure 3-4: Christchurch Earthquake Sequences from the CBGS: 3 September 2010 (Mw 7.1) at 16:35, 21 February 2011 (Mw 6.2) at 23:51, 13 June 2011 (Mw 6.0) at 2:20 and 23 December 2011 (Mw 6.0) at 2:18 respectively in the North-South direction.

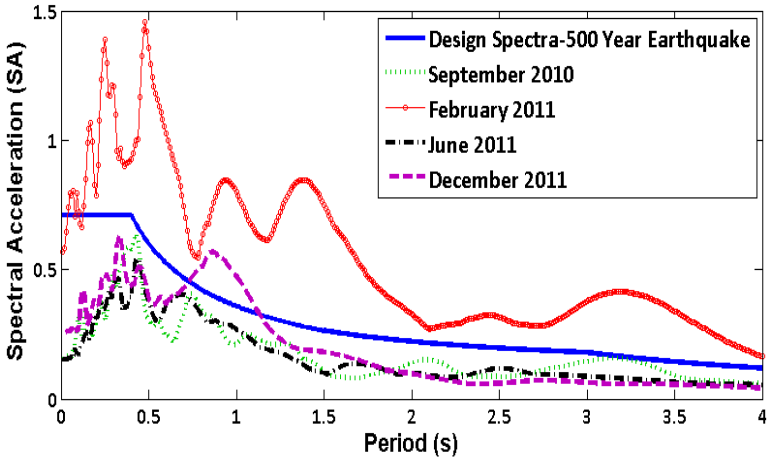

Figure 3-5: Spectral Acceleration of 3 September 2010 (Mw 7.1) at 16:35, 21 February 2011 (Mw 6.2) at 23:51, 13 June 2011 (Mw 6.0) at 2:20 and 23 December 2011 (Mw 6.0) at 2:18 from the CBGS in the North-South direction and NZ Design Spectra for Category C soil for 500 year shaking

The dynamic inelastic time history computer program RUAUMOKO-2D (2004) was used to run the analysis. The shear columns were modelled assuming bi-linear hysteretic behaviour with a story shear force-displacement post-yield stiffness ratio of 4%, as shown in Figure 3-6, in order to represent steel buildings. The continuous column was assumed to remain elastic during an earthquake. Caughey damping (Caughey, 1960) was implemented with a damping ratio of 5% is assumed for all modes and P-delta was considered in analysis. Input files for

RUAUMOKO-2D (2004) are generated using MATLAB (2008). The two programs were automated to run and extract the peak and residual inter-story drift ratio, (*PISDR* and *RISDR*, respectively), for each site and orientation over all stories. There are defined as the relative peak and residual horizontal displacement between adjacent floors normalized by the story height, respectively.

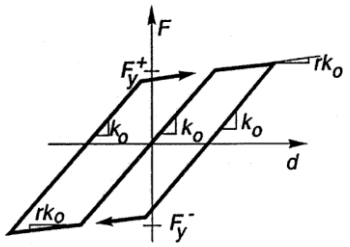

Figure 3-6: Bi-linear Hysteretic models

3.4. Building Drift Response under Seismic Sequence

3.4.1. General Peak Inter-Story Drift Observations

Median peak inter-storey drift ratios, *PISDR*, were computed for Canterbury seismic sequences recorded for 3, 6, 9 and 12 story buildings for the 10 sequences as shown in Figure 3-7. The *PISDR* following the 2011 February event (mainshock) was generally larger than that following the 2010 September for all cases, which is due to the relatively greater shaking intensity of the February event compared to the September event as seen previously in Figure 3-4 and Figure 3-5. Figure 3-7 also shows that the maximum median *PISDR* over the height was slightly increased by 10% with post-February aftershocks.

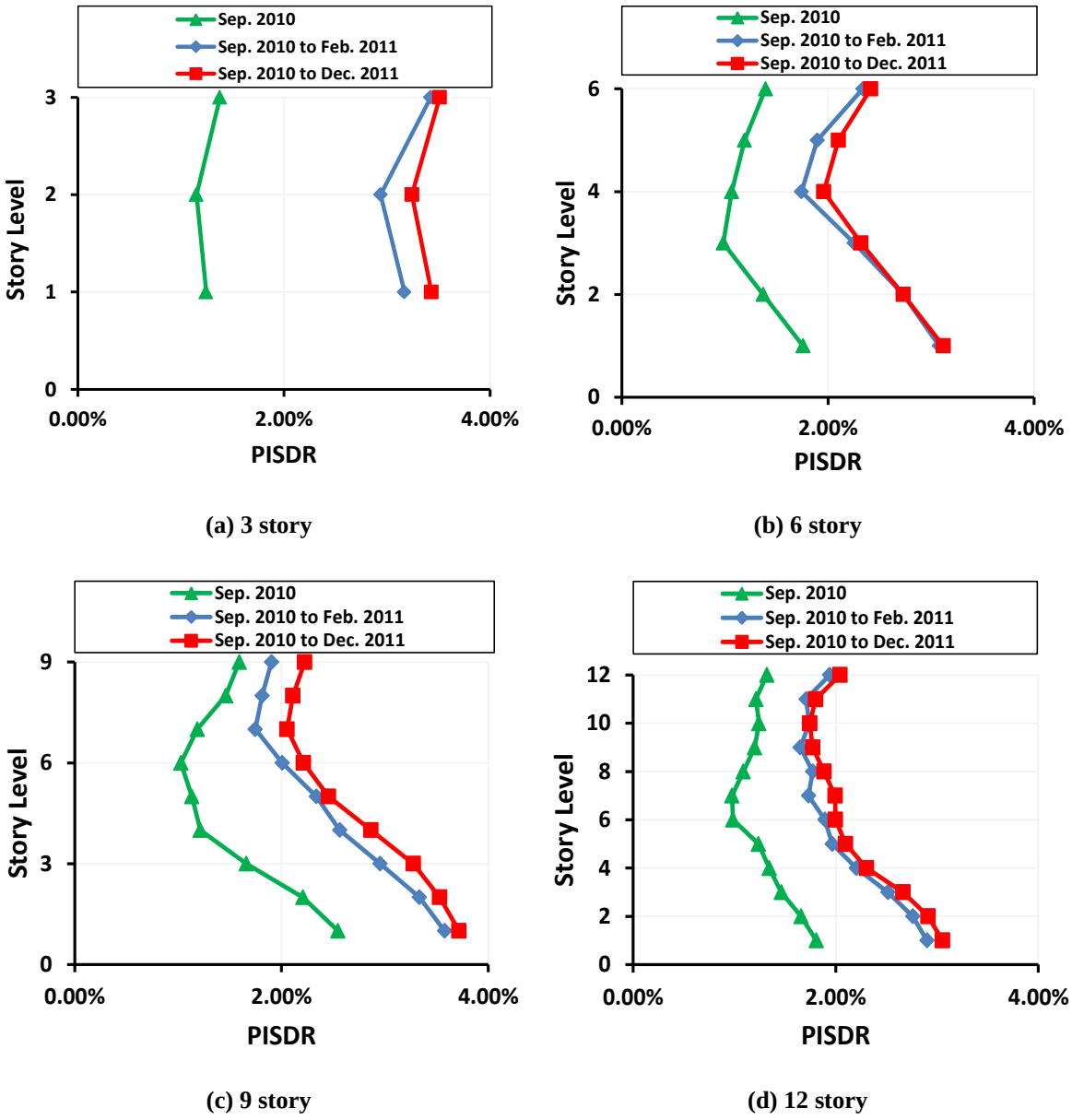

Figure 3-7: Effect of sequence of ground motions on PISDR (R = 4, Design drift of 2%)

A key reason for the generally small increase (by 5%) in overall peak interstorey drift following the February 2011 event was due to the relatively low amplitude displacement response of the structures under June and December 2011

aftershocks. This can be observed from Figure 3-8, which shows the moment-displacement hysteresis curves of the first floor shear column of the 3 story structure with *R* of 4 subjected to the Sep. 2010, February 2011, June and December 2011 ground motions from CBGS station individually. It clearly shows that the displacement response of the structure under February 2011 event is larger than the September 2010, June 2011, and December 2011 events.

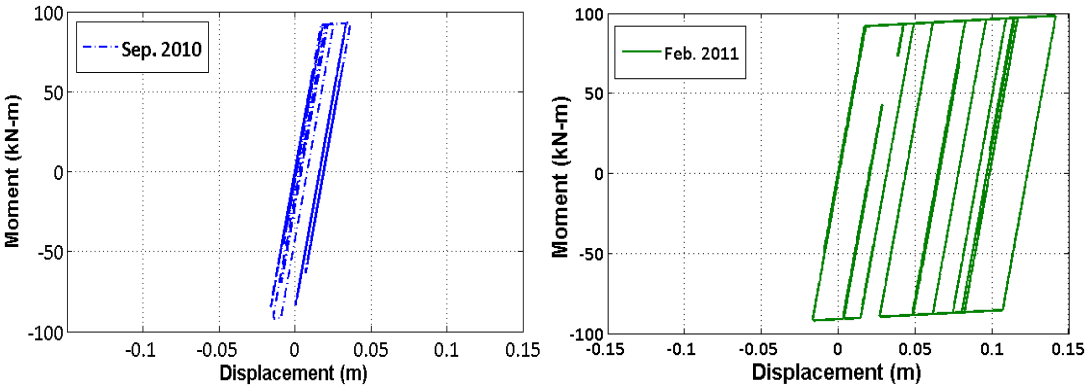

(a) September 2010

(a) February 2011

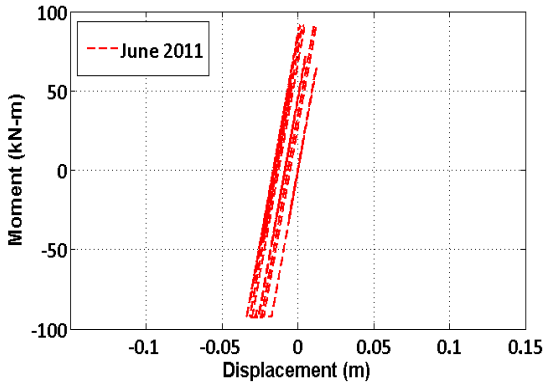

(c) June 2011

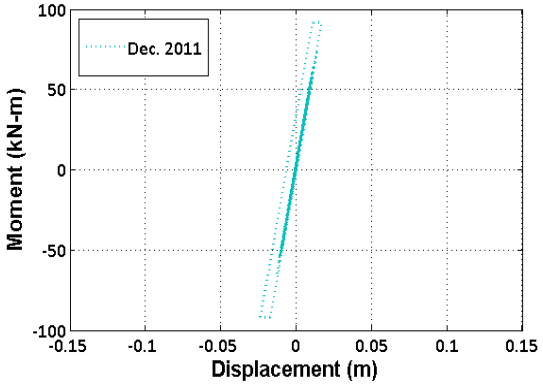

(d) December 2011

Figure 3-8: Moment-displacement hysteresis curve of first floor element of the 3 story structure (R of 4, design drift of 2%) under CBGS (N-S) earthquake records.

3.4.2. General Residual Inter-Story Drift Observations

Median *RISDR* is computed for Canterbury seismic sequences recorded for 3, 6, 9 and 12 story buildings with *R* of 4 for the 10 sequences as shown in Figure 3-9. The effect of September earthquake on residual drift of the buildings is small as the February event produce larger residual drifts compared to the September earthquake, which is consistent with findings from Figure 3-8. Moreover, Figure 3-9 shows that June and December sequence records increase the maximum median *RISDR* of the buildings by 30%. It indicates that aftershocks may potentially continuously push the structure to ratchet in one direction only.

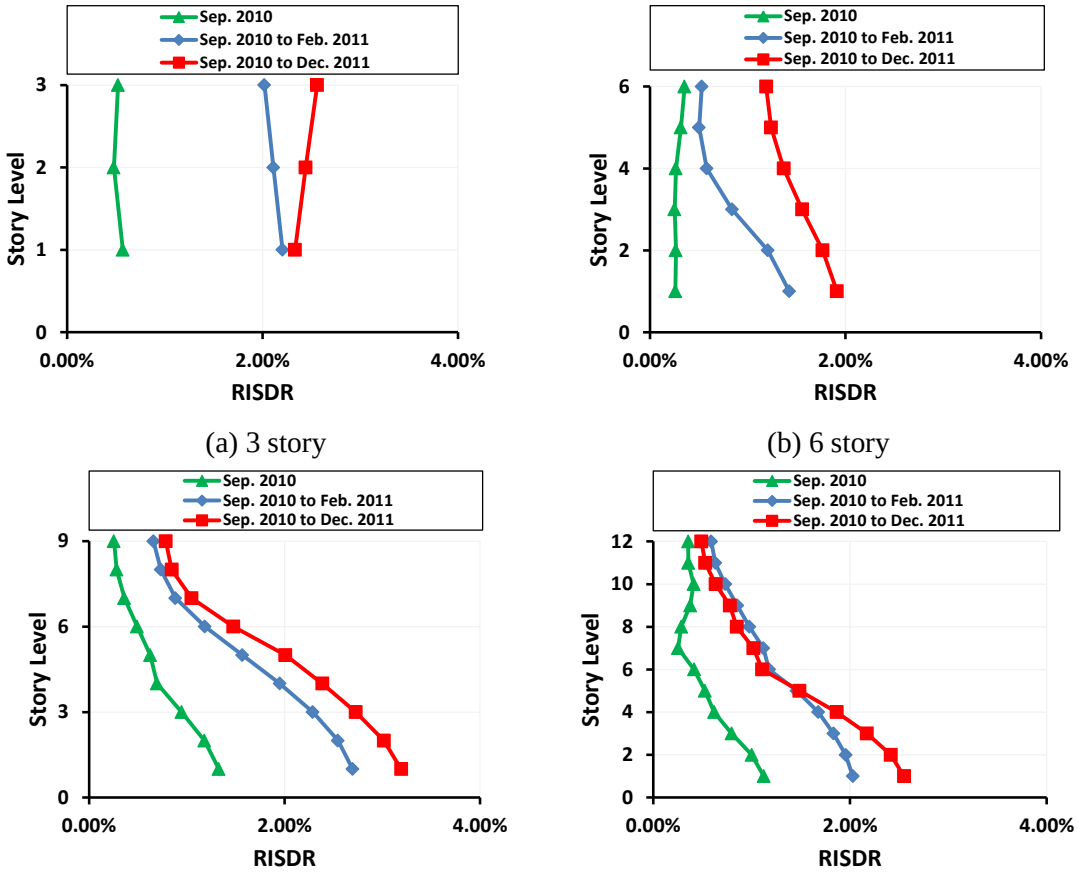

(a) 3 story (b) 6 story

(c) 9 story (d) 12 story

Figure 3-9: Effect of aftershocks on median RISDR (Design drift of 2%, R =4)

3.4.3. Effect of Lateral Force Design Reduction Factor

Figure 3-10 compares the median *RISDR* over the height of the structure of the 3, 6, 9 and 12 story buildings for the 10 sequences with and without the June and December aftershocks for different *R*. The trend shows that June and December aftershocks tend to increase the *RISDR* of the structures. In addition, the *RISDR* value itself increases with increasing *R*. It shows that the structures would experience predominant ratcheting in one direction. The tendency for ratcheting was with increasing *R*.

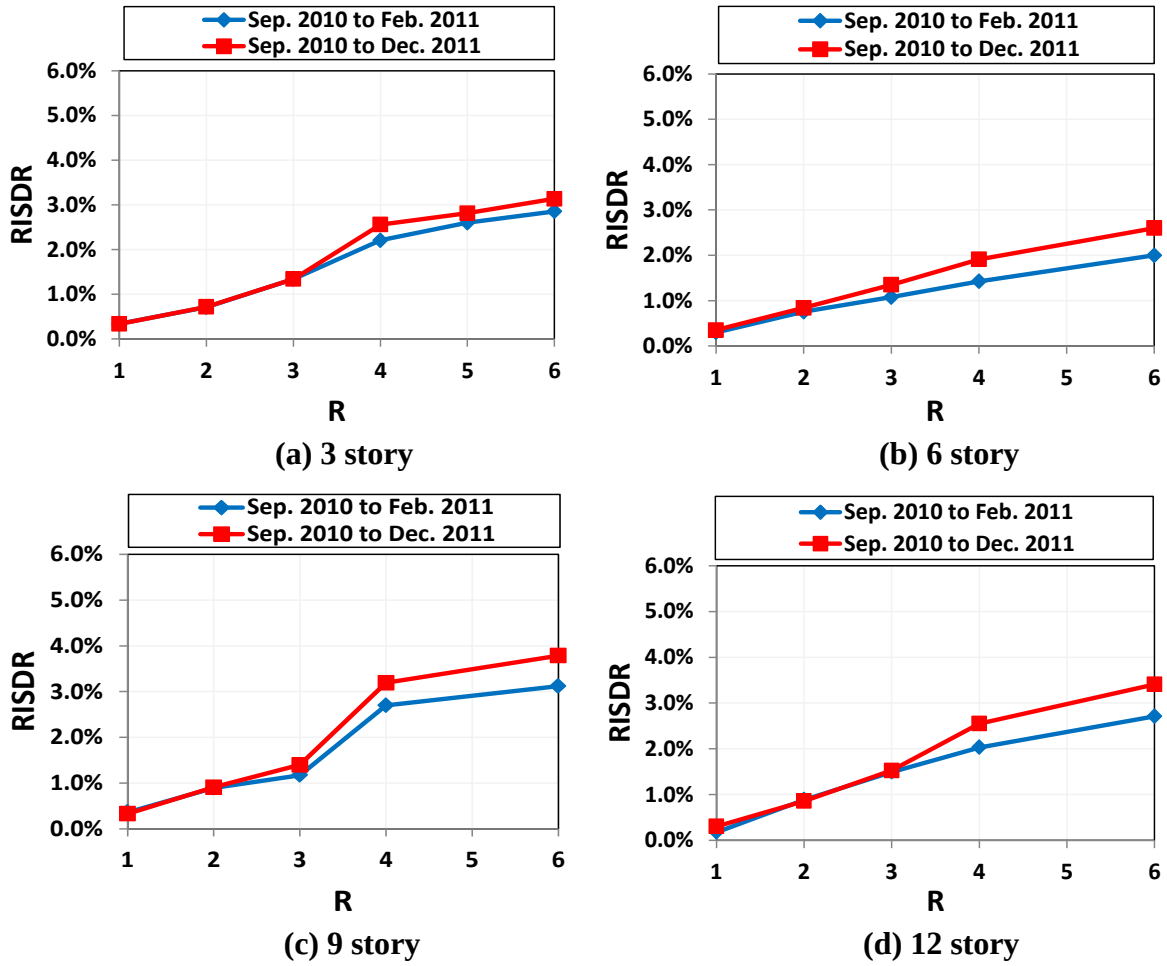

Figure 3-10: Effect of force design reduction factor (R) on RISDR (Design drift of 2%)

3.4.4. Effect of Design Drift

Figure 3-11 compares the maximum median *RISDR* of 3, 6, 9 and 12 story buildings over the height for the 10 sequences with different design drift and *R* of 4. The trend shows that with increasing of design drift (i.e. increased period and spectral displacement), the *RISDR* of the structures is also increased.

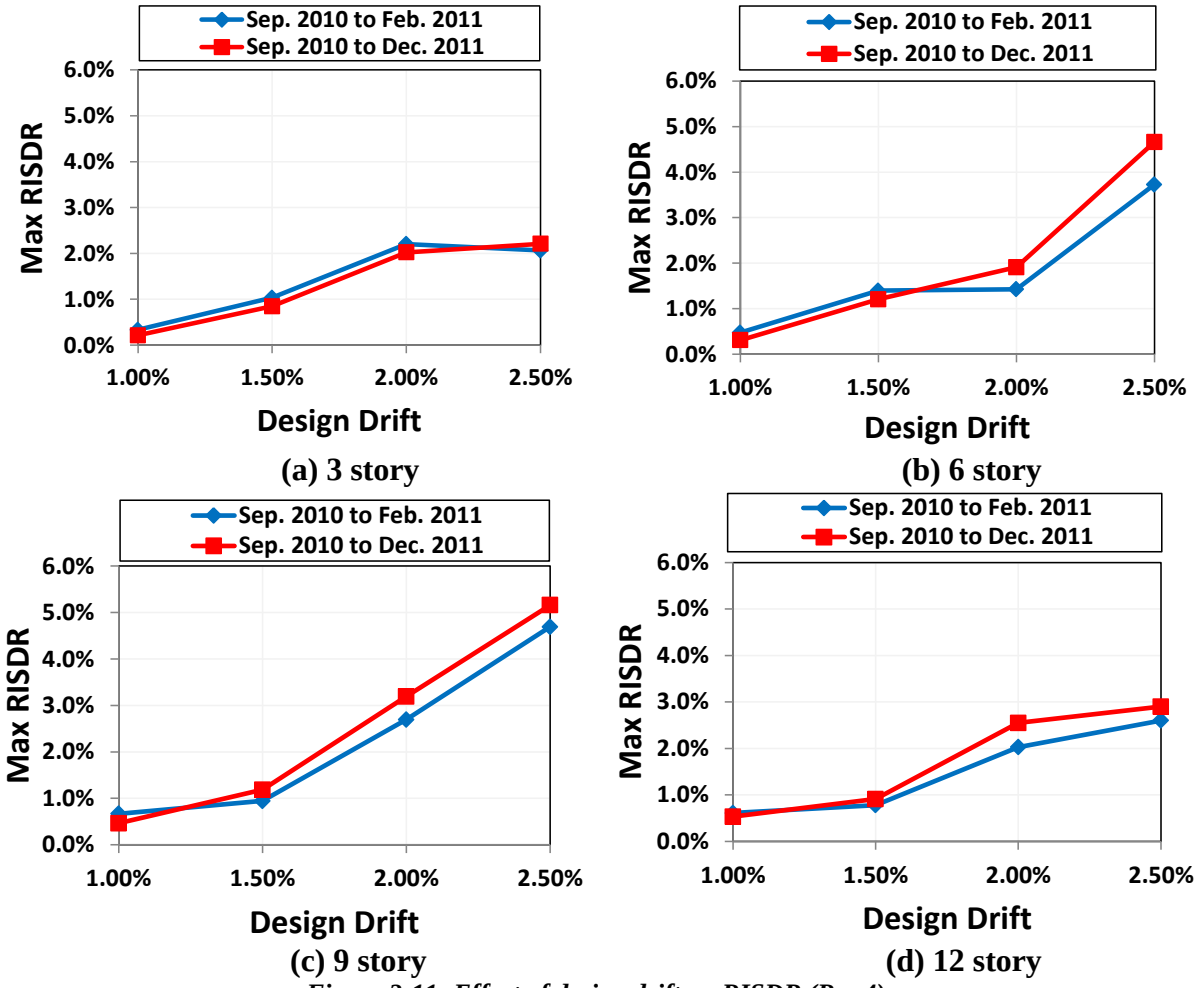

Figure 3-11: Effect of design drift on RISDR (R = 4).

3.4.5. Effect of Direction of Shaking

Figure 3-12 shows the effect of changing the direction of the June and December ground motions by 180 degrees of the 10 sequences on *RISDR* for structures

compared to that using as recorded data. It shows that generally there is higher tendency of *RISDR* to increase for all structures due to aftershock irrespective of direction of motions. This is also can be seen in first story time history drift response of the 3 story structure as shown in Figure **3-13**.

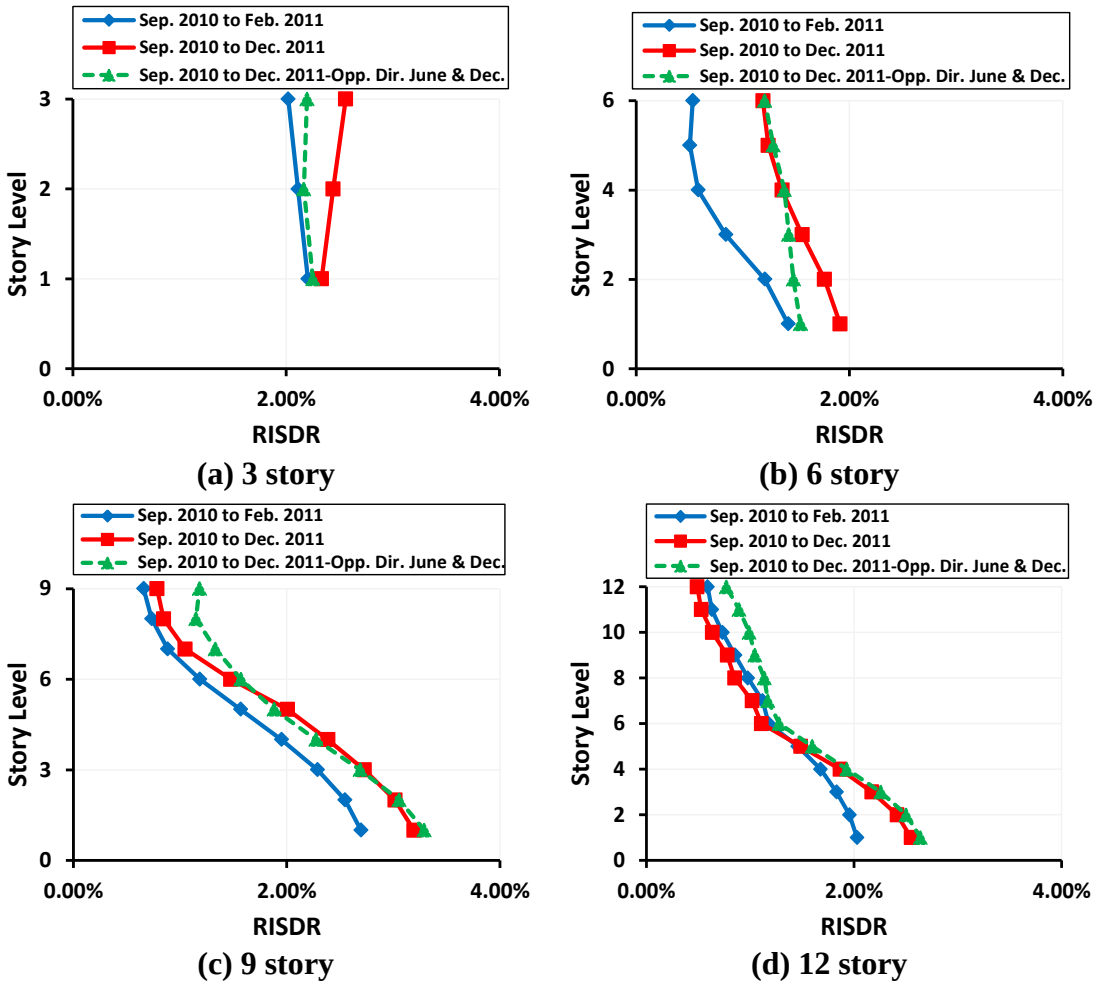

Figure 3-12: Effect of direction of earthquake sequence records on the RISDR of the structures (R of 4 and design drift of 2%) under 10 sequences.

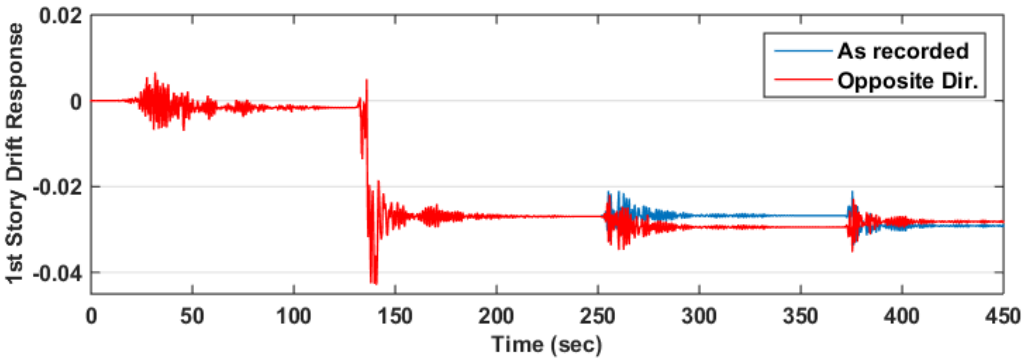

Figure 3-13: Effect of direction of earthquake sequence records (CBGS) on 1st story drift response of the structure (3story, R of 4, Design drift of 2%).

3.5. Conclusion

Time history analyses were conducted of shear-type steel structures with force design reduction factors, *R*, of 1, 2, 3, 4, 5 and 6; number of stories, *N*, of 3, 6, 9, and 12; and design drifts of 1%, 1.5%, 2%, and 2.5% in order to evaluate peak and residual inter-story drift ratio (*PISDR* and *RISDR*) under Canterbury sequence of ground motions. The main findings are:

1) The September 2010 and the February 2011 ground motion events caused the major peak interstorey drift demands, while the June and December 2011 aftershocks increased the maximum observed peak inter-story drift response across the entire height of the building by up to 10%.

2) The residual interstorey drift ratio (*RISDR*) increased under post February aftershocks by up to 30%. This implies that these aftershocks had an overall tendency to cause the structures ratchet in one direction. This was irrespective of the earthquake directionality.

3) The residual interstorey drift ratio (*RISDR*) under a sequence of ground motions was strongly dependent on the force design reduction factor and design drift. The tendency for ratcheting was with increasing lateral force reduction factor, *R*, and design drift.

3.6. References

Abdelnaby A. E. and Elnashai A. S. . "Performance of degrading reinforced concrete frame systems under the Tohoku and Christchurch earthquake sequences", J. Earthquake Eng., 2014, 18:1009–1036.

Amadio C., Fragiacomo M., and Rajgelj S. "The effects of repeated earthquake ground motions on the non-linear response of SDOF systems" Earthquake Eng. Struct. Dyn., 2003, 32, 291–308.

Bradley B. A. "Strong ground motion characteristics observed in the 4 September 2010 Darfield, New Zealand earthquake" Soil Dyn. Earthquake Eng., 2012, 42:32–46,

Bradley B. A. and Cubrinovski M. "Near-source strong ground motions observed in the 22 February 2011 Christchurch earthquake" Seismol. Res. Lett., 2011, 82(6): 853-865.

Canterbury Earthquake Royal Commission. "The performance of Christchurch CBD buildings", 2012, Final Report, 2, 1-236.

Carr A.J. Ruaumoko 2D. "Inelastic dynamic time-history analysis program" Department of Civil Engineering, University of Canterbury, Christchurch, 2004.

Caughey T. K. "Classical normal modes in damped linear dynamic systems", Transactions of ASME, J Appl. Mech.,1960, 27, 269-271.

Cornell C.A., Fatemeh J.F., Hamburger R.O., and Foutch D.A. "Probabilistic basis for 2000 SAC FEMA steel moment frame guidelines" J. Struct. Eng., 2002, ; 128(4):526–533.

Erochko, J., Christopoulos, C., Tremblay, R., and Choi, H. (2011). "Residual drift response of SMRFs and BRB frames in steel buildings designed according to ASCE 7-05" J. Struct. Eng., 137, 589–599.

Fragiacomo M., Amadio C., and Macorini L. "Seismic response of steel frames under repeated earthquake ground motions" Eng. Struct., 2004, 26, 2021–2035.

Goda K. and Taylor C.A. "Effects of aftershocks on peak ductility demand due to strong ground motion records from shallow crustal earthquakes", Earthquake Eng. Struct. Dyn., 2012, 41, 2311-30.

Hatzigeorgiou G. D. “Ductility demand spectra for multiple near- and far-fault earthquakes” Soil Dyn. Earthquake Eng., 2010, 30, 170–83.

Hatzigeorgiou G. D. and Beskos D. E. “Inelastic displacement ratios for SDOF structures subjected to repeated earthquakes” Eng. Struct.,2009, 31: p. 2744-25.

Hatzigeorgiou G. D. and Liolios A. A. “Nonlinear behaviour of RC frames under repeated strong ground motions” Soil Dyn. Earthquake Eng., 2010, 30, 1010–25.

Li Q. and Ellingwood B. R. “Performance evaluation and damage assessment of steel frame buildings under main shock-aftershock sequences” Earthquake Eng. Struct. Dyn., 2007, 36, 405–427.

MacRae G. A. (1994). “P-delta effects on single-degree-of-freedom structures in earthquakes”, Earthquake Spectra, 1994, 10(3), 539–568.

MacRae G.A. “The Continuous Column Concept - Development and Use” Proc. 9th Pac. Conf. on Earthquake Eng., Building an Earthquake-Resilient Society, Auckland, New Zealand. 2011.

MacRae G. A. and Clifton G. C. “Low Damage Steel Construction”, Steel Innovations Conference, Steel Construction New Zealand, Christchurch. 2013.

MacRae G. A., Clifton, G. C., Bruneau, M., Kanvinde, A., and Gardiner, S. “Lessons from steel structures in Christchurch earthquake”, 8th Int. Conf. on Behav. Steel Struc. in Seismic Areas, Shanghai, China. 2015.

MacRae G. A. and Kawashima, K. “The seismic response of bilinear oscillators using Japanese earthquake records.” J. Res. Public Works Res. Inst., Ministry of Construction, Tsukuba, Japan.1993.

MacRae G. A., Kimura, Y. and Roeder, C. W. “Effect of column stiffness on braces frame seismic behavior.” J. Struct. Eng., American Society of Civil Engineers, 2004, 130 (3): 381-391.

Masuno T., MacRae G.A., Sadashiva V.K. and Wada A. “Response of Out-of-Plumb Structures in Earthquake.” Proc. 9th Pac. Conf. on Earthquake Eng., Building an Earthquake-Resilient Society, Auckland, New Zealand. 2011.

NZS 1170.5. “Structural Design Actions Part 5: Earthquake actions New Zealand”, Standards New Zealand, Wellington, New Zealand. 2004.

Rad A. A., MacRae G., Bull, D. and Yeow T. “Seismic Behavior of Steel Buildings with Initial Out-of-Plumb.” Earthquake Eng. Struct. Dyn., 2015, 44 (14), 2575-2588

Ruiz-García J. “Mainshock-Aftershock Ground Motion Features and Their Influence in Building's Seismic Response.” J. Earthquake Eng., 2012, 16, 719-737.

Ruiz-García J. and Aguilar J. D. “Aftershock seismic assessment taking into account post mainshock residual drifts.” Earthquake Eng. Struct. Dyn., 2015, 44:1391–1407.

Ruiz-García J. and Negrete-Manriquez J. “Evaluation of drift demands in existing steel frames under as-recorded far-field and near-fault mainshock–aftershock seismic sequences.” Eng. Struct., 2011, 33, 621–634.

Sadashiva VK, MacRae GA, Deam BL. “Determination of structural irregularity limits – mass irregularity example.” Bull. N. Z. Soc. Earthquake Eng., 2009, 42(4): 288–301.

Tagawa H. “Towards an understanding of seismic response of 3D structures-stability & reliability.” Doctoral Thesis, University of Washington, Seattle. 2005.

Tagawa H., MacRae G.A. and Lowes L. “Continuous column effects of gravity columns in U.S. steel moment-resisting frame structures- continuous column effects in steel moment frames in perspective of dynamic stability.” (Part 2), J. Struct. Constr. Eng., Trans. Arch. Inst. Jpn., 2010, AIJ, 75(650): 761-770.

The MathWork (2008). Inc., Matlab R2008a.

Wilson N. and Bradley B. “Cumulative ground motion effects on structures in the Canterbury earthquake sequence.” undergraduate report, University of Canterbury. 2012.

Yeow T. Z., MacRae G. A., Sadashiva V. K., and Kawashima K. “Dynamic Stability and Design of C-Bent Columns.” J. Earthquake Eng., 2013, 17:5,750-768.

Chapter 4: Seismic Response of Elastic Single Story Structures with Unbalanced Stiffness

4.1. Introduction

Most structures built around the world have approximately the same stiffness in both forward and backward horizontal loading directions. However, some structures may have different stiffnesses and this means that the response from earthquake shaking in one direction will not be the mirror image of that from shaking in the other direction. Different stiffnesses/strengths in opposite horizontal directions can cause progressive yielding and displacements in one direction. This is sometimes termed ratchetting (e.g. MacRae 1994, Yeow 2014, Rad et al. 2015) and the displacement demands may become significantly larger than for structures without a ratchetting tendency. Some seismic standards (e.g. NZS3404:2007, NZS1170.5:2016) have limitations on the permissible stiffness or strength difference to limit ratcheting. Nevertheless, many older structures, as well as newer structures in countries which do not have such provisions, may have stiffness/strength differences. Examples of structures with a ratcheting tendency include: single T-shaped reinforced concrete walls which are stiffer/stronger with the flange in tension than in compression. If such walls are not placed in a balanced manner around the structure, the lateral stiffness and strength of the structure will be higher in one direction than the other, structures with slender bracing elements which are not placed in a balanced configuration around the structure. These will have a greater stiffness/strength in the brace tension direction

than the opposite direction, and structures where gravity forces, which cannot be redistributed out, cause an overturning moment in one direction that is not balanced by appropriately by increasing the strength in that direction. The gravity overturning forces increase the lateral forces to cause the frames to yield in one direction, while decreasing the lateral forces to cause the frames to yield in the opposite direction. Such structures include some C-bent bridge columns where gravity loading is provided eccentric to the column, some T-bent bridge columns where the traffic is all on one side causing an overturning moment, and some structures on a lean. These may be on a lean due to initial design considerations, significant permanent displacements from earthquake shaking, or other reasons.

Currently there are no methods to estimate the displacement demands of such structures with different strength/stiffness in the different directions.

Based on the discussions above, it may be seen that there is a need to evaluate the likely seismic displacements of structures with different stiffness/strengths in opposite horizontal directions.

The scope of this chapter is to address this need for single-story elastic frame structures with different stiffnesses in opposite horizontal directions. In particular, answers are sought to the following questions for structures with different stiffnesses in the different horizontal directions:

1) What is the ratio of the displacements in each direction?

2) How can peak horizontal displacements be estimated?

3) Can simple methods be developed?

4.2. Literature Review

No studies are known to have specifically addressed the estimation of displacements of structures with different stiffnesses in opposite horizontal directions. The majority of methods used to estimate structural response displacements are for symmetric structures. They are based on an initial stiffness, or equivalent stiffness which is the same in both directions. Such methods are difficult to generalize to structures with different stiffnesses in opposite directions. However, one approach which may be relevant considers energy concepts which are described below.

Housner (1956) stated that the earthquake energy transmitted into a structure, termed the input energy E_I, is defined as Eq. 4-1. This input energy consists of the kinetic energy (E_k), the potential energy (E_p) (consists of the recoverable elastic strain energy and the irrecoverable hysteretic energy) and damping energy (E_ξ). Kinetic energy reflects the work of the inertia force; potential energy is the portion of the input energy stored in the structure, and damping energy is the work of the damping force.

$$E_I = E_k + E_p + E_\xi \tag{4-1}$$

McKevitte et al. (1980) computed the input energy and the hysteretic energy for SDOF and MDOF structures (three- and ten-story) subjected to four earthquake records (El Centro 1940, Taft 1952, Parkville 1956, and Pacoima Dam 1971). They concluded that the ratio of the maximum hysteretic energy to the maximum input energy for an MDOF structure can be estimated from an SDOF structure with the same fundamental period, yield strength, and damping.

Zahrah and Hall (1984) computed the input energy for eight earthquake records and they considered that ductility, damping and past-to-pre yield stiffness ratios have small effects on the input and hysteretic energies for a structure with bilinear behavior.

Akiyama (1985) computed the input energy for a five-story building with different structural properties and for an equivalent one-story building having the same fundamental period, total mass and yield strength using the S00E component of the 1940 El Centro record. He compared these two buildings and showed the total input energy transmitted to a five-story building is as much as the input energy transmitted to the equivalent one-story building, and consequently, it was concluded that input energy transmitted to one of them can be computed from the other. Akiyama (1985) also defined an energy spectrum based on the relationship between input energy and natural period of the system. He expressed input energy in terms of equivalent pseudo-velocity, V_E, which is defined in Eq.4- 2 where E_I is the input energy and M is the mass of the structure.

$$V_E = \sqrt{2E_I/M} \tag{4-2}$$

Akiyama (1985, 1988) suggested that a bilinear curve may be appropriate to provide the energy spectrum in terms of pseudo-velocity, V_E. For structures with low periods, T, V_E linearly increases with T and at higher T it becomes constant as shown in Figure 4-1. He also stated that the input energy spectrum obtained for elastically responding structures is also valid for inelastic systems with the total input energy in both cases being similar.

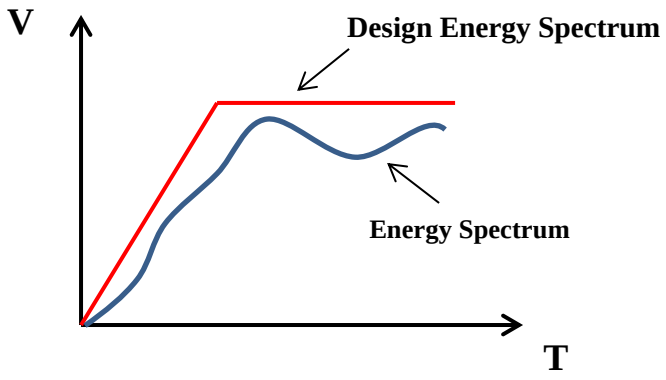

Figure 4-1: Energy Spectrum

Uang and Bertero (1990) showed that earthquake input energy may be obtained two ways; one based on the relative motion and the other on absolute motion. By multiplying $\dot{x}dt$ to both sides of the equation of motion of a damped SDOF system (Eq.4-3) and integrating, the ***relative energy balance equation*** is obtained as Eq.4- 4 where *m* is mass of the structure, *c* is the damping coefficient, f_s is the restoring force equal to *Kx*, *K* is equal to the structural lateral stiffness, *x* is the relative displacement of the mass with respect to ground, $\ddot{x}_g$ is the ground acceleration and *t* is time.

$$-m\,\ddot{x}_g = m\,\ddot{x} + f_s(=kx) + c\dot{x} \tag{4-3}$$

$$-\int_0^t m\,\ddot{x}_g\,\dot{x}\,dt = \int_0^t m\,\ddot{x}\,\dot{x}\,dt + \int_0^t f_s(=kx)\,\dot{x}\,dt + \int_0^t c\,\dot{x}^2\,dt \tag{4-4}$$

The left-hand-side term in equation (4) is the relative input energy E_I; the first term on the right-hand side of the above equation is the 'relative' kinetic energy E_k; the second term is the potential energy E_p; and the third term is the damping energy E_ξ.

To calculate the results of the above integrations for 'relative' kinetic energy, E_k, and potential energy, E_p, partial integration method ($\int uv' = uv - \int u'v$) was applied where for E_k, $u = \dot{x}$, $v' = \ddot{x}$, $u' = \ddot{x}$, $v = \dot{x}$ and for E_p, $u = x$, $v' = \dot{x}$, $u' = \dot{x}$, $v = x$. Therefore:

$$E_k = \int_0^t m\,\ddot{x}\,\dot{x}\,dt = {m(\dot{x})^2}/{2} \tag{4-5}$$

$$Ep = \int_0^t kx\,\dot{x}\,dt = {kx^2}/{2} \tag{4-6}$$

The *absolute energy balance equation* is given by Eq.4- 7. This is done by replacing x by x_t in the left hand side term of the Eq.4- 4 and the first term in the right-hand side of the Eq.4- 4 where x_t is the absolute displacement of the mass ($x_t = x + x_g$).

$$-\int_0^t m\,\ddot{x}_g\,(\dot{x}_t - \dot{x}_g)dt = \int_0^t m\,(\ddot{x}_t - \ddot{x}_g)(\dot{x}_t - \dot{x}_g)dt +$$

$$\int_0^t f_s(=kx)\,\dot{x}\,dt + \int_0^t c\,\dot{x}^2\,dt \tag{4-7-a}$$

$$-\int_0^t m\,\ddot{x}_t\,\dot{x}_g\,dt = \int_0^t m\,\ddot{x}_t\,\dot{x}_t\,dt + \int_0^t f_s(=kx)\,\dot{x}\,dt + \int_0^t c\,\dot{x}^2\,dt \tag{4-7-b}$$

The left-hand-side term in Equation 7 is the absolute input energy E'_I; the first term in the right-hand side of the above equation is the 'absolute' kinetic energy E'_k. Here, the second and third terms on the right side of the equation - the potential and damping energies - remain unchanged, but the first term on the left side of the equation (kinetic energy) and a term in left side of the equation (input

energy) change. Based on partial integration method, the absolute kinetic energy, E'_k, can be written as:

$$E'_k = \int_0^t m\,\ddot{x}_t\,\dot{x}_t\,dt = {m(\dot{x}_t)^2}/{2} \qquad (4\text{-}8)$$

Uang and Bertero (1990) noticed a difference in the magnitude of relative and absolute input energies, E_k and E'_k, for the very short and long period structures. For long period structures the mass of the structure almost does not move. Therefore, the absolute input energy, E'_I, for the relatively long period structure should be low.

Chopra (1995) and Bruneau and Wang (1996) state that the relative motion input energy, E_I, is more meaningful than the absolute motion input energy, E'_I, since internal forces and damage within a structure are related to relative displacements and velocities. Bruneau and Wang (1996) also indicated that damping ratios smaller than 5% have a minor influence on input energy, E'_I.

Nakashima et al. (1996) investigated the effect of damping ratios and large post elastic stiffness ratios (up to 0.75) for bilinear SDOF and MDOF structures. They concluded that in general, damping and large post elastic stiffness ratios have a minor effect on the input energy.

Rahnama and Manuel (1996) studied the effect of duration of ground motions on the input and hysteretic energy. They concluded that as the duration increases, the input and hysteretic energies increase. However, the duration did not influence the ratio of cumulative hysteretic energy to input energy.

Goel (1997) investigated the distribution of energy in asymmetric structures. He concluded that the input energy transmitted to a symmetric or to an asymmetric one-story building is approximately the same.

Decanini and Mollaioli (1998) proposed a three part curve for an elastic input energy spectra that in low and middle periods parts (two initial parts) are similar to the Akiyama curve (Akiyama 1985). However, at higher periods this curve is not constant and decreases. Decanini and Mollaioli (2001) also developed design inelastic energy spectra as a function of ductility, soil type, source-to-site distance and magnitude considering a large set of strong motion records.

Khashaee et al. (2003) studied the effects of the viscous damping of structure on input energy. They observed that for damping ratios smaller than 5%, it has little influence on input energy, but for damping ratios greater than 5%, there is a significant influence on input energy spectra.

Yeow et al. (2014) performed dynamic 2D shaking table tests of sliding components being obstructed in one direction and unobstructed. The obstructed components had a very high (almost infinite) stiffness in the negative direction. These tests indicated that obstructed sliding displacements were approximately 3 times that for the unobstructed sliding tests. However, the experimental work clearly showed impact where there was loss of energy. That tends to decrease displacements.

4.3. Modelling and Evaluation Approach

In this study, an elastic single story frame structure is considered for analysis as shown in Figure 4-2. The structure has a floor mass, *m*, of 20 Tons, floor height, *h*, of 3m and bay width, *L*, of 6m. Structures with periods ranging from 0.5 to 5s are considered. Here, column bases are modelled as pinned, and column stiffnesses are assumed constant for all period ranges. Column moments of inertia, I_c, are 0.000388m^4 each. Since the columns are stiff, changing of the period of the structure is controlled by the beam second moment of area, I_b. The story stiffness is calculated as $\frac{12EI_b}{Lh^2}$ (Sadashiva, 2010) where E is elastic modulus of steel. To provide the unbalanced stiffness structures, an "elastic compression-only" brace was added to the structure to increase stiffness in the negative displacement direction up to 100 times that in the opposite direction. The addition of such a brace to a frame with an initial negative displacement from a previous earthquake event may be provided to limit further frame negative displacements. However, as this study relates to the fundamental behaviour of different stiffness in different directions alone, no initial permanent displacement is considered here.

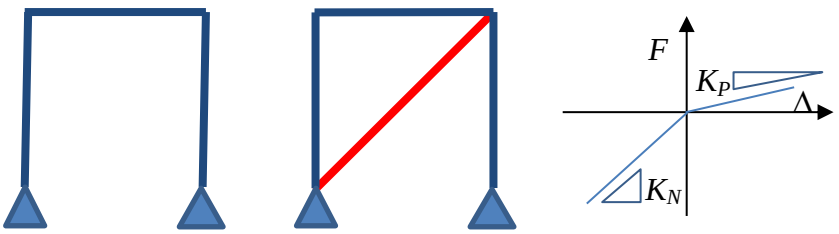

(a) Frame Building (b) Building with compression-only braces (c) Unbalanced hysteresis loop

Figure 4-2: Structure Models

The SAC (SEAOC-ATC- CUREE, 2000) suite of 20 earthquake ground motion records for Los Angeles, with a probability of exceedance of 10% in 50 years, was used. To eliminate the directionality effects from the ground motion records, the analysis was repeated by applying the same ground motion in the opposite direction. All earthquake ground motions have a scale factor of 1.0. The median spectral displacement of the records with a scale factor of unity is consistent with NZS1170.5 (2004) for Soil Type C as shown in Figure 3.

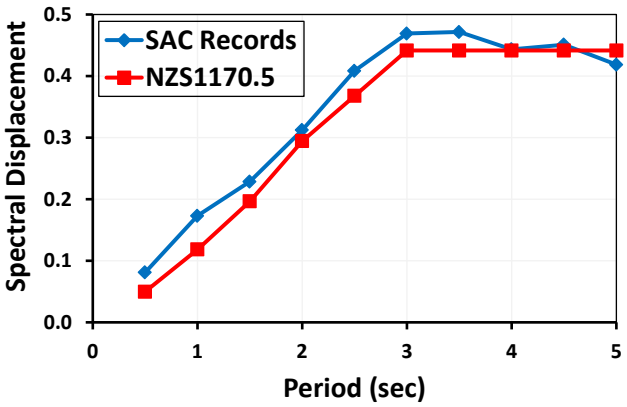

Figure 4-3: NZ Standard and SAC La10in50 Record Average Spectral Displacement (5% damping, Z=0.4, Soil C, S_p=1.0)

Elastic dynamic time history analysis was performed using OpenSees (2015). MATLAB (2008) was used to extract the peak positive and negative displacements (*PPD* and *PND*), peak forces in positive and negative directions (*PPF* and *PNF*), and response quantities to calculate the kinetic and potential energies. For the unbalanced structure model used in this study, the more flexible direction is associated with positive displacements and the stiffer direction with negative displacements. Analysis was conducted considering 0% and 5% damping. These damping ratios were specified as being a proportion of the

positive (more flexible) stiffness. The hysteresis loops were considered to already consider P-delta effects which were not explicitly considered.

The potential energies in the negative (PE_P) and positive (PE_N) directions were calculated based on Eq.4- 6 using Eq.4- 9 and 10 where K_P is the stiffness of the positive side, K_N is the stiffness of the negative side, Δ_p is the relative displacement response in positive direction and Δ_n is the relative displacement response in negative direction.

$$PE_P = K_p \Delta_p^2/2 \tag{4-9}$$

$$PE_N = K_n \Delta_n^2/2 \tag{4-10}$$

An empirical distribution function (EDF) of the potential energy in positive and negative direction for all 40 records were calculated based on Equation 11 where $x_{(1)}, \dots, x_{(n)}$ is the sample (potential energy) ordered from the smallest to the largest and n is the total number of the sample (= 40).

$$EDF_n(x) = \begin{cases} \frac{1}{n}, & x_{(1)} \le x < x_{(2)} \\ \frac{2}{n}, & x_{(2)} \le x < x_{(3)} \\ \vdots & \\ \frac{n-1}{n} & x_{(n-1)} \le x < x_{(n)} \\ 1, & x \ge n \end{cases} \tag{4-11}$$

A normalized *PPD, NPPD*, describing the effect of stiffness imbalance on the positive displacements, is computed as the peak positive displacement, *PPD*, obtained for a structure with unbalanced stiffness (PPD_{UBS}) divided by the *PPD* obtained from the structure with balanced stiffness (PPD_{BS}) for each record and direction.

$$NPPD = \frac{[PPD_{UBS}]}{[PPD_{BS}]} \quad (4\text{-}12)$$

Also, the ratio of positive-to-negative displacement, known as the positive-negative ratio (*PNR*), is computed as PPD_{UBS} of unbalanced stiffness structures was divided by PND_{UBS} for each record:

$$PNR = \frac{[PPD_{UBS}]}{[PND_{UBS}]} \quad (13)$$

The median absolute values of *NPND* and *PNR* were obtained for all records and directions.

The stiffness ratio, K_{ratio}, is defined as the ratio of stiffness in stiffer (negative) direction, K_N, to that in the positive direction, K_P, where these terms are shown in Figure 2c.

4.4. Seismic Energy Response

4.4.1. Structures with Balanced Stiffness

Absolute kinetic energy, E_k, relative kinetic energy, E'_k, and relative potential energy, E_p, of the structures under a suite of records were calculated at each time step according to Eqs. 8, 5 and 6. Figure 4-4 shows these versus time for an elastic structure with a period, *T*, of 1s and damping ratio of 0% under the Imperial Valley (El Centro, 1940) record. It may be seen that the peak E'_k and E_k differ by less than 25%, but have the same approximate shape. Also the shape of E_p is similar. Once the ground stops shaking, $\ddot{x}_g = \dot{x}_g = 0$ so $E'_I = E_I$ which is

constant and does not change with time in Equations 8 and 5. It is the energy that is within the system. Since there is no energy dissipation $E_\xi = 0$ so there is no energy leaving or entering the system. This means that $E'_k = E_k$ and $E_p = E'_I - E'_k$ according to Equation 4. That is, the potential energy, E_p, is out-of-phase with the kinetic energy ($E'_k = E_k$) but it has the same magnitude. The potential energy is maximum at peak displacement when $E'_k = E_k = 0$. Similarly, the kinetic energy is maximum at maximum velocity which occurs at zero displacement as shown in Figure 4.

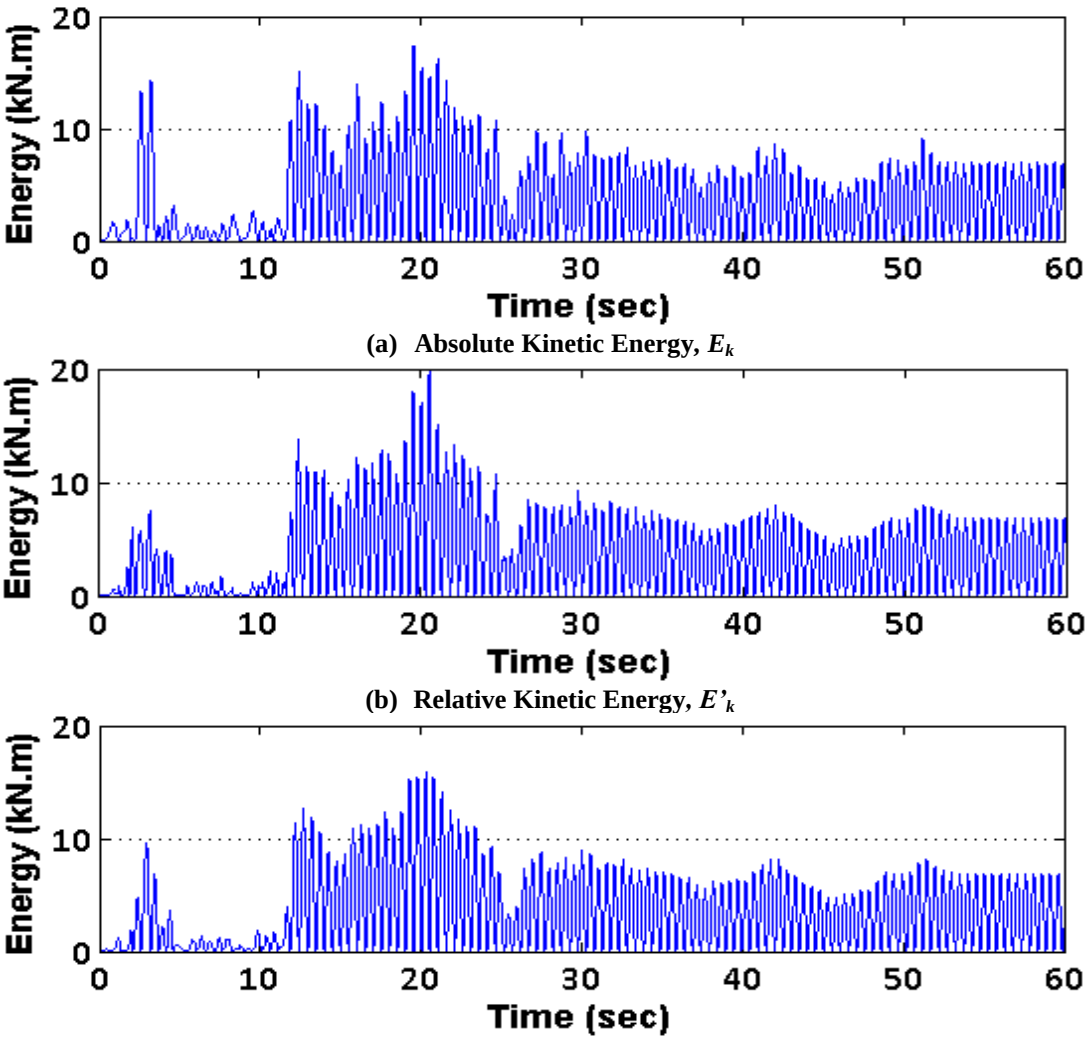

(a) Absolute Kinetic Energy, E_k

(b) Relative Kinetic Energy, E'_k

(c) Relative Potential Energy, E_p

Figure 4-4: Energy time history of the elastic structure (T=1s, Damping=0) under Imperial Valley (El-Centro, 1940, NS) record

Figure 4-5 shows the median absolute and relative kinetic energy and potential energy spectra of elastic structures considering 0% and 5% damping for various periods using the 20 SAC La10in50 records. Note that values obtained are the same irrespective of whether the record is applied in the forward or backward direction. It shows that absolute and relative kinetic energies E_k and E'_k are similar near a period of about 2s, but the absolute kinetic energy, E_k, is higher for shorter periods, and E'_k is higher for longer periods. This is consistent with Uang and Bertero (1990). Also, it can be seen that E_k, E'_k and E_p spectra decreases in higher periods and matches with Decanini and Mollaioli (1998) study. Moreover, the kinetic and potential energies at 5% damping levels are about 50% of that at 0% damping. A decrease in potential energy of 50% is consistent with a change in displacement of $\sqrt{0.5} = 0.707$ based on Eq. 4-6.

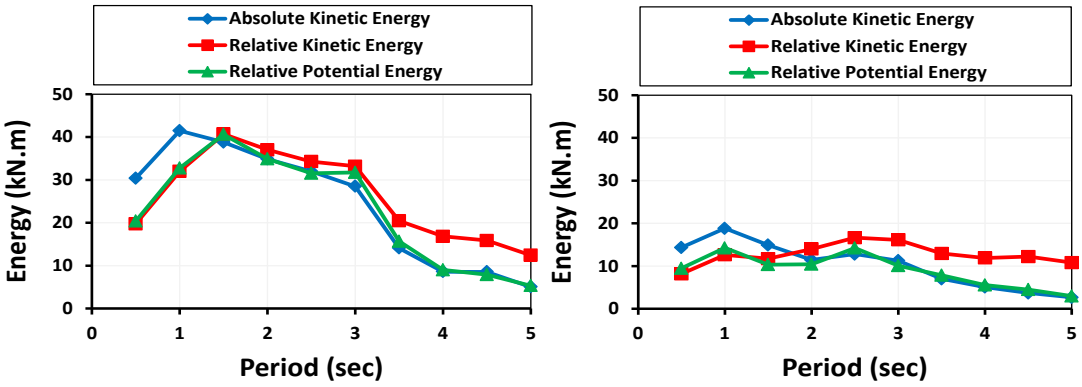

(a) 0% damping (b) 5% damping

Figure 4-5: Spectral energy of elastic structures with balanced stiffness using the 40 SAC La10in50 records (both directions).

Since the relative potential energy is related to the relative displacement and this energy remains unchanged for both absolute and relative methods of Uang and Bertero (1990), a procedure based on relative potential energy is used for the rest

of the study. Here, the relative potential energy in the positive and negative sides is calculated to quantify the effect of stiffness in displacement of both directions. Figure 4-6 shows the median spectral relative potential energy of the structures with the same stiffness in positive and negative sides using the 20 SAC La10in50 records. The potential energies in the positive and negative sides are identical because the ground motion records were applied in both directions. If the records were applied in one direction, the displacement would likely be different in each side, and the potential energies similarly different.

It can also be seen that the potential energies in Figure 4-6 and Figure 4-5 are not identical. For example, the potential energy for T=3s is 31kN.m in Figure 4-6a. this is slightly less than the value of 33kN.m in Figure 4-5a. This is because, in Figure 4-5, the maximum absolute response (ignoring directionality) was considered for the 40 records and the median was obtained. In Figure 4-6 the maximum response at each side (positive or negative) was considered and the median was obtained for the 40 records. It may be seen that in Figure 4-6 the median in positive and negative sides are identical. However, they are about 6% lower than that for the median of the peak absolute responses in Figure 4-5a, since for individual records the response in one direction was bigger than that in the other direction.

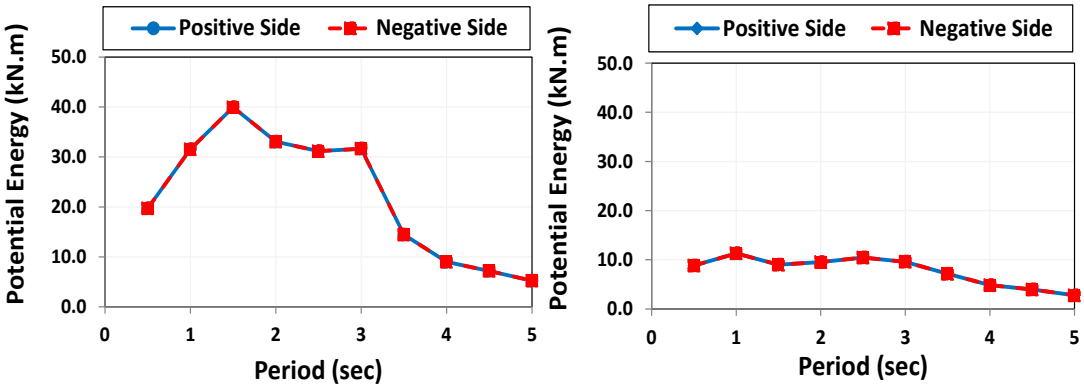

(a) 0% damping (b) 5% damping

Figure 4-6: Potential spectral energy of elastic structures with balanced stiffness in positive and negative sides using the 40 SAC La10in50 records applied in both directions.

4.4.2. Structures with Unbalanced Stiffness

While Figure 6 indicates that elastic structures have about the same displacement in each direction, which results in the same potential energy in each direction, there is no reason to expect that for an oscillator with different stiffnesses in each direction, that the displacements in the different directions would be the same. In fact they are not. However, the energy in both directions may be similar. This is investigated in Figure 4-7 which compares the empirical distribution function (EDF) of the potential energy in the stiffer and more flexible sides of unbalanced stiffness structures with K_{ratio} of 2 and 5. The initial period is 1.0s and the 20 SAC La10in20 records were used in both directions with 0% and 5% damping. Figure 4-7 is shown that the potential energy in stiffer and more flexible sides of this structure with unbalanced stiffness is similar for all 40 records. Figure 4-8 also shows the median spectral potential energy of the structures under 40 records with different K_{ratio} are approximately equal.

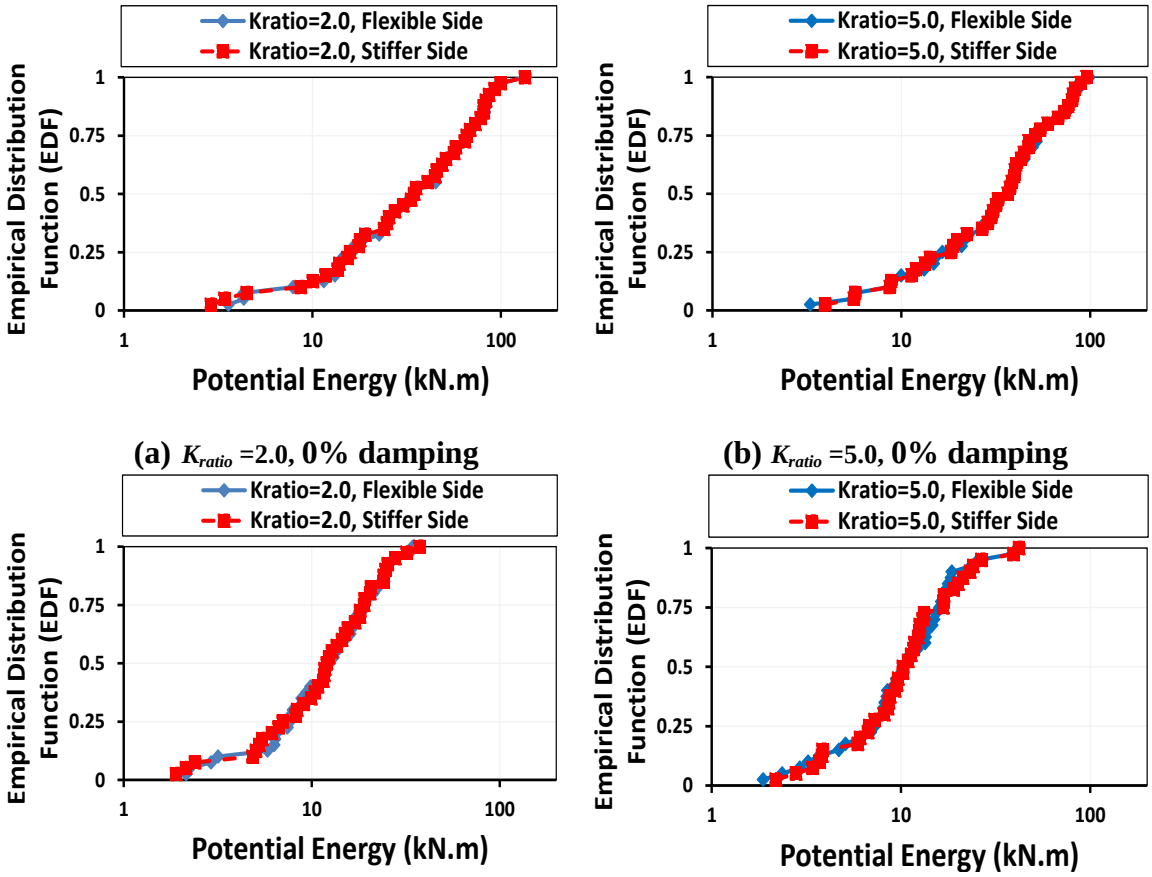

(a) K_{ratio} **=2.0, 0% damping** **(b)** K_{ratio} **=5.0, 0% damping**

(c) K_{ratio} **=2.0, 5% damping** **(d)** K_{ratio} **=5.0, 5% damping**

Figure 4-7: EDF of the potential energy for structure with K_{ratio} of 6 and initial T of 1.0s using the 40 SAC La10in50 records (both directions).

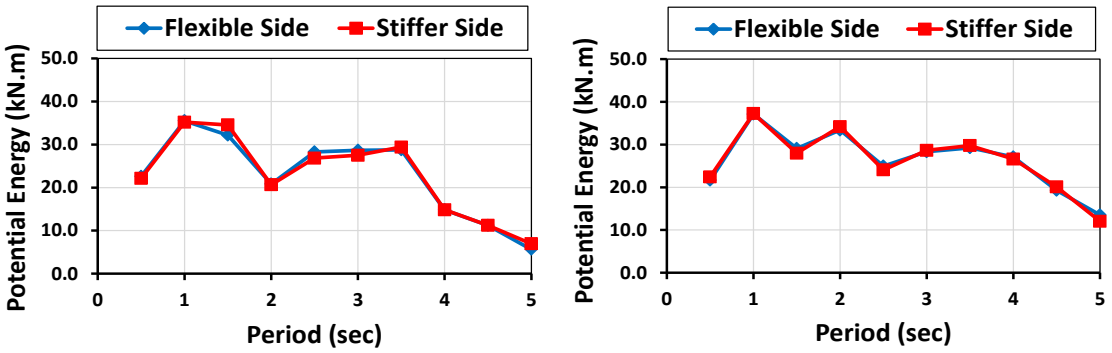

(a) K_{ratio} **= 2.0, 0% damping** **(b)** K_{ratio}**= 5.0, 0% damping**

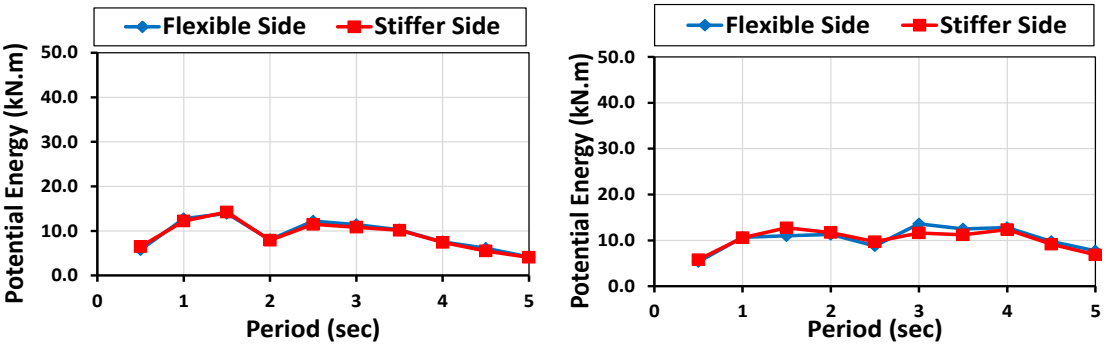

(c) K_{ratio} = 2.0, 5% damping **(d) K_{ratio} = 5.0, 5% damping**

Figure 4-8: Median spectral potential energy of the structures with different initial periods and K_{ratio} in positive and negative directions using the 40 SAC La10in50 records (both directions).

Figure 4-9 shows the roof displacement time history response of the unbalanced stiffness structure with period of 1.0s under Imperial Valley (El Centro, 1940) ground motion record (SAC, la01). It shows that by increasing the stiffness of the structure on the compression side by 5 times, the displacement in this direction decreased. However, although the displacement of the stiffer side is decreased, since the stiffness of that side is also increased. The peak potential energy in both directions remains similar.

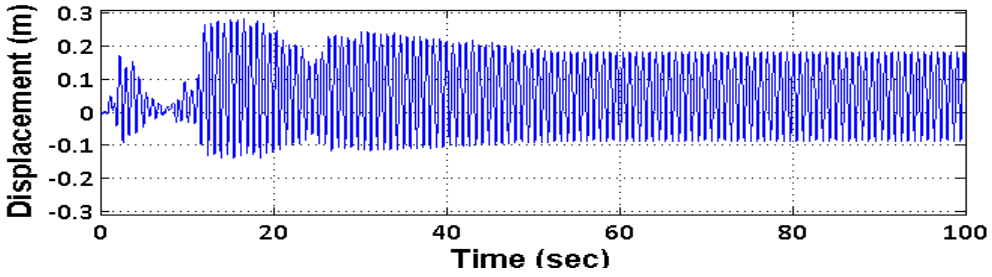

Figure 4-9: Time history roof displacement response of the unbalanced stiffness structure (K_{ratio} =5) with initial period of 1s under la01 from SAC record (Imperial Valley, El-Centro, 1940), Damping=0%.

Figure 4-10 also shows the hysteresis loop of the structure with unbalanced stiffness ratio of 6 under the Imperial Valley (El Centro, 1940) ground motion

record. It shows that displacement of the structure in the stiffer direction is less than in the more flexible one. Also, the base shear in stiffer direction is larger than in the other. Therefore, the potential energies in the negative (stiffer) and positive (flexible) directions, which equal the area under the hysteresis loop ($A_p \approx$ 0.285m*220kN/2=31, $A_n \approx$ 0.14m*460kN/2=32kNm) are approximately equal.

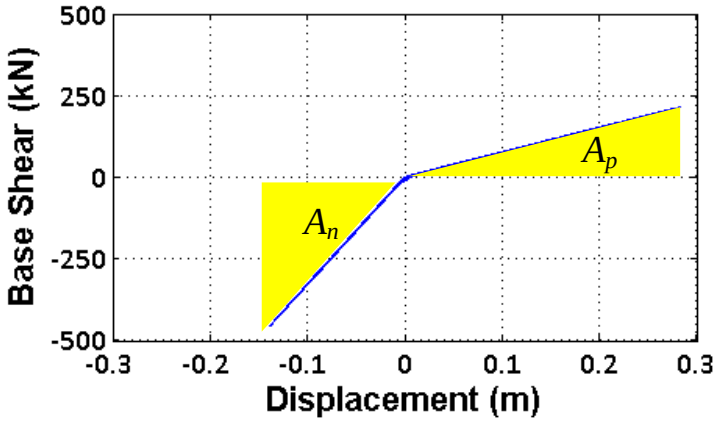

Figure 4-10: Hysteresis loop of the structure with unbalanced stiffness (K_{ratio} =5.0) and initial period of 1s under la01 from SAC record (Imperial Valley, El-Centro, 1940), Damping=0%.

4.5. Seismic Displacement Response

The median peak negative and positive displacement (PND & PPD) defined earlier is given in Figure 4-11 considering 5% damping and different stiffness ratios (K_{ratio}) for structures with different initial periods. These initial periods, T_i, are the same in each direction of displacement for the linear structure when K_{ratio} = 1. For different K_{ratio}, T_i is equal to the period in the positive direction, T_p (i.e. T_i = T_p). The period in the negative direction, T_n, changes with K_{ratio}. Figure 4-11 indicates that:

1) The *PND* and *PPD* for K_{ratio} of 1 have identical magnitude because the ground motions are applied in both directions. They are equal to the spectral displacement of the structure. *PPD*, and hence spectral displacement, S_d, increase linearly until a period in the positive direction of 3s. Then they become almost constant at greater initial periods, T_i.

2) By increasing the stiffness in the negative direction, and hence K_{ratio}, the displacement in the negative direction (i.e. median *PND*) generally decreased.

    a. For small K_{ratio} (such as K_{ratio} = 2) the *PND* has the same trend as the balanced stiffness structures (i.e. K_{ratio} =1) and S_d. The absolute value of *PND* first increases linearly up until an initial period, T_i, of 3s, then it stops increasing and slightly decreases.

    b. For high K_{ratio}, the absolute value of *PND* increases linearly up to the maximum initial period, T_i, plotted of 5s.

    c. The different trends of *PND* with K_{ratio} can be explained using the spectral displacement as follows:

        i. For low K_{ratio} and high T_i, S_d is in the constant spectral displacement region; therefore, the trend of those is similar to the balanced stiffness structures.

        ii. For high T_i and K_{ratio}, the period of the structure in the negative direction, T_n, is less than 3s. For linear structures with periods,

T, in this range, S_d tends to increase linearly with T as seen here and as shown in Figure 4-3.

iii. For high T_i and intermediate K_{ratio}, the response seems to be intermediate between the cases given above.

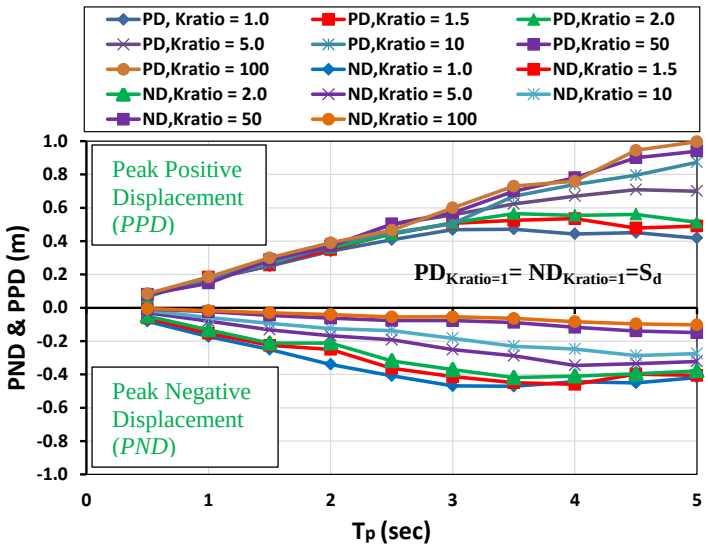

Figure 4-11: Effect of K_{ratio} and T_p on median peak positive and negative displacement (PPD and PND) response of the unbalanced stiffness structures (5% damping, 40 SAC Records-both directions).

Figure 4-12 illustrates the trends shown above by plotting the *PND* versus negative period, T_n. It shows that by increasing K_{ratio}, T_n and *PND* decrease. For low K_{ratio} and high T_i, T_n is more than 3s, so the trend of the *PND* is similar to S_d. For high T_i and K_{ratio}, T_n, is less than 3s, so *PND* tends to increase linearly with period. Figure 4-12 also compares spectral displacements (S_d) of the balanced stiffness structure with the peak negative displacements (*PND*) of the unbalanced stiffness structure. It the shows that the S_d can be used to estimate the peak displacements in the negative (or stiffer) direction although it is conservative at T_n values near 3s.

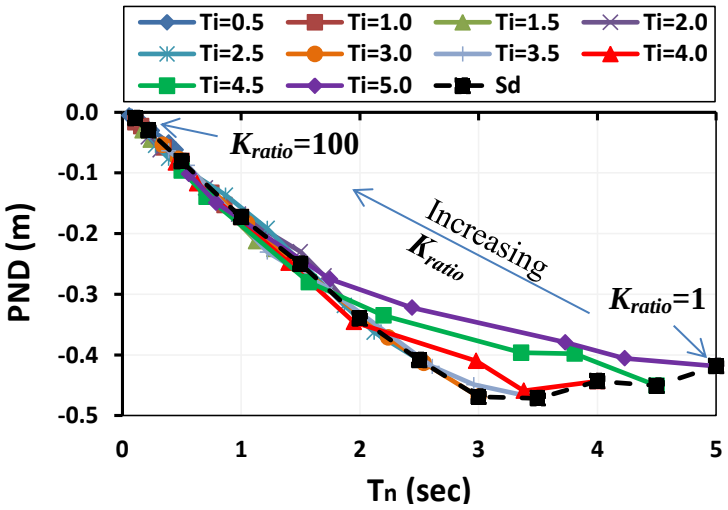

Figure 4-12: Effect of K_{ratio} and T_n on PND

3) The median displacement in the positive direction, PPD, is described below:

   a. For initial periods, T_i less than about 3s, the *PPD* generally increased with T_i. The increase is approximately linear with T_i and the *PPD* followed the S_d (i.e. K_{ratio}=1) response but was slightly greater for greater K_{ratio}. The amount is greater up to about 30% as shown in Figure 4-13. It shows that by increasing K_{ratio} the normalized *PPD*, *NPPD*, defined as the peak positive displacement of an unbalanced structure divided by that of a balanced structure, increases.

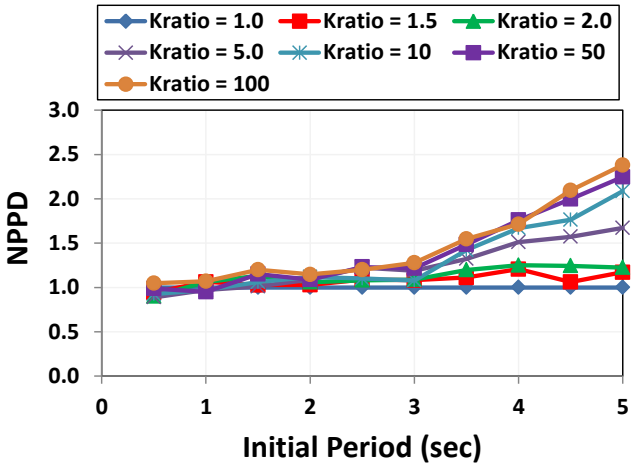

Figure 4-13: Effect of initial period and K_{ratio} on NPPD

b. For low K_{ratio} and T_i greater than 3s, S_d is approximately constant and the *PPD* followed the S_d trends.

c. For high K_{ratio} and T_i greater than 3s, *PPD* tends to increase linearly with T_i. Some possible reasons for this are:

   i. In this range of K_{ratio} and T_i, T_n is less than 3s which is in the linearly increasing region of S_d with T. Since S_d is linearly increasing here, so does *PPD*.

   ii. The absolute value of *PND* in this range tends to increase linearly with T_p. If it is assumed that the energy concept holds, where structures tend to have similar relative potential energies in the different directions, then it would be expected that the *PPD* would follow the linear trends of the *PND*.

   iii. By increasing initial period of the structure, the relative velocity response of the structure increases. Therefore, the peak relative

kinetic energy for the structures over this range increases. Because of this, when this energy is turned into potential energy, it will result in greater relative *PPDs*.

Figure **4-14** and Figure **4-15** illustrate the trends shown above for a single oscillator. It is shown that the displacement and velocity increase more for oscillators with T_i of 4.5s than for T_i of 1.0s due to greater K_{ratio}.

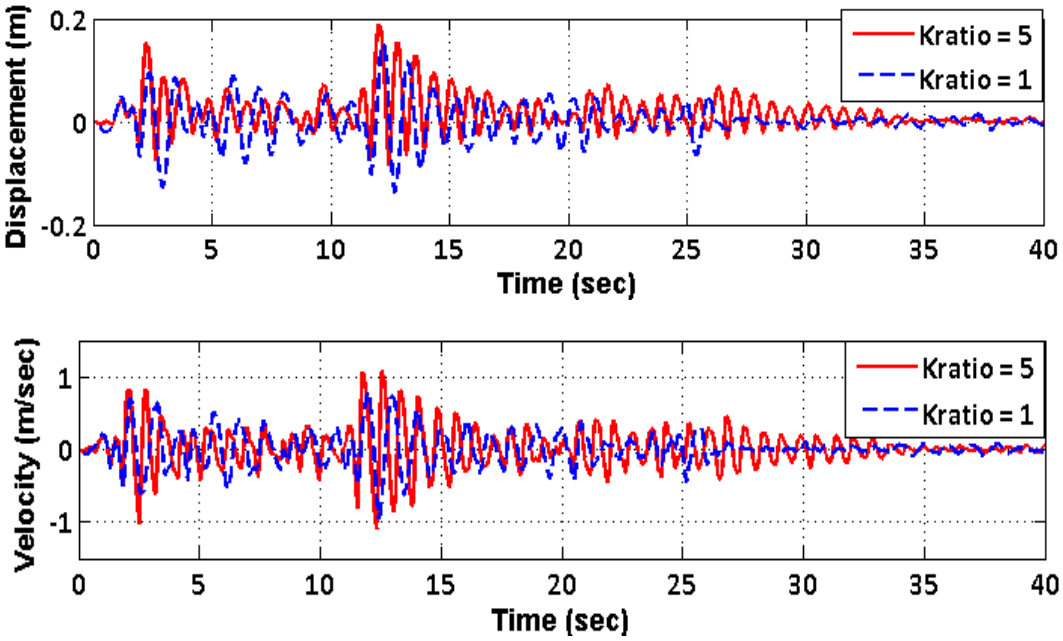

Figure 4-14: Time history response of the unbalanced stiffness structure (Kratio =5) with initial period of 1s under Imperial Valley (El-Centro, 1940) ground motion.

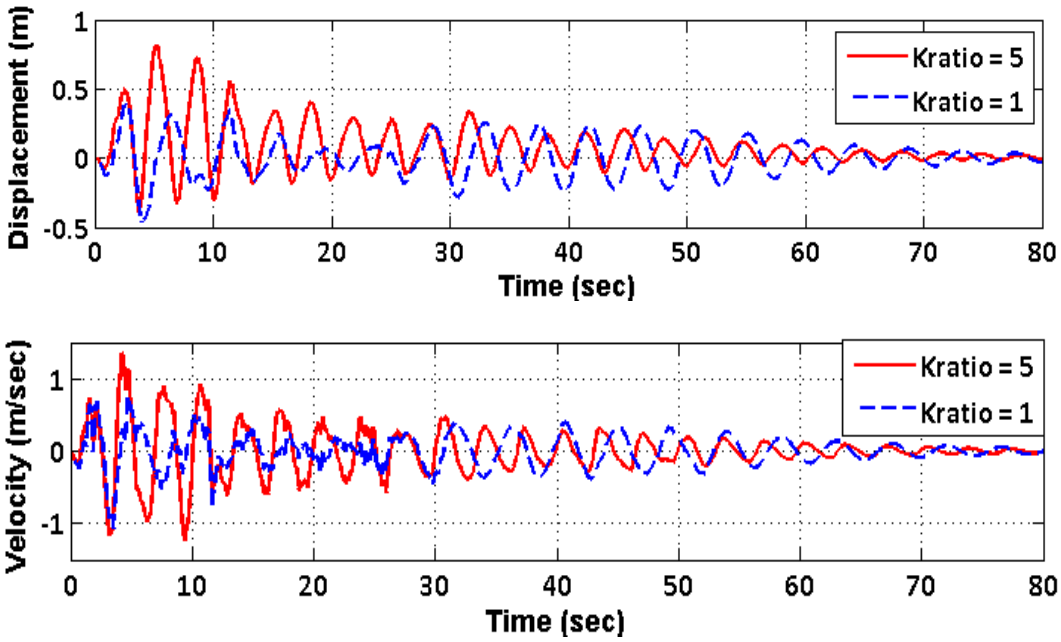

Figure 4-15: Time history response of the unbalanced stiffness structure (Kratio =5) with initial period of 4.5s under Imperial Valley (El-Centro, 1940) ground motion.

The range of displacement, *PPD-PND*, for T_i less than 3s tends to decrease with increasing K_{ratio} and period as shown in Figure 4-16 because the *PND* tends to decrease significantly with K_{ratio} while the *PPD* increases slightly with period. For T_i greater than 3s, as *PPD* increases more than decreasing of *PND*, the range of displacement increased.

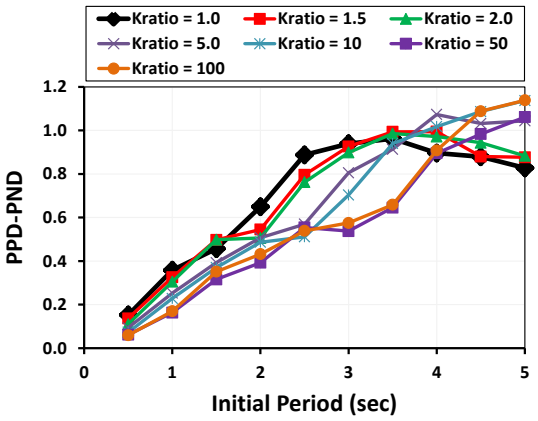

Figure 4-16: Effect of initial period and K_{ratio} on range of displacement (PPD-PND) using the 40 SAC La10in50 records (both directions).

Figure 4-17 shows that the median *PNR*, defined in Equation 13 as the peak positive displacement of an unbalanced structure (PPD_{UBS}) divided by the peak negative displacement of an unbalanced structure (PND_{UBS}), is independent of the period of the structures and it only changes with K_{ratio}. This can be explained based on the potential energy of the two sides of the structures which was explained in Section 4.2. As shown in Figure 4-7 and Figure 4-8 the potential energy in the positive (flexible) and negative (stiffer) directions are approximately equal. Therefore, based on Eqs.4- 9 and 10:

$$\text{Since } EP_p = EP_n, \qquad \Delta_p = \Delta_n \,.\, \sqrt{(K_n/K_p)} \tag{4-14}$$

where K_p is the stiffness of the positive side, K_n is the stiffness of the negative side, Δ_p is the displacement response of positive side and Δ_n is the displacement response of negative side. For example, based on Figure 4-17, the average *PNR* for K_{ratios}(=K_n/K_p) of 2, 5, 10, 100 is about 1.39, 2.2, 3.05 and 9.8 which is similar to the results of the Eq.4-14 which give 1.41, 2.23, 3.16 and 10 as shown on the beside the left hand axis of the figure.

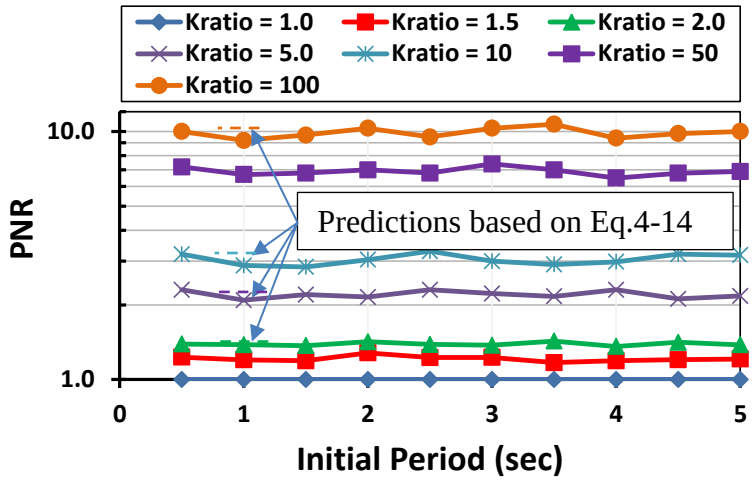

Figure 4-17: Effect of K_{ratio} and initial period of the unbalanced structures on median PNR with 5% damping using the 40 SAC La10in50 records (both directions).

4.6. Design Considerations

A simple prediction procedure for peak displacements in the negative (for the stiffer) and positive (for the more flexible) directions are developed here for elastic structures with unbalanced stiffness. Spectral displacements balanced stiffness structure can be predicted based on procedures in seismic design standards. As shown in Figure 4-12, the peak displacements in the negative (for the stiffer) direction can be estimated by spectral displacements (S_d) balanced stiffness structure. Therefore, the stiffer side displacement can be predicted. Moreover, using the independence of the median *PNR* on period and its dependence only on K_{ratio}, the more flexible side displacement of the structure can be estimated from the negative displacement using energy methods according to Eq. 4-14.

4.7. Design Application

The displacements of a structure with unbalanced stiffness are given in the following steps:

Step 1: The period of the stiffer side of the structure is obtained by $T_n = T_i/\sqrt{K_{ratio}}$.

Step 2: The peak negative (stiffer) direction displacement ($\Delta_{unbal,n}$ = *PND*) of the structures with unbalanced stiffness is obtained from design spectral displacement (S_d) from appropriate standard considering the period of the stiffer side, T_n.

Step 3: Compute the peak positive (more flexible side) displacement ($\Delta_{unbal,p}$ = *PPD*) of the structures with unbalanced stiffness from Eq.4- 14.

Example:

For a structure with an initial period, T_i, of 2.0s and stiffness ratio, K_{ratio}, of 2.0, the likely $\Delta_{unbal,p}$ and $\Delta_{unbal,n}$ displacements are calculated as:

Step 1: The period of the stiffer side of the structure is $T_n = 2s/\sqrt{2} = 1.43s$.

Step 2: By assuming the design spectra is given by NZS117.5 as shown in Figure 4-3, the peak negative displacement, *PND,* of the unbalanced stiffness structure with T_n of 1.43 is -0.25m.

Step 3: The peak positive displacement, *PPD,* from Eq.4-14 is +0.35m. Also, the displacement range is 0.35m - -0.25m = 0.6m.

4.8. Discussion

It has also been argued that in many cases strength may be proportional to stiffness (e.g. Priestley, et al., 2007). This may be stated that Δ_y (yield displacement) = F_y/k is constant. Therefore, a structure with a high ratio of peak force demand to stiffness (i.e. high F/k, or displacement demand Δ) will have a greater likelihood of yielding than one with a low $F/k = \Delta$. As shown in Figure 4-11, *PPD*($=\Delta_p$) is generally greater than *PND*($=\Delta_n$). Because of this, the chance of exceeding Δ_y is therefore greater in the positive direction than in the negative direction, indicating that yielding is more likely in the unstrengthened direction.

Moreover, Figure 4-17 shows that when *PNR* ($=\Delta_p/\Delta_n$) is equal to unity, there is a similar likelihood of yielding in each direction. It may be seen that the ratio is independent of period, and that it increases with increasing K_{ratio}. Increasing values of this ratio may be regarded as an indicator of the likelihood of yielding predominantly in the positive direction.

All of the discussion above is based on the premise that strength is proportional to stiffness, implying a constant yield displacement as per Priestley and Kowalsky (1998), Aschheim and Black (2000), and Priestley, et al., 2007 is true only in the cases when this premise holds.

4.9. Conclusion

Time history analyses were conducted of elastic single story structures with unbalanced stiffness ratios ranging from 1.0 to 100, initial flexible direction periods, ranging from 0.5 to 5s and considering 0 and 5% damping. The main findings are the following:

1) The average potential energy of the stiffer and more flexible sides of the structures with unbalanced stiffness from time history analyses with records applied in different directions was found to be similar for all period ranges with both 0% and 5% damping. This allows the likely peak displacement in one direction to be predicted if the peak displacement in the other direction is known.

2) The median peak negative (stiffer) direction displacement (*PND*) of the unbalanced stiffness structures decreased with increasing stiffness ratio (K_{ratio}). The median displacement in the positive direction, *PPD*, generally increased with initial periods (T_i). It was shown that the peak displacements in the flexible direction were generally larger than the spectral displacements associated with the period in the flexible direction. However, the peak displacements in the stiffer direction were similar to, and sometimes less than, the spectral displacements associated with the period in the stiffer direction.

3) A step-by-step methodology to obtain the displacements in negative (stiff) and positive (more flexible) directions of simple single story elastic structures is developed using (i) the spectral displacement in the stiff

direction, and (ii) the energy relationship between the displacements in each direction. A design example was also provided. In yielding structures where stiffness is proportional to strength, it is shown that yielding is more likely in the flexible direction indicating that placing devices in a structure to increase the stiffness and strength is likely to effectively mitigate the possibility of increased displacements in a direction where they are not desired.

4.10. References

Akiyama H. Earthquake-resistant limit-state design for buildings. the University of Tokyo Press, Tokyo, Japan, 1985.

Akiyama H. Earthquake-resistant design based on the energy concept. Proc. of the 9th World Conference on Earthquake Engineering, Tokyo-Kyoto, Japan, 1988.

Aschheim MA, Black EF. Yield point spectra for seismic design and rehabilitation. Earthquake Spectra, EERI; 2000, 16(2): 317–35.

Bruneau M. and Wang N. Some aspects of energy methods for the inelastic seismic response of ductile SDOF structures. Eng. Struc., 1996, 18(1), pp. 1-12.

Chopra A. Dynamics of structures: Theory and applications to earthquake engineering. Perntice Hall, 1995.

Decanini LD, Mollaioli F. Formulation of elastic earthquake input energy spectra. Earthquake Engineering and Structural Dynamics, 1998, 27, pp. 1503-22.

Decanini LD, Mollaioli F. An energy-based methodology for the assessment of seismic demand. Soil Dynamics and Earthquake Engineering, 2001, 21, pp. 113-137.

Goel, R. Seismic Response of Asymmetric Systems: Energy-Based Approach. J.

Housner G.W. Limit design of structures to resist earthquakes. Proc. of the 1st World Conference on Earthquake Engineering, California, USA, 1956, 5, pp. 5-1 to 5-13.

MacRae GA. P-Δ effects on single-degree-of-freedom structures in earthquakes. Journal of Earthquake Spectra 1994; 10(3):539–568.

NZS3404. Steel Structures Standard. Standards New Zealand: Wellington, New Zealand, 2007.

McKevitt W. E., Anderson D.L., and Cherry S. Hysteretic energy spectra in seismic design. Proc. of the 2nd World Conference on Earthquake Engineering, 1980, Vol. 7, pp. 487-494.

Nakashima M., Saburi K., and Tsuji B. Energy input and dissipation behaviour of structures with hysteretic dampers. Earthquake Eng. & Struct. Dyn., 1996, 19(1), pp. 77-90.

NZS 1170.5. Structural Design Actions Part 5: Earthquake Actions New Zealand. Standards New Zealand: Wellington, New Zealand, 2016.

Priestley M.J.N., Calvi G.M., Kowalsky M.J. Direct displacement-based seismic design of structures. NZSEE conference, 2007.

Priestley MJN, Kowalsky MJ. Aspects of drift and ductility capacity of rectangular cantilever structural walls. Bulletin of the New Zealand National Society for Earthquake Engineering, NZNSEE, 1998, 31(2): 73–85.

Rad A. A., MacRae G. A., Yeow T. Z. and Bull D. K. Seismic behavior of steel buildings with out-of-plumb. Earthquake Engineering & Structural Dynamics 2015; DOI: 10.1002/eqe.2598.

Rahnama M. and Manuel L. The effect of strong motion duration on seismic demands. Proc. of the 11th World Conference on Earthquake Engineering, Mexico, 1996, paper No. 924.

Struct. Eng. ASCE), 1997, 123:11, 1444-1453.

Uang C.-M., Bertero V. V. Evaluation of seismic energy in structures. Earthquake Eng. & Struct. Dyn, 1990, 19(1), pp. 77-90.

Yeow TZ, MacRae GA, Sadashiva VK, Kawashima K. Dynamic stability and design of C-bent columns. Journal of Earthquake Engineering 2013; 17:5,750–768.

Zahrah T.F. and Hall W.J. Earthquake energy absorption in SDOF structures. J. Struct. Eng., ASCE, 1984, 110(8), pp. 1757-1772.

Khashaee P., Mohraz B., Sadek F., Lew H.S., and Gross J.L. Distribution of earthquake input energy in the structures. NISTIR 6903, Washington, D.C., 2003.

Sadashiva V.K. Quantifying structural irregularity effects for simple seismic design. PhD thesis, University of Canterbury, Christchurch, New Zealand, 2010.

SAC (SEAOC-ATC-CUREE). The SAC Steel Project. Berkeley, Ca, 2000.

OpenSees (2015), Open System for Earthquake Engineering Simulation- Home Page: http://opensees.berkeley.edu/, 2015.

The MathWork, Inc., Matlab R2008a.

Yeow, T.Z., MacRae, G.A., Dhakal, R.P. and Bradley, B.A. Experimental studies on the sliding behavior of building contents. Anchorage, AK, USA: 10th US National Conference on Earthquake Engineering (NCEE10), 2014, 21-25 Jul 2014. 10pp.

Chapter 5: Seismic Response of Nonlinear Single Story Steel Structures with Unbalanced Stiffness/Strengths

5.1. Introduction

Structures are usually designed to have the same stiffness/strength in forward and reverse horizontal directions because they are expected to perform similar ways under wind and earthquake loading. However, some structures may have different stiffness/strength in one horizontal direction compared to the opposite direction. For example, T-shaped reinforced concrete walls which are stiffer/stronger with the flange in tension than in compression, or structures with slender bracing elements not placed in a balanced configuration around the structure as shown in Figure 5-1, may have a greater stiffness/strength in one direction than the opposite direction. Structures with significant unbalanced lateral force resistance have a tendency for inelastic deformation in predominantly one direction under strong earthquake shaking. This is sometimes termed ratcheting (e.g. MacRae 1994, Yeow et al. 2014, Rad et al 2015).

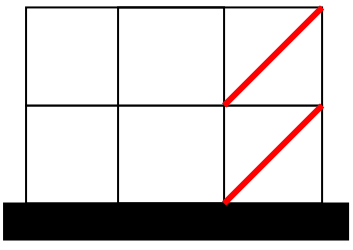

Figure 5-1: Unbalanced Stiffness/Strength Building

Also, structures with residual displacements due to earthquakes may be strengthened/stiffened to limit the likelihood of further increase in displacement in that direction due to aftershocks. Such stiffening/strengthening can act as a permanent measure, as an interim measure until the building is manually straightened and repaired, or until it is deconstructed. While the concept regarding these mitigation measures is clear, simple methods to estimate the displacement demands of such structures with different strength/stiffness in the different directions are not available.

Based on the discussions above, it may be seen that there is a need to evaluate the likely seismic displacements of structures with different stiffness/strengths in opposite horizontal directions. The scope of this chapter is to address this need for single-story non-linear frame structures with different stiffness/strengths in opposite horizontal directions. In particular, answers are sought to the following questions:

1) How can the peak horizontal displacements in the stiffer direction be estimated?

2) How can the peak horizontal displacements in the flexible direction be estimated?

3) How do the peak absolute displacements change?

4) How can residual horizontal displacements be estimated?

5) What procedures are appropriate for design?

5.2. Literature Review

Rad and MacRae (2017) showed that the peak displacements of elastic single story structures in the stiffer direction could be predicted by the spectral displacement associated with the period in that direction. Also, it was shown that the average potential energy of the stiffer and more flexible sides of the elastic structures with unbalanced stiffness to be similar for all period ranges. Therefore, this was allowed the likely peak displacement in a flexible direction could be estimated from the displacement in the stiffer direction by using energy considerations irrespective of the level of damping or period as shown in Eq.5-1 where $\Delta_{e,f}$ and K_f are the peak displacement and stiffness in more flexible direction and $\Delta_{e,s}$ and K_s are the peak displacement and stiffness in stiffer direction. However, this study only considered the effect of unbalanced stiffness for elastic structures and the yielding characteristics of the structure was not considered.

$$\Delta_{e,f} = \Delta_{e,s} \cdot \sqrt{(K_s/K_f)} \quad (5\text{-}1)$$

While some works have been conducted to determine the response of the structures with different strength in different direction (e.g. Yeow et al. 2013, Saif et al. 2017), no studies are known to have specifically addressed the estimation of displacements of yielding structures with different stiffnesses/strength in opposite horizontal directions.

Priestley, et al. (2007) also argued that in many cases strength may be proportional to stiffness. This may be stated that Δ_y (yield displacement) = F_y/k is constant.

Moreover, Paulay and Priestly (1992) also showed that for structures with periods more than 0.7s, the ductility (μ) is often similar to force reduction factor (R). However, for structures with period less than 0.7s, they are not equal and a relationship between them was given in Eq.5-2 which has been adapted in NZS1170.5. Here for a specific R value, by decreasing T, the corresponding μ is increased. Therefore, the ratio of (μ/R), is increased by decreasing the period T, of the structure. Eq.5-3 to 6 and Figure 5-2 shows that this ratio (μ/R) equals to ratio of ultimate to elastic displacement response (Δ_u/Δ_e). In Figure 5-2, F_e and F_y are elastic and yielding strength of the structure, and Δ_e, Δ_y, and Δ_u are the elastic, yielding and ultimate displacement of the structure. Thus, ratio of ultimate to elastic displacement response (Δ_u/Δ_e) is increased by decreasing T of the structure.

$$\mu = min\begin{cases} 1 + (R-1)\frac{0.7s}{T} \\ 1 \end{cases} \tag{5-2}$$

$$R = \frac{F_e}{F_y} = \frac{\Delta_e}{\Delta_y} \tag{5-3}$$

$$\mu = \frac{\Delta_u}{\Delta_y} \tag{5-4}$$

$$\Delta_y = \frac{\Delta_e}{R} \tag{5-5}$$

$$\frac{\Delta_u}{\Delta_e} = \frac{\mu}{R} = max\begin{cases} 1 + {(R-1)\frac{0.7s}{T}}\Big/{R} \\ 1 \end{cases} \tag{5-6}$$

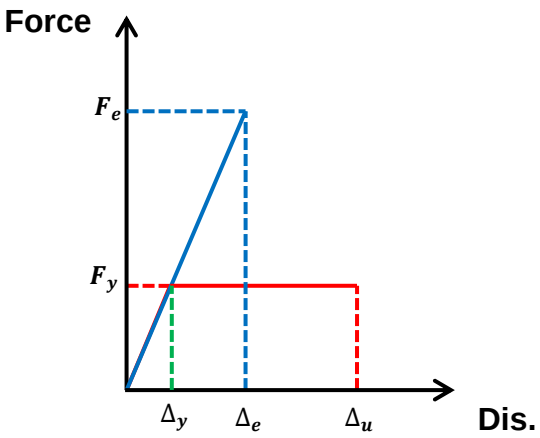

Figure 5-2: Effect of R and μ on peak displacement response.

5.3. Modelling and Evaluation Approach

In this study, a nonlinear single story steel frame structure is considered for analysis as shown in Figure 4-2. The basic structure was designed with target maximum interstory drifts of 1.5%, 2.0% and 2.5% and force reduction factors of 1, 2, 4 and 6 according to the equivalent static method in NZS1170.5 (2016). The structure has a floor mass of 20 Tons, floor height of 3m and a span length of 6m. For this model, the bases of the columns were modelled as pinned, and column stiffnesses was assumed to be constant with moments of inertia of 0.000388m^4 and module of elasticity of 200GPa each for all design drifts. Changing of the design drift of the structure is controlled by the beam stiffness. The periods of the structure with these design drifts of 1.5%, 2.0% and 2.5% are 0.45s, 0.55s and 0.7s respectively.

To make unbalanced stiffness/strength structures, a "nonlinear tension-only" brace with slackness was added to the structure to increase the stiffness (*K_ratio*) in positive direction from 1 to 10 times that in the opposite (negative) direction. This range of *K_ratio* is only considered for parametric study. A building with high dramatic discrepancy of strength/stiffness in both directions may not be permitted in to be designed. Moreover, such a brace may also be used to limit the further positive displacements in a frame with an initial permanent positive displacement from a previous earthquake event. However, as the study conducted here is to study the fundamental behaviour of different stiffness/strength in different directions alone, no initial permanent displacement is considered here. Moreover, based on study by Priestley et al. (2007), the strength was assumed to be proportional to stiffness. Therefore, the balanced and unbalanced structure have same yield displacement (Δ_y) as shown in push-pull curve of the structures in Figure 5-4. The hysteretic behaviour was assumed to be elastic perfectly plastic with no gapping. The stiffness and strength ratio, K_{ratio}, is defined as the ratio of stiffness/strength in stiffer direction, K_s, to that in the more flexible direction, K_f, where these terms are shown in Figure 5-4.

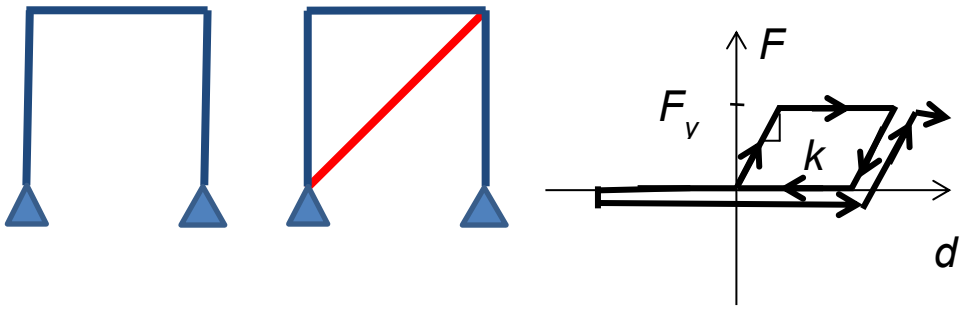

(a) Frame Building (b) Building with tension-only braces (c) Brace hysteresis loop

Figure 5-3: Structure Models

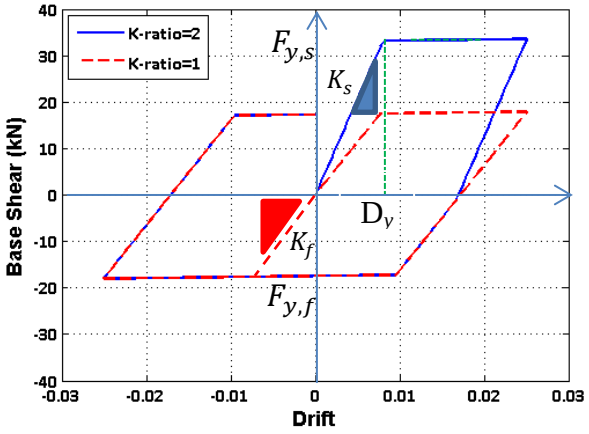

Figure 5-4: Comparing Push & Pull behaviour of the balanced and unbalanced stiffness/strength structures (R=4, T=1.0s).

The SAC (SEAOC-ATC- CUREE, 2000) suite of 20 earthquake ground motion records for Los Angeles, with a probability of exceedance of 10% in 50 years, was used. To eliminate directionality effects from individual ground motion records, the analysis was repeated by applying the same ground motions in the opposite direction. All earthquake ground motions records are scaled to elastic design spectral acceleration at fundamental period of the frame structure without a brace.

The dynamic inelastic time history analysis was performed using OpenSees (2017). MATLAB (2008) was used to extract the peak and residual drift in both stiffer and more flexible directions. Initial mass proportional Rayleigh damping with a damping ratio of 5% was considered. These damping ratios were specified as being a proportion to the more flexible stiffness. The hysteresis loops were considered to already consider P-delta effects which were not explicitly considered.

5.4. SEISMIC BEHAVIOUR

5.4.1. Absolute Peak Drift Response

Figure 5-5 shows that median absolute peak drift response of the structure from both stiffer and more flexible directions changes less than10% for *K_ratio* from 1.0 to 10. While increasing *K_ratio* the median peak stiffer direction drift is decreased, but the median peak flexible direction drift for most of the *R* values and design drifts does not change significantly.

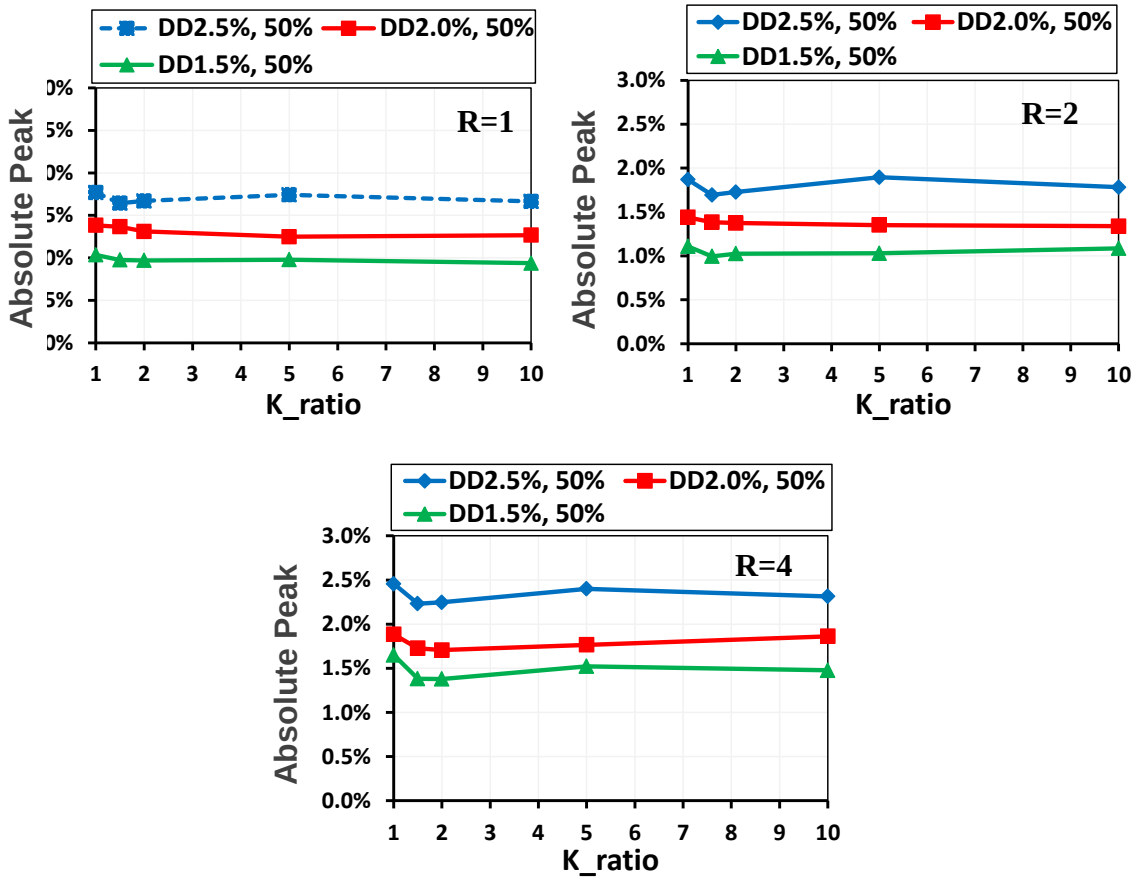

Figure 5-5: Absolute Peak Drift Response using the 40 SAC La10in50 records (both directions).

5.4.2. Peak Stiffer Direction Drift

Figure 5-6 shows that as *K_ratio* increases the stiffer direction drift tends to decrease. For *K_ratio* of 1, although the design drifts of the structures are 2.5%, 2.0% and 1.5%, the median peak stiffer direction drifts are less than about 1.6%. This is because the maximum drift of the structure can occur either direction under different earthquake records and shaking direction. Therefore, by choosing only one direction, the median peak drift of that direction is less than median maximum drifts shown in Figure 5-5.

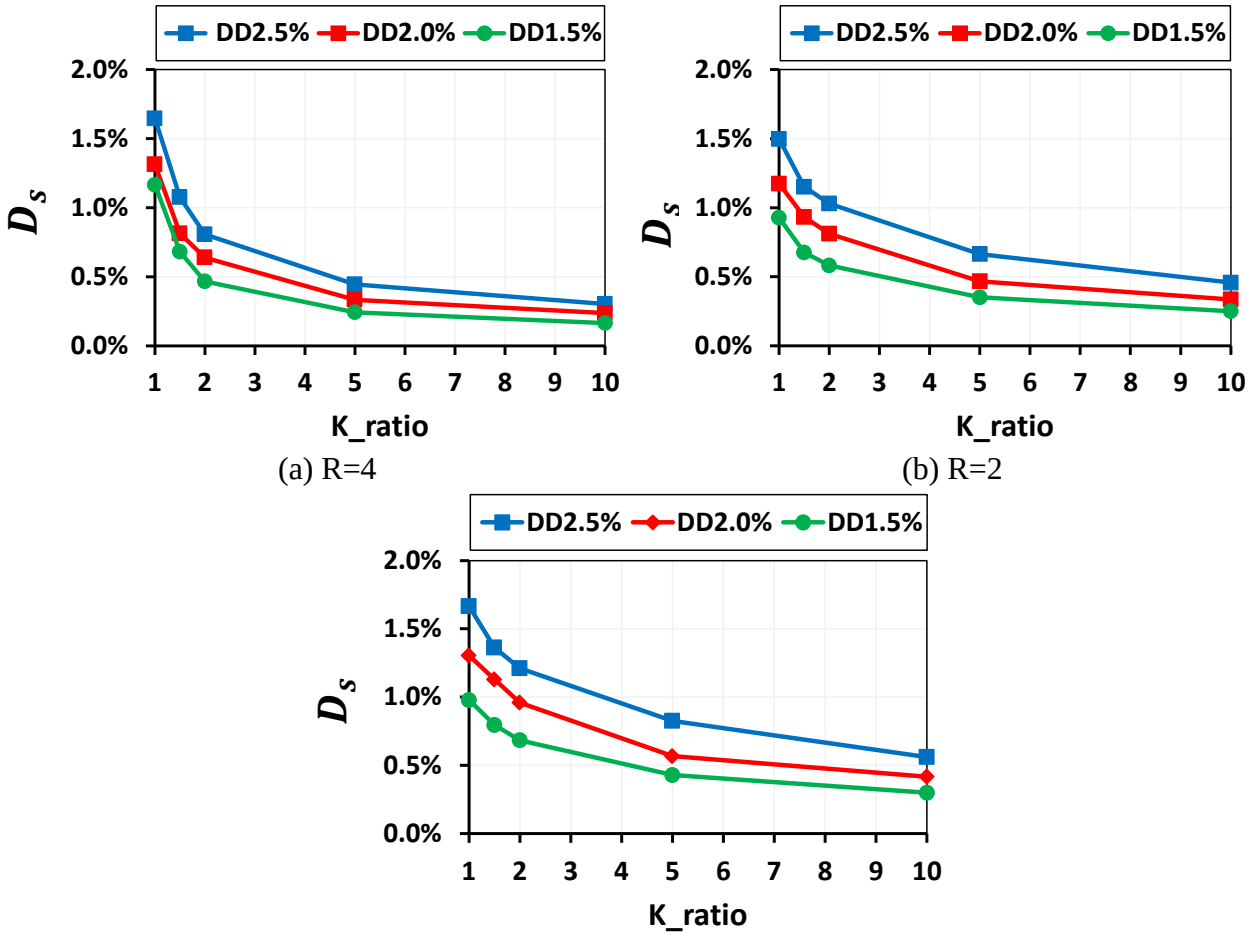

(a) R=4 (b) R=2

(c) R=1

Figure 5-6: Effect of K_ratio, Design drift and R on Peak Positive Drift (Stiffer direction) using the 40 SAC La10in50 records (both directions).

Figure 5-7 shows that the stiffer direction displacement is similar to spectral displacement for the period of the stiffer side, $S_d\,(T_s)$. Therefore, $S_d\,(T_s)$ can be used conservatively to estimate the peak displacements in the stiffer direction. The stiffer side of the structure remains in almost elastic especially for high *K_ratio*. Therefore, consistent the study by Rad and MacRae, (2017), the displacements follow the spectral displacements of the balanced stiffness structures.

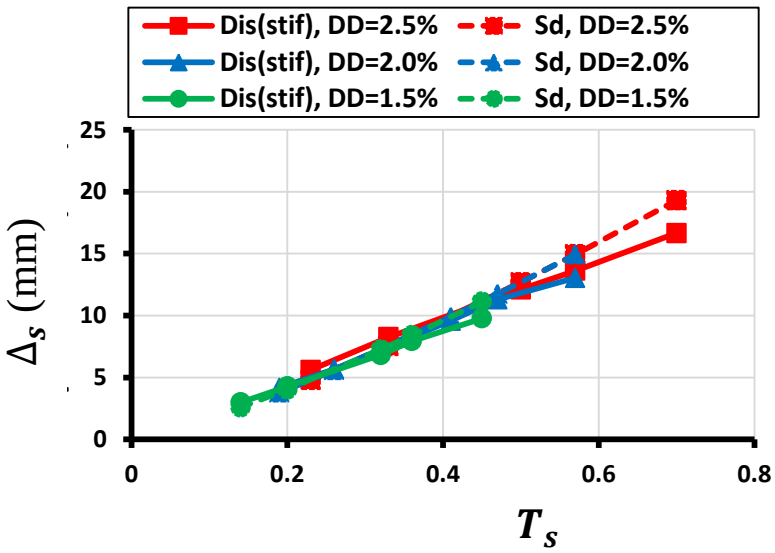

Figure 5-7: Stiff direction peak displacement, Δ_s, and spectral displacement versus stiff direction period, T_s.

5.4.3. Peak Flexible Direction Drift

Figure 5-8 shows that the absolute peak drift in the flexible direction, Δ_f can do increase and become almost constant with greater *K_ratio*. This increase is greater with higher design drift and force reduction factors (*R*). For low design drifts and force reduction factors (*R*) remain almost constant. This is consistent with Rad and MacRae, (2017) for an elastically response structure.

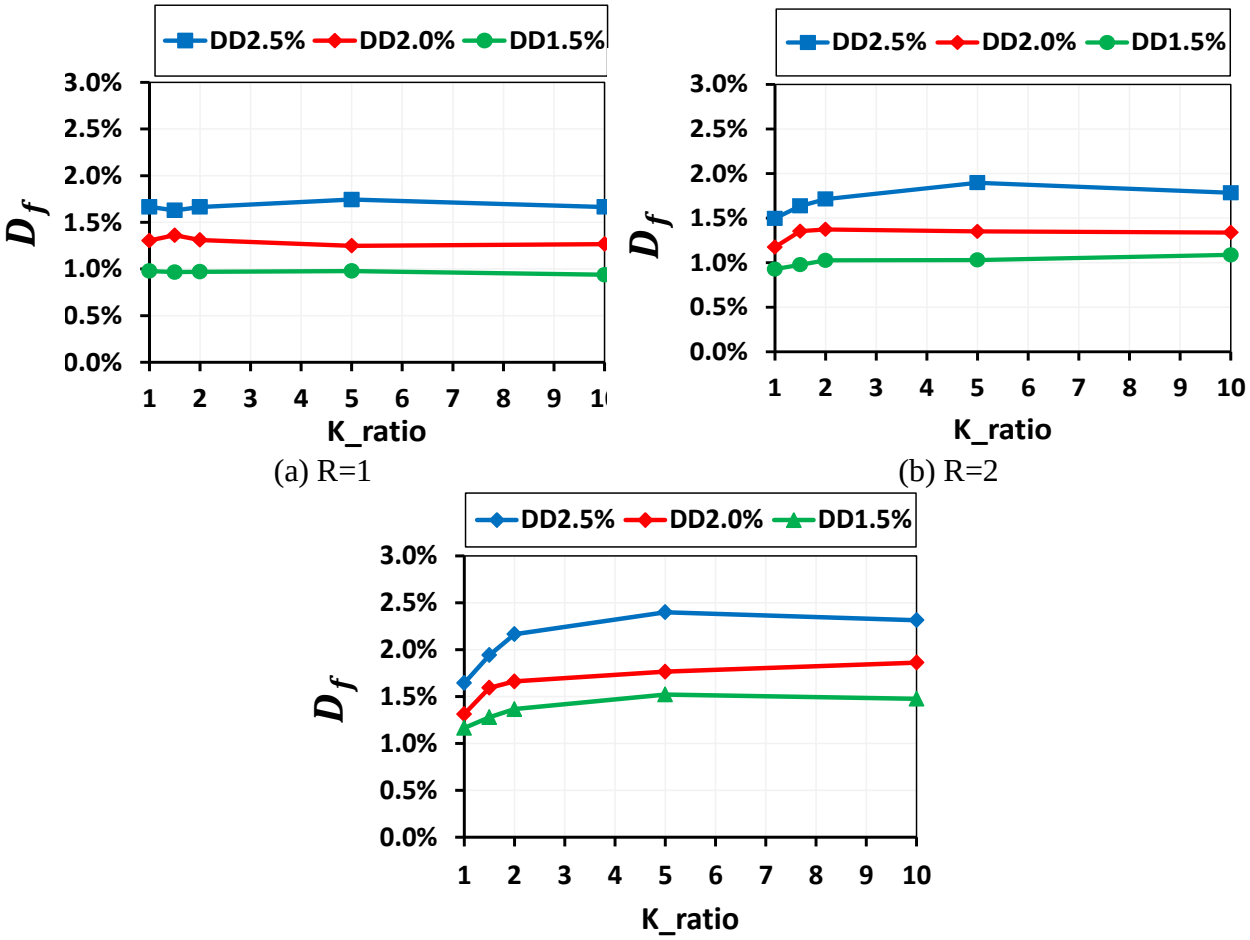

(a) R=1

(b) R=2

(c) R=4

Figure 5-8: Effect of K_ratio, Design drift and R on Peak Negative Drift (flexible direction) using the 40 SAC La10in50 records (both directions).

5.4.4. Drift Range

Figure 5-9 shows that drift range of the structures, D_range, calculated as $D_f - D_s$, is decreased by increasing the *K_ratio*. This is because by increasing *K_ratio*, peak relative drift in the stiffer direction, D_s is decreased as shown in Figure 5-6, but peak relative drift in the flexible direction does not change as much as shown in Figure 5-8. Therefore, the range of drift for structures with different design drifts and force design reduction factor is decreased.

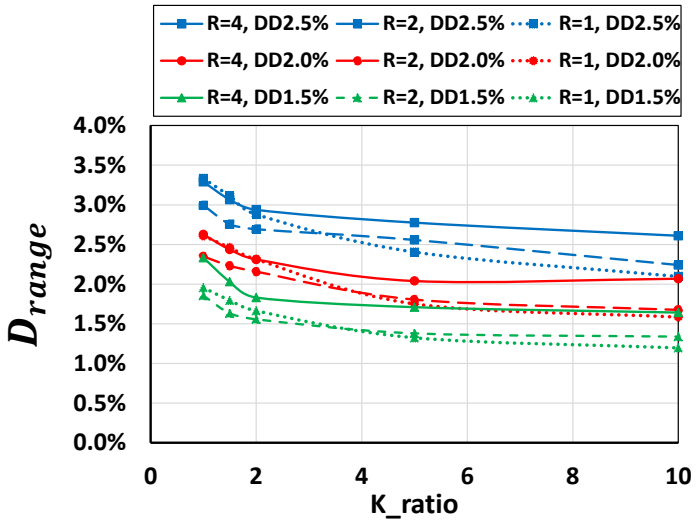

Figure 5-9: Effect of K_ratio, Design drift and R on Drift Range

Figure 5-10 also shows that the centre of the drift range, $D_{centre,\ range}$ calculated as $(D_f + D_s)/2$, for a balanced stiffness structure (K_ratio =1) is equal to zero because the ground motion records were applied in both directions. By increasing K_ratio, $D_{centre,\ range}$ becomes negative. This is also shown for specific records in Figure 5-11.

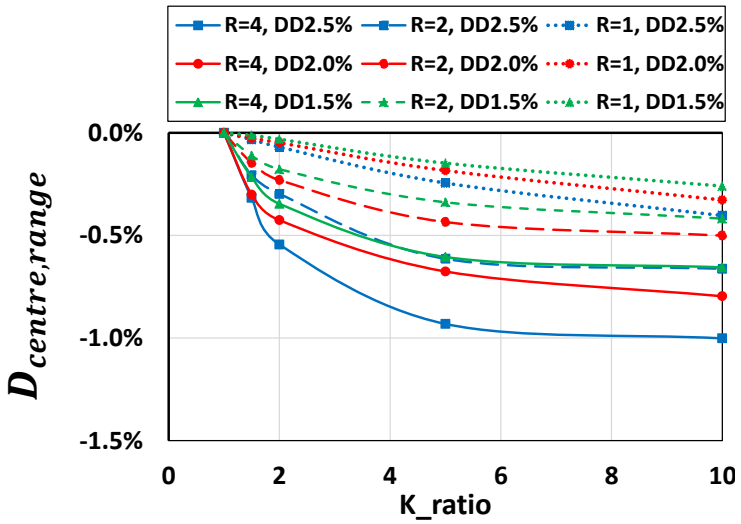

Figure 5-10: Effect of K_ratio, Design drift and R on Centre of Range

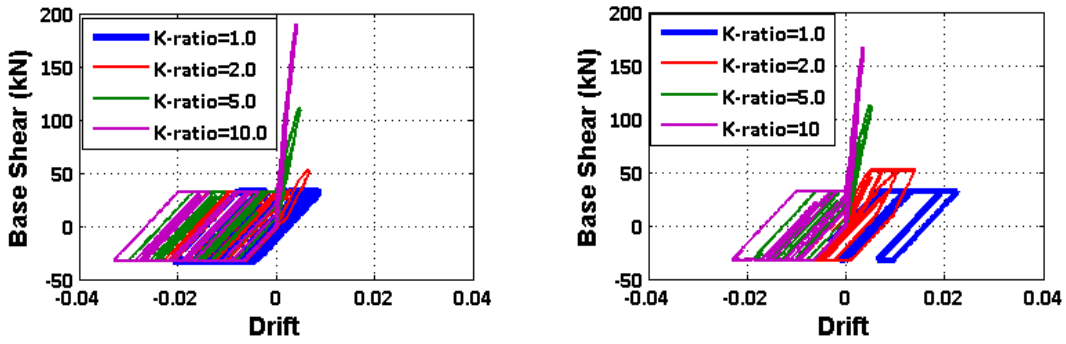

(a) Imperial Valley, El Centro, 1940 *(b) Imperial Valley, Array 05, 1979*

Figure 5-11: Effect of K_ratio on base shear vs drift response of structure with R of 4 and design drift of 2.5%.

5.4.5. Residual Drift Response

Figure 5-12a shows that by increasing *K_ratio*, the median absolute value of residual drift, $D_{res,abs}$, for all structures with *R* of 4, slightly decreases then again increases and becomes almost constant. This is because by an increased stiffness/strengths in positive direction, the residual drift moves from being positive toward the more negative direction as shown in Figure 5-12b. Here, the residual drift changes is defined as, $\Delta D_{res} = D_{res,K_{ratio}=i} - D_{res,K_{ratio}=1}$. Residual drift does not continue to increases with *K_ratio* because it is limited by the peak drift of which also becomes constant as shown in Figure 5-8.

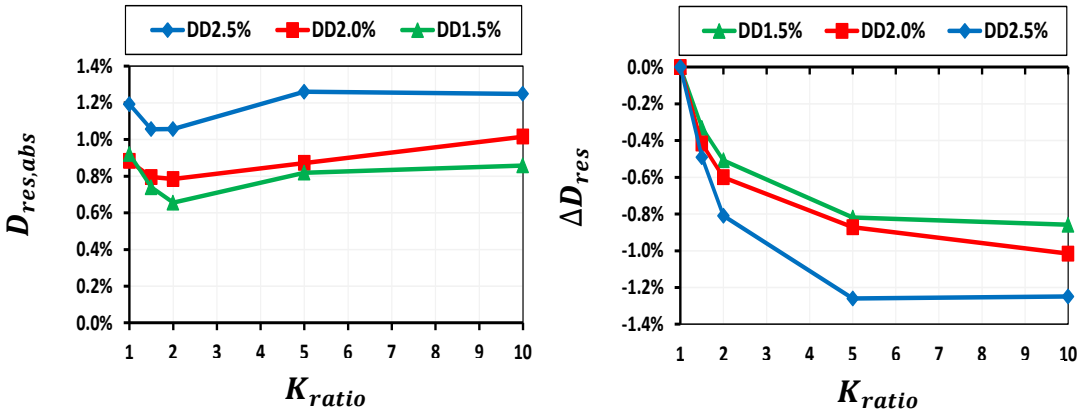

(a) Absolute Residual Drift (b) Residual Drift Changes

Figure 5-12: Residual Drift Response of the unbalanced stiffness/Strengths (R=4).

5.5. Ultimate to Elastic Response Ratio

5.5.1. Balanced Stiffness/Strength Structure

Figure 5-14 shows that the ratio of ultimate peak flexible direction displacement ($\Delta_{u,f}$) to elastic peak flexible direction displacement, $\Delta_{e,f}$, of the balanced stiffness structures, K_{ratio}=1, is increased with increasing design drifts and *R*. This ratio is consistent with Eq.5-6 obtained from Eq.5-2 to 5 and Figure 5-2 where *T* is the period of the flexible direction, T_f. However, it can be seen that the NZ Standard (NZS1170.5, 2004) is conservative. This can be because of the ground motions or type of the soils. Eq.5-3 from NZ standard was generalized for all different soil types for simplicity.

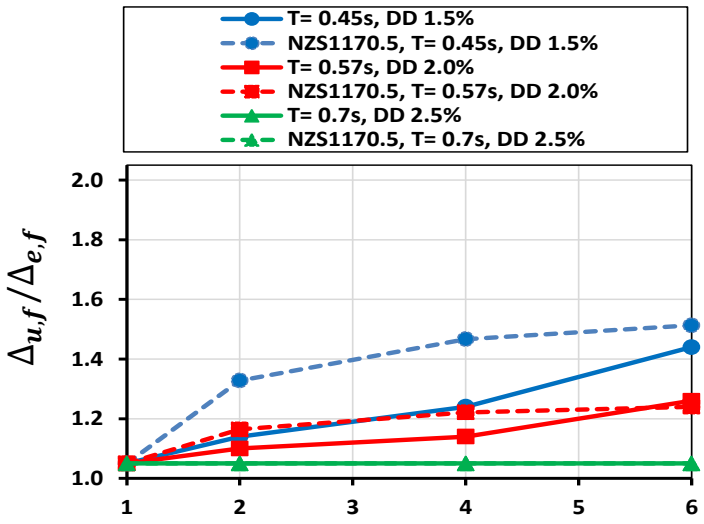

Figure 5-13: Effect of R and Design drifts on $\Delta_{u,n}/\Delta_{e,n}$ ratio using the 40 SAC La10in50 records.

5.5.2. Unbalanced Stiffness/Strength Structure

Figure 5-14a shows that $\Delta_{u,f}/\Delta_{e,f}$ of the unbalanced stiffness structures increases with increasing *K_ratio* and *R*, then becomes constant. However,

Figure 5-14b shows that $\Delta_{u,f}/\Delta_{e,f}$ is not sensitive to design drifts.

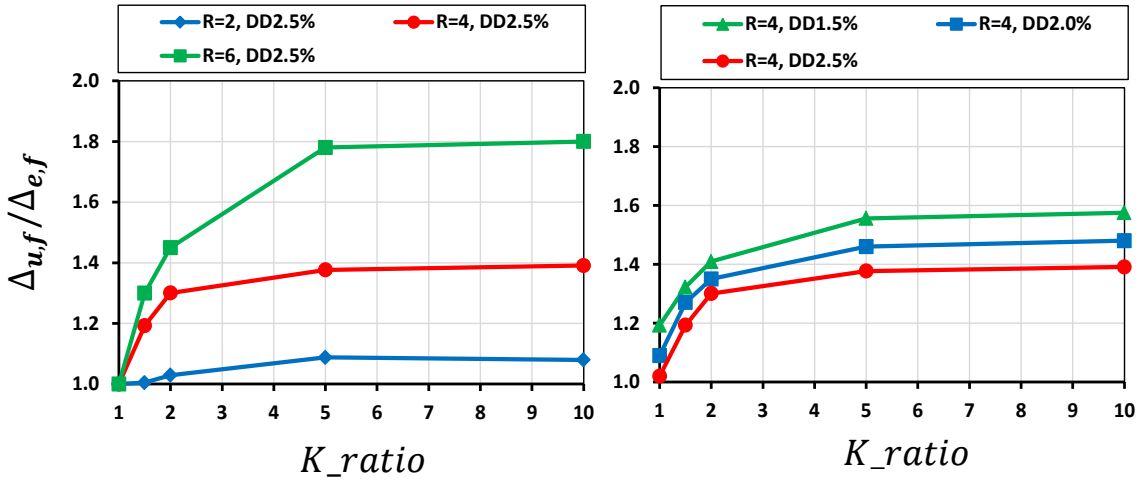

(a) Effect of R **(b) Effect of Design Drift**

Figure 5-14: Effect of K_ratio, and R on $\Delta_{u,f}/\Delta_{e,f}$ ratio using the 40 SAC La10in50 records (both directions).

5.6. DESIGN CONSIDERATIONS

A number of different methods could be proposed for design based on the relationship observed. These would all use the fact that the elastic peak displacement in the stiffer direction can be obtained by from the spectral displacements. This would use the fact from Figure 5-8 that $\Delta_{u,f}$ does not change much with *K_ratio*. Others could use the elastic responses and variation of them to account for ductility.

One method is proposed below which is considered to be suitable for design because it is both consistent with that used in standard as well as with observation related to fully elastically responding structures with unbalanced stiffness (Rad et al., 2017).

Methodology is as follows:

1) Estimate elastic displacement of the stiffer side, $\Delta_{e,s}$, from *Sd* (*Ts*).

2) Estimate elastic displacement of the flexible side from Eq.5-1, $\Delta_{e,f} = \Delta_{e,s} . \sqrt{(K_s/K_f)}$.

3) For each direction, calculate inelastic displacements using Eq.5-6. Here, *R* can be taken as $R_s = \frac{\Delta_{e,s}}{\Delta_y}$ for stiffer direction and $R_f = \frac{\Delta_{e,f}}{\Delta_y}$ for flexible direction from Eq.5-3 and Figure 5-2 until further information is available. Here, based on Priestley, et al. (2007), Δ_y (yield displacement) is constant for both stiffer and flexible directions.

$$\Delta_{u,s} = \Delta_{e,s} \times max \begin{cases} 1 + (R_s - 1)\frac{0.7s}{T_s}\Big/ R_s \\ 1 \end{cases}$$

$$\Delta_{u,f} = \Delta_{e,f} \times max \begin{cases} 1 + (R_f - 1)\frac{0.7s}{T_f}\Big/ R_f \\ 1 \end{cases}$$

5.7. DESIGN APPLICATION

The displacements of a structure with unbalanced stiffness are given in the following steps:

Step 1: The period of the stiffer side of the structure, T_s is obtained by $T_s = T_i/\sqrt{K_{ratio}}$ where T_i is the initial period of the structure.

Step 2: The elastic peak displacement in stiffer direction ($\Delta_{e,s}$) of the structures is obtained from design spectral displacement (S_d) from appropriate standard considering the period of the stiffer side, T_s.

Step 3: The elastic peak displacement in more flexible direction ($\Delta_{e,f}$) of the structures can be estimated from the stiffer displacement using energy method and Eq.5-1.

Step 4: Calculating Δ_y, and $R_s = \frac{\Delta_{e,s}}{\Delta_y}$ and $R_f = \frac{\Delta_{e,f}}{\Delta_y}$.

Step 5: The ultimate peak stiffer direction displacement ($\Delta_{u,s}$) of the structures is obtained from Eq.5-6 considering $R = R_s = \frac{\Delta_{e,s}}{\Delta_y}$.

Step 6: The ultimate peak flexible direction displacement ($\Delta_{u,f}$) of the structures is obtained from Eq.5-6 considering $R = R_f = \frac{\Delta_{e,f}}{\Delta_y}$.

Example:

For a structure with mass of 20 Tons, an initial design drift of 2.0%, period, T_i, of 0.57s, story height of 3m, R of 4 and stiffness ratio, K_{ratio}, of 4.0, the likely $\Delta_{u,s}$ and $\Delta_{u,f}$ displacements are calculated as:

Step 1: The period of the stiffer side of the structure is $T_s = 0.57/\sqrt{4} = 0.285s$.

Step 2: By assuming the design spectra is given by NZS117.5 for Wellington, soil type C, the elastic peak stiffer displacement, $\Delta_{e,s}$, of the unbalanced stiffness structure with T_s of 0.285s is $\Delta_{e,s}$ = 0.019m.

Step 3: The elastic peak more flexible displacement, $\Delta_{e,f}$, equals to $0.019\times\sqrt{4}$ = 0.038m.

Step 4:

$$\Delta_y = {V}/{K} = {c.w}\Big/{\left(\frac{4\pi^2 m}{T^2}\right)} = \frac{0.18\times 9.81\times 20{,}000}{2427725.45} = 0.0145$$

$$R_s = \frac{\Delta_{e,s}}{\Delta_y} = {0.019}/{0.0145} = 1.3$$

$$R_f = \frac{\Delta_{e,f}}{\Delta_y} = {0.038}/{0.0145} = 2.6$$

Step 5: The ultimate peak stiffer displacement, $\Delta_{u,s}$, equals to

$$\Delta_{u,s} = 0.019\times\left(1+ {(1.3-1)\times\frac{0.7}{0.285}}\Big/{1.3}\right) = 0.019\times 1.56 = 0.029\text{m}$$

Step 6: The ultimate peak more flexible displacement, $\Delta_{u,f}$, equals to

$$\Delta_{u,f} = 0.038\times(1+ (2.6-1)\times \frac{0.7}{0.57}/_{2.6}) = 0.038\times 1.76 = 0.067\text{m}$$

5.8. CONCLUSION

In this study, peak and residual seismic displacements of nonlinear single story structures with different stiffness/strength in opposite directions are obtained using response history analysis. Parameters considered were the relative stiffness/period in the different directions, the force design reduction factor (*R*), and the design drift. It was found that by increasing the stiffness/strength in one direction

(i) peak displacement in the stiffer direction tend to decrease and may be predicted by the spectral displacement associated with the period in that direction,

(ii) the likely displacement in a flexible direction could be estimated from the displacement in the opposite direction using energy considerations,

(iii) the median maximum peak displacement of the structure does not change,

(iv) the residual displacement decreases in the stiffer direction. However, the absolute residual drift does not decrease, but remain relatively constant as it tends to occur in the flexible direction.

(v) A methodology to estimate peak displacements is developed that is consistent with current standards and with fully elastic response. An example is also provided.

5.9. REFERENCE

Paulay and Priestly (1992), "Seismic design of reinforced concrete and masonry buildings", Willey, ISBN: 978-0-471-54915-4, 768 pages.

Priestley M.J.N., Calvi G.M., Kowalsky M.J. (2007), Direct displacement-based seismic design of structures NZSEE conference.

SAC (SEAOC-ATC-CUREE) (2000), The SAC Steel Project. Berkeley, Ca.

Rad, A. A., MacRae, G., Bull, D. and Yeow, T. (2015). "Seismic Behavior of Steel Buildings with Initial Out-of-Plumb." Earthquake Eng. Struct. Dyn., 44 (14), 2575-2588,

Rad, A.A. and MacRae, G. (2017) "Seismic response of elastic single story structures with unbalanced stiffness". Submitted to Earthquake Eng. Struct. Dyn.

MacRae GA. P-Δ effects on single-degree-of-freedom structures in earthquakes. Journal of Earthquake Spectra, 1994; 10(3):539–568.

NZS 1170.5:2016. Structural Design Actions Part 5: Earthquake Actions New Zealand. Standards New Zealand: Wellington, New Zealand, 2004.

OpenSees (2017), Open System for Earthquake Engineering Simulation- Home Page: http://opensees.berkeley.edu/.

The MathWork, Inc., Matlab R2008a.

Yeow TZ, MacRae GA, Sadashiva VK, Kawashima K. Dynamic stability and design of C-bent columns. Journal of Earthquake Engineering 2013; 17:5,750–768.

Chapter 6: Shake Table Testing of a Low Damage Steel Building with Asymmetric Friction Connections (AFC)

6.1. Introduction

In light of recent major seismic events worldwide, it has become apparent that while modern design provisions ensure life safety in modern structures during severe earthquake events, structures may be damaged and require extensive repair or replacement. A recent research effort is to develop new solutions that will also minimize the possibility of structural damage. Such low-damage structures may be achieved by developing a behaviour that is elastic, or by incorporating the use of energy dissipaters such as friction connections.

In friction connections, energy is dissipated as two surfaces slide against each other. The sliding resistance is determined by the clamping force provided by pre-tensioned high strength bolts and the friction coefficient between the sliding materials. Beam end friction connections for steel MRFs have been studied by Yang and Popov (1995) where the researchers utilized symmetric friction connections (SFCs) in the top and bottom flanges of steel beams. The experimental test results showed a reliable frictional behaviour with limited degradation. However, most realistic moment frames cannot deform in this manner since there is a slab on top of the beam. Connections which do not slide at the top flange have also been developed and tested (Clifton (1996, 2005), MacRae et al. (2010)). These rotate about the top flange plate and sliding only occurs in the

bottom flange plate thus minimizing interactions with the overlaying floor slab and the effects of beam elongation as shown in Figure 6-1.

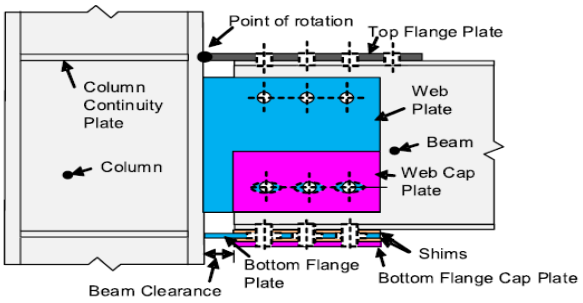

Figure 6-1: Asymmetric friction connection (AFC) in beam column joint (MacRae et al. 2010).

In such asymmetric friction connections (AFC) the top flange of the beam is fixed to a plate extending from the column called the bottom flange plate. One shim is placed between the bottom-flange plate and beam. Another shim is placed between the column-flange plate and cap plate. When beam ends starts to rotate about the top flange plate, initial sliding occurs between the bottom-flange plate and beam. Later sliding occurs between the column-flange plate and cap plate. Since sliding does not initiate at both locations at the same time, it is referred to as an asymmetric friction connection.

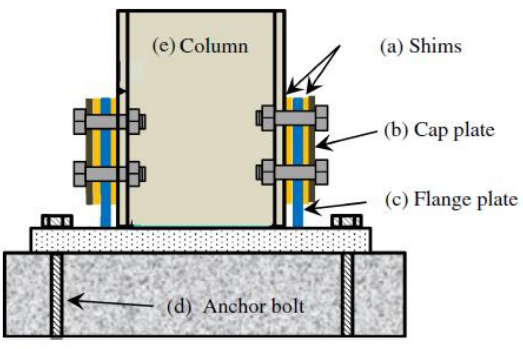

(a) Base column joint (Bourzouie et al. 2015a).

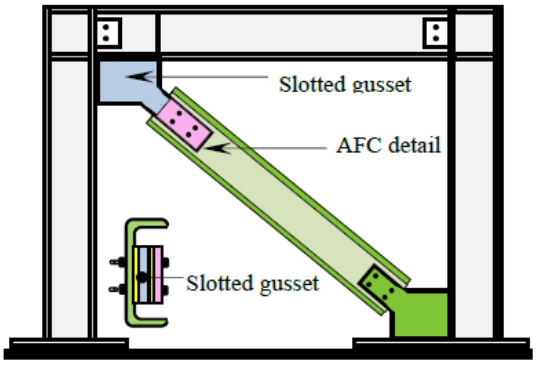

(b) Braces (Chanchí et al. 2014).

Figure 6-2: Asymmetric friction connection (AFC) in base column and braces

Past studies of AFC were mostly experimental with AFCs applied to beam-to-column moment resisting joints (Clifton, 2005; MacRae et al. 2010), base-columns connections (Bourzouie et al. 2015a, b, Figure 6-2a) and braces (Chanchí et al. 2012 & 2014, Figure 6-2b). All of these configurations can possess good seismic performance. However, the conceptual model for hysteretic behaviour of beam end AFC was not matched with experimental studies and also, the dynamic performance of AFCs in steel moment resisting frames (SMRFs) under earthquake type excitation has not been validated.

It is clear that there is a need to experimental validates the seismic performance of whole AFC frame systems to develop further confidence amongst engineers for their adoption. This chapter seeks to address this need by describing the shake table testing of a half-scale steel frame building with AFCs at the column bases and beam ends. In particular, answers are sought to the following questions:

1) What is the peak and residual response for this particular structure?

2) How do these beam and column friction connections behave during excitation?

3) Can numerical modelling predict the experimental performance?

4) Can beam and column AFCs be considered “low damage”?

6.2. Literature Review

Conceptual hysteretic behaviour of beam end AFC connection, known as sliding hinge joints, was described by MacRae et al. (2010). It was defined over 5 different stages as shown in Figure 6-3 beginning with (a) before sliding, where beam flexure dominates the response before there is sliding in the connection; (b) initial sliding, where sliding occurs between the bottom of the beam flange and the bottom flange plate. At this stage the bottom flange cap plate is not sliding because the shear force imposed on it is relatively small. Stage (c) cap plate sliding occurs as the shear force and deformations become greater. Stage (d) reverse loading first sliding occurs between the bottom of the beam flange and the bottom flange plate and finally stage (e) occurs at larger displacements in the opposite direction. The sliding on both surfaces causes approximately twice the resistance than from one surface.

However, in this model the prying effect of the bottom flange plate was not explicitly considered. Also, the sliding force for reverse loading, Stages (d) and (e), were considered to have same magnitude at Stages (b) and (c) respectively. Furthermore, the experimental studies by Clifton (2005) showed that the conceptual model was not matched with the experimental.

The nominal sliding force for each AFC bolt equals to $F_s = \mu \times \eta \times N_{tf}$, where F_s is the sliding force of each bolt, μ is the friction coefficient, η is the number of shear planes (η = 2, for both surface sliding; η = 1, for one surface sliding), and N_{tf} is the proof load per bolt. The median friction coefficient of steel on Bisalloy 500 is equal to 0.21 according to Chanchí et al. (2012).

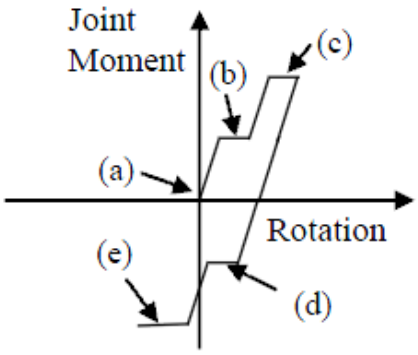

Figure 6-3: Hysteretic behaviour of asymmetric friction connection (AFC) at beam end (MacRae et al., 2010).

Column base AFC hysteretic behaviour has been studied by Bourzouie et al. 2015a. The column base AFC could be modelled by a bilinear hysteresis loop. It was found that sliding, prying, and axial force are three mechanisms that provide moment resisting in the base connection as shown in Figure 6-4. Based on this the maximum base moment from lateral loading causing strong-axis bending, M_{Tot}, was calculated by Eq.6-2 where M_{Slide} is the moment resulting from sliding friction, M_{Prying} is the elastic-prying moment mainly from flange plate bending on the compression side of the column, and M_{Axial} is the moment from axial force. In the equation, n_{Bolt} is the number of the bolts in each AFC, F_s is the sliding force for each bolt as defined in Eq. 6-6, θ_{Base} is the base rotation, H_{fp} is the distance from the top of the flange plate to the base plate, I_{fp} is the second moment of area about the weak axis of the flange plate, d is the distance from the sliding bolts to the neutral axis, and D_{Axial} is the perpendicular distance from the center of axial force to the neutral axis.

$$M_{Tot} = M_{Slide} + M_{Prying} + M_{Axial} = (n_{Bolt} \times F_s \times d) + \left(\frac{\theta_{base} \times 3EI_{fp}}{H_{fp}}\right) + (P \times D_{Axial}) \qquad (6\text{-}2)$$

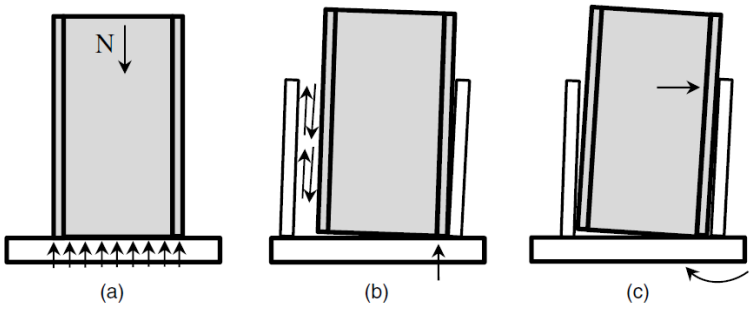

Figure 6-4: Mechanisms of load transfer at the base column: (a) axial force; (b) sliding; (c) prying (Bourzouie et al. 2015a).

Residual displacement prediction methods have been developed by MacRae and Kawashima (1997) for elasto- plastic single-degree-of-freedom (SDOF) oscillators with specified ductilities of 2, 4 and 6, post elastic stiffness ratios ranging from 0.25 to 1 and fundamental periods from 0 to 3s. It was shown that the ratio of the residual displacement to the maximum possible residual displacement is almost totally dependent on the post-elastic stiffness ratio of the force-displacement hysteretic curve. The oscillators with positive stiffness ratios generally have small residual displacements, while those with negative stiffness ratios have larger residual displacements. The residual displacement, D_r, was calculated by Eq.6-3 where D_{mr} is the maximum possible residual displacement based on slow unloading from the peak displacement and D_{rr} is a non-dimensional residual displacement ratio which has values ranging from zero to unity. D_{mr} was calculated by Eq. 6-4 where μ is ductility, r is post elastic stiffness ratio and D_y is yield displacement.

$$D_r = D_{rr} \times D_{mr} \tag{6-3}$$

$$D_{mr} = \begin{cases} (\mu - 1)(1 - r)D_y & r(\mu - 1) < 1 \\ \frac{(1-r)}{r} D_y & r(\mu - 1) \geq 1 \end{cases} \quad (6\text{-}4)$$

Peak interstory drifts can be estimated according to methods of MacRae et al. (2004). They showed that if the structure deforms with a linear distribution of displacements and columns are continuous over several stories of a structure, then the stiffness of the columns will limit the possible drift concentration. This is known as the "continuous column concept" and it emphasizes the continuous column stiffness. The drift concentration factor (DCF), is defined by Eq.6-5 and Figure 6-5 where the roof drift, δ_{roof}, is simply the roof displacement, Δ_{roof}, divided by the height of the roof from the ground, *H*, and the story drift, δ_s, is the maximum value of interstory displacement, Δ_{si}, divided by story height, h_i, for all stories, *i*, as shown in Eq. 6-6. If the columns are very stiff, then the structure is moves over linearly, there is no drift concentration, and the *DCF* is unity. Otherwise, *DCF* is greater than unity.

$$DCF = \frac{\delta_s}{\Delta_{roof}} \quad (6\text{-}5)$$

$$\delta_s = \max_i \left\{ {\Delta_{si}}/{h_i} \right\} \quad (6\text{-}6)$$

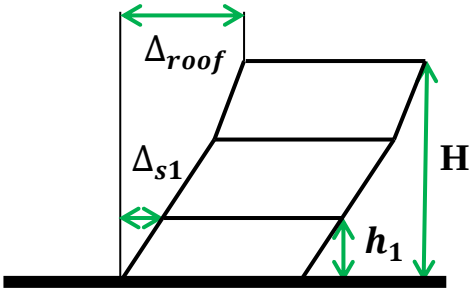

Figure 6-5: DCF Definition

6.3. Test Specimen Design

The test specimen was designed as a full-scale prototype building according to the Equivalent Static Method in NZS1170.5 (2016). The structure was assumed to be located Wellington, with Z=0.4 and soil type C. It was designed assuming beam end and base column connections were fixed. Assuming rigid and strong connections the design ductility was unity and the design drift in the Design Level (DL) earthquake event (1-in-500 year earthquake shaking) was 2.0%. AFC connections at the column bases and beam ends were then designed to have drifts corresponding to design ductilities of 3 and 6 respectively. Capacity design consideration were checked to ensure that the beams and columns remained elastic during both design level (DL) and maximum considered events (MCE). The MCE shaking had a probability of exceedance of 1-in-2500 year). The test specimen is composed of two steel frames (which are yellow in Figure 6-6) with AFC connections at the base column and beam ends. The beam end AFC shown in Figure 6-7a is designed to rotate about the top flange plate and slide only on the bottom flange plate. The moment is carried by friction between plates as no web plate exists. The friction plates are designed with sufficient tension capacity to carry the plastic moment capacity of the beam section ($M_n = F_y \times S = 24\ kN.m$ where S is the plastic section modulus and F_y is the minimum specified yield stress for the steel grade) and capacity design requirements based on frictional sliding were checked. These involved an overstrength factor of 1.4 (MacRae et al, 2015). The nut-rotation method with half a turn after snug tightening according to NZS3404 (2007) was used for tightening 4M12 Grade 8.8 bolts in the AFCs to their proof load (45kN). At the base connection, the moment is carried by friction.

Axial force is transferred directly by the column to the base plate as shown in Figure 6-7b. In the transverse direction, the two frames are joined by short transverse beams. The lengths of beams and columns, and the amount of the total mass at each floor, are provided in Table 6-1. The black beams under the yellow frame are part of a catch frame to provide safety during tests. The white channels on top of the yellow beams form a tray into which steel is placed to increase the mass at that level.

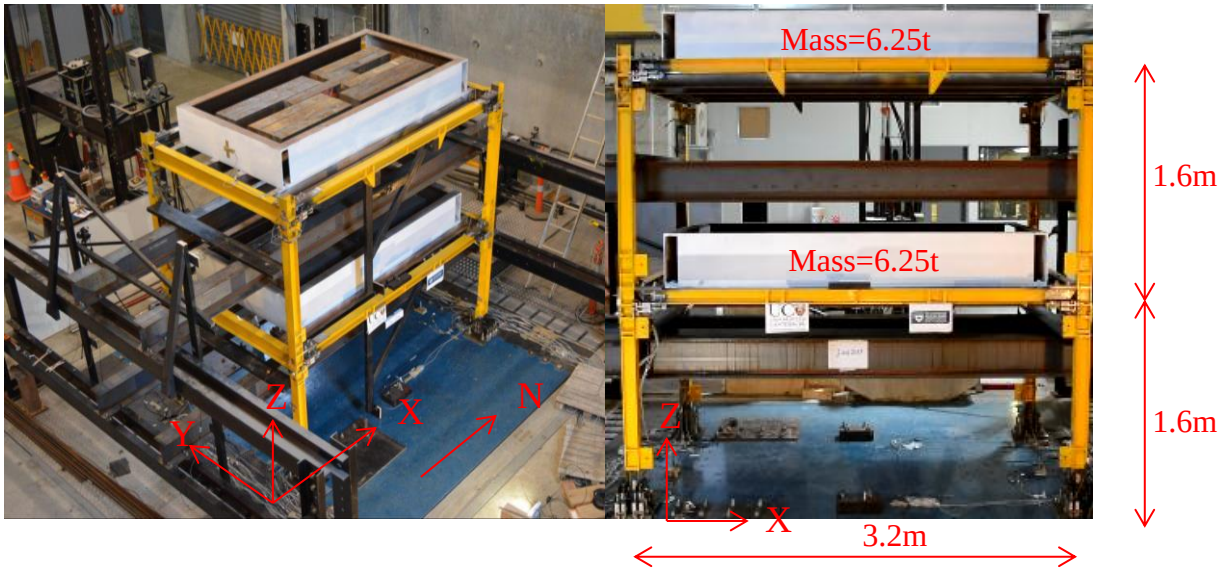

(a) Above view (b) Front Frame, NS direction.

Figure 6-6: Test building constructed frame

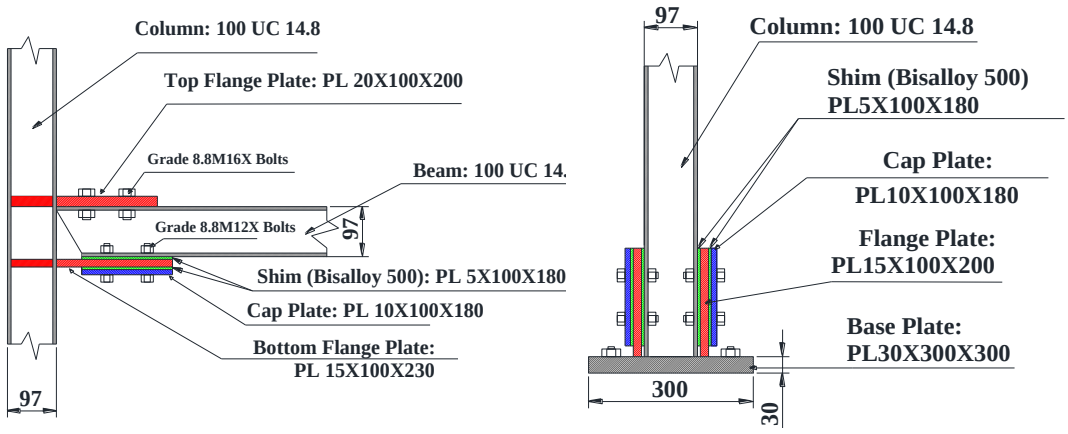

(a) AFC at the beam ends **(b) AFC at the column ends**

Figure 6-7: AFC details (All units mm)

Table 6-1: Properties of Test Building

Items	Properties
Inter-storey height [m]	1.6
Bay length [m]	3.2
Building width [m]	2
Mass per floor [Tons]	6.25
Column section	100 UC 14.8 Grade 320
Beam section	100 UC 14.8 Grade 320

The prototype was scaled to meet the requirements of the shake table. Considering the limitations of the shake table, as well as the added artificial mass, the three fundamental scaling factors (SF) specified were α_l for length, α_m for mass, and α_s for stress. These were set to 0.5, 0.25 and 1, respectively. Thereafter, other SFs such as time, acceleration, force were calculated based on the above three factors as shown the relationship in Table 6-2. In Table 6-2 the similitude relationships for key quantities often considered in structural engineering are presented. Here, the symbol M refers to the model and symbol P refers to the prototype.

Table 6-2: Similitude Relationships

Quantity	Symbol	Relationship	Parameter	Similitude
Length	α_l	Specified	0.5	$L_M = 0.5\ L_P$
Mass	α_m	Specified	0.25	$m_M = 0.25\ m_P$
Stress	α_s	Specified	1.0	$S_M = S_P$
Area	α_A	${\alpha_l}^2$	0.25	$A_M = 0.25\ A_P$
Time	α_t	$\sqrt{(\alpha_m/(\alpha_s\alpha_l))}$	0.7	$t_M = 0.7\ t_P$
Velocity	α_v	α_l/α_t	0.7	$v_M = 0.7\ v_P$
Acceleration	α_a	$\alpha_l/{\alpha^2}_t$	1	$a_M = a_P$
Force	α_f	$\alpha_m\alpha_a$	0.25	$F_M = 0.25\ F_P$
Moment	α_M	$\alpha_f\alpha_l$	0.125	$M_M = 0.125 M_P$
Strain	α_ε	α_s	1	$\varepsilon_M = \varepsilon_P$

6.4. Instrumentation

For this study, instrumentation of the test frame consisted of a combination of string pots, accelerometers, strain gauges, potentiometers, and load cells as shown in Figure 6-8. The relative displacement of each story, along with the location of each string pot allowed for the determination of the inter-story drifts. They were attached between the columns and a fixed reference frame as shown in Figure 6-8. The string pots had a maximum displacement of 1000mm in each direction from the resting position and a resolution of 0.001m. The local behaviour of the beam-column connections and column base connections were recorded by two and four parallel potentiometers respectively. These were placed across each connection interface (Figure 6-9). The neutral axis and rotation of the connection are subsequently estimated by interpolation assuming a linear strain profile across connections. Six horizontal accelerometers (two at each floor level (both sides) and two on each side of the shake table) were placed on the structure in the direction of loading as shown in Figure 6-8. Tension of some bolts during and after tightening was measured directly with donut load cells as shown in Figure 6-9. Strain gauges were also attached at beam and column ends before sliding plates on both top and bottom sides of the sections to measure the strain and moment force at each connection.

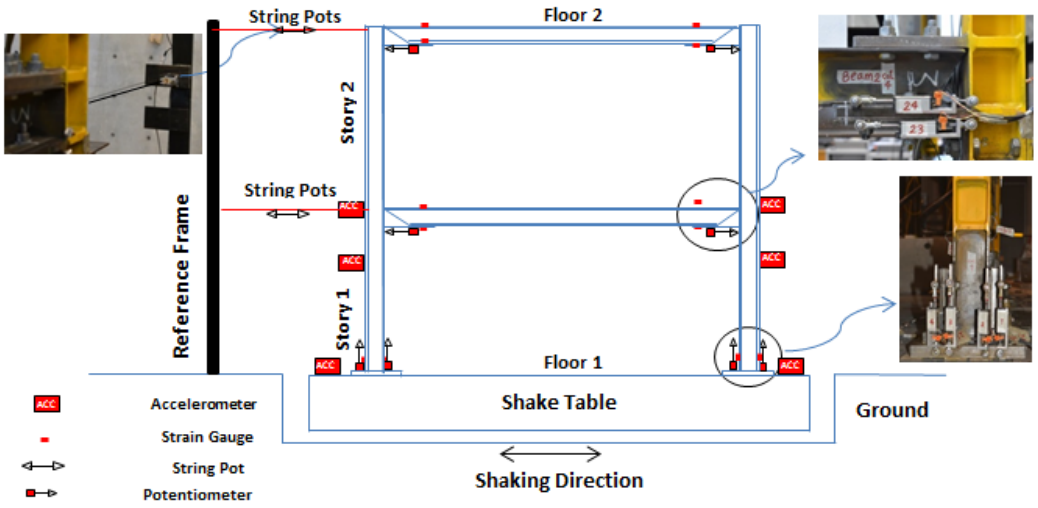

Figure 6-8: Instrumentation arrangement

(a) Beam ends (b) Base Column

Bolt Load Cell **Bolt Load Cell**

Figure 6-9: Bolt Load cells to measure the bolts tension

6.5. Test Protocols

The testing input was a set of 6 earthquake ground motions selected from both NZ local earthquake events (Bradley and Cubrinovski, 2011) and the NGA database (Campbell and Bozorgnia, 2008) as shown in Table 6-3. The time-step of each ground motion was reduced by a factor of 0.7 to fulfil similitude requirements and

to ensure similar peak acceleration. Figure 6-10 compares the NZ code (NZ1170.5) spectra with spectral acceleration of ground motions.

Table 6-3: Ground motions (Unscaled properties)

No	EQ name	Station	Orientation	Date	M_w	PGA (g)	PGV (mm/s)	PGD (mm)
1	Christchurch, NZ	CCCC	N-S	22/02/2011 12:51pm	6.2	0.49	480	100.8
2	Christchurch, NZ	REHS	N-S	22/02/2011 12:51pm	6.2	0.71	587	143.8
3	Northridge, US	Sylmar	N-S	1994	6.7	1.02	467.6	110.9
4	Kobe, Japan	KJM	N-S	1995	6.9	0.82	569.1	86.7
5	Tabas, Iran	Tabas	N-S	1978	7.4	0.85	694.5	175.7
6	Bam, Iran	Bam	N-S	2003	6.6	0.81	868.84	166.7

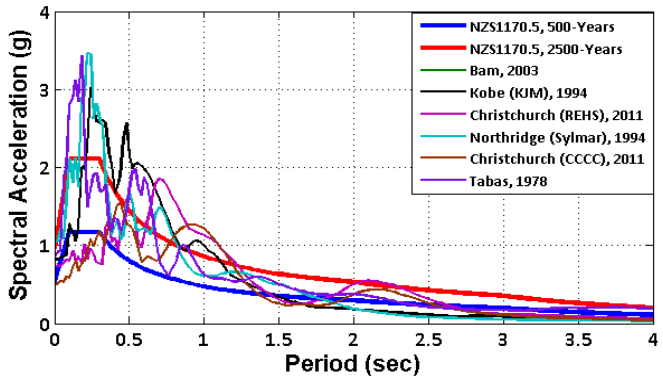

(b) Spectral Acceleration

Figure 6-10: Spectral Acceleration of ground motions compared with NZ Code Spectra (NZ1170.5), (3.4% damping, Z=0.4, Soil C, S_p=1.0), Time scale=0.7.

6.6. SHAKE TABLE RESPONSE

6.6.1. **Dynamic characteristics of the test model**

Snap-back (free vibration) tests were performed on the test structure to determine the natural period and damping ratio of the structural system before the shake table excitations were applied. The top floor of the model was pulled from both sides to a displacement of about 3mm, then it was released. Figure 6-11 shows the fundamental period of the structure which was found to be 0.47s. The damping ratio was calculated by Eq. 6-7, which was found to be 3.4%. Torsional displacements of the frame were negligible (<0.1%).

$$\xi = \log\left(\frac{A_0}{A_1}\right)/2\pi \qquad (6\text{-}7)$$

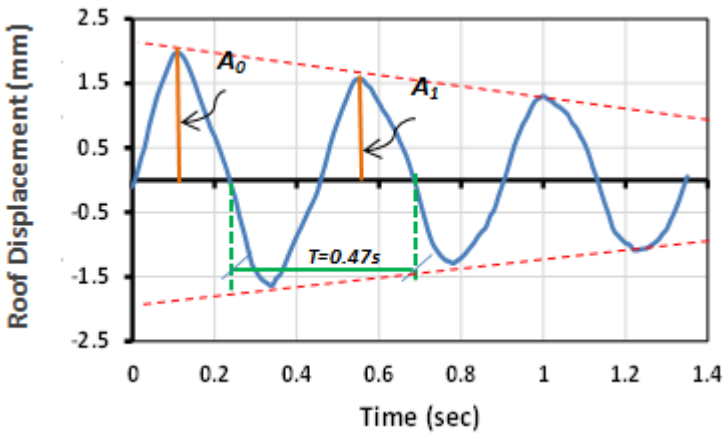

Figure 6-11: Free Vibration Response

6.6.2. **Earthquake Records Response**

6.6.2.1. Peak Displacement Response

Figure 6-12 shows how peak roof displacement response of the structure changes with spectral displacement of different ground motion records with different intensity levels (α_a=50%, 75% and 100%). It shows that for most of the records with low intensity levels (α_a=50%), the spectral displacements of the records was close to, but generally less than, the peak displacement of the structure. Also, with increasing ground motion intensity the peak roof displacement of the structure increases relative to the spectral displacement of the records. These effects are because: (i) the multi-storey structure mass centroid is below the roof level, (ii) higher mode effects occur, (ii) the structure has non-linear behaviour; and (iii) the record pulse characteristics may increase the inelastic response.

6.6.2.2. Base Shear Response

Floor design forces at any time were obtained by multiplying the floor accelerations by the floor mass. The building base shear at any time was obtained by summing these together. Figure 6-13 shows some base shear vs. roof displacement plots under different ground motions. It is compared with a bi-linear approximation with a post-elastic stiffness factor, *r*, of about 0.3 as shown by simple red lines.

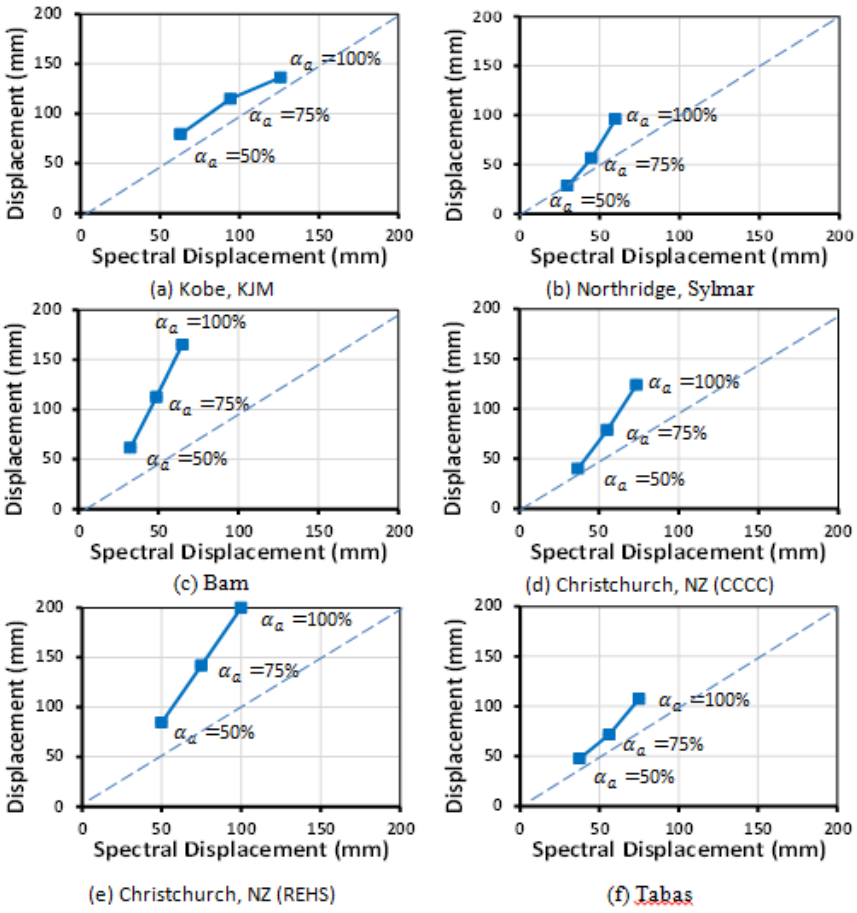

Figure 6-12: Roof Displacement Variation with Spectral Displacement

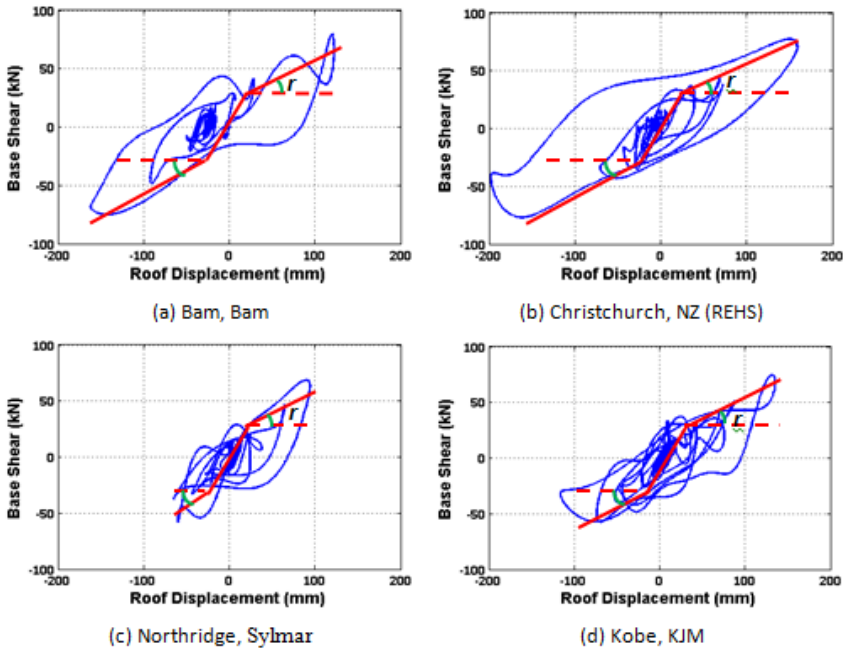

Figure 6-13: Roof displacement vs Base shear

6.6.2.3. Peak and Residual Drift Response

Figure 6-14 shows the peak and residual drift response of the structure over the height under different ground motion records with different intensity levels. The frame was manually returned to its initial vertical position, and new bolts were inserted and tightened before each run. The number shown after "Residual and Peak Drift" is the record acceleration scale factor considered. Peak drifts are generally similar at both floor levels. Often these occur at similar times indicating that the structure moves with an almost linear pattern with little drift concentration (i.e. the DCF is close to unity) as shown in Table 6-4 based on the calculation in Eq. 6-5. It may also be seen that up to a peak drift response of 3% the residual drift response is not more than 0.2%, but with increasing the peak drift response up to 6.0%, the residual drift response increases up to 0.7%.

To verify the results, the residual drift is also calculated by Eqs. 6-3 and 4. Here the ductility, μ, post elastic stiffness ratio, *r*, and yield displacement, D_y, are calculated from Figure 6-13. The ductility, μ, is taken as the maximum peak displacement, D_{max}, (which is about 150mm) divided by yield displacement, D_y, (which is about 25mm). Therefore, the ductility, $\mu = D_{max}/D_y$ = 150/25 = 6; and post elastic stiffness ratio is 0.3. The D_{mr} is 58.5mm according to Eq. 6-4, and D_{rr} is 0.25 for a ductility of 6 from Eq. 6-3. Therefore, the average residual displacement, D_r, is 14.6mm. Moreover, to calculate the drift, the equivalent height of SDOF substitute structure, H_e, is considered from the centre mass of the structure to the ground level which is 2.4m. Therefore, the residual drift demand,

is $\delta_r = D_r/H_e = 14.6mm/2400mm = 0.6\%$. This value is consistent with the value was obtained from the shake table tests shown in Table 4.

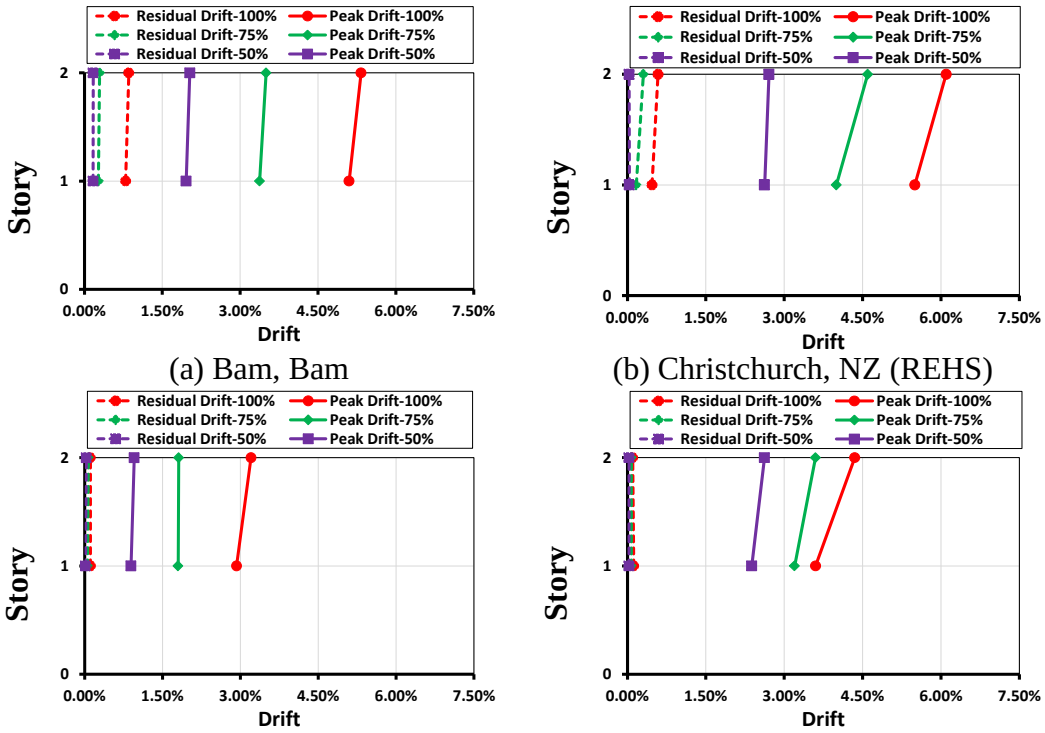

(a) Bam, Bam (b) Christchurch, NZ (REHS)

(c) Northridge, Sylmar (d) Kobe, KJM

Figure 6-14: Peak and Residual Storey Drift Response

Table 6-4: Drift concentration factor,* DCF*, at 100% of each record

EQ	Max. Roof Drift	Max. Interstory Drift Ratio	Max Residual Drift Ratio	*DCF* at Peak Drift
Bam, Iran	5.31%	5.20%	0.72	0.98
Northridge (Sylmar)	3.13%	3.21%	0.11	1.03
Christchurch (REHS)	6.25%	6.10%	0.59	0.98
Kobe (KJM), Japan	4.38%	4.35%	0	0.99

6.6.2.4. Asymmetric Friction Connection (AFC) Behaviour

Figure 6-15 shows the moment rotation relationship at the beam end (1st floor, front frame, North end, previously shown in the Figure 6-6) during different earthquake records. In addition, a red line is provided. It is used to represent key feature of behaviour especially for a largest displacement cycle behaviour firstly in a positive direction then in negative direction. It is defined empirically based on the observe response to the Bam record in Figure 6-15a where there is almost monotonic behaviour initially. For the other records, the first and second lines have the same magnitude and slope, the third line is extended to the peak positive displacement and the unloading on the 4th line has the same magnitude and slope. The 5th line has same slope, but the magnitude of point (e) is dependent on magnitude at point (c) which is explained in next paragraph and the last line is extended to the peak negative displacement.

The hysteretic behaviour of AFC can be defined by 5 different points. Here at Point (a) sliding initiates between bottom flange plate and beam flange, and at Point (b) sliding initiates between cap plate and beam flange. In both stages flange plate prying also occurred. This prying increases the moment resistance. This was not explicitly considered in the model described by MacRae et al. (2010) for beam-end AFCs as shown in Figure 6-3. The moment force at Points (a) and (b), (M_a=3kN.m and M_b=7kN.m) are the same for all records. At Points C the maximum positive rotation occurred causing the moment force at Point (c), M_c, to be vary depends on different events (e.g. $M_c \approx$ 10kN.m for Bam record). Points (d) and (e) occur during reverse loading. First, initial sliding occurs between the

bottom of the beam flange and the bottom flange plate (d to e). At larger reverse loading displacements sliding of cap plate occurs (from e). Point (e) does not occurr at the same absolute moments as Point (b). This is different from the model described by MacRae et al. (2010) for thr beam end AFC where the sliding occurs with the same absolute moment in each direction as shown in Figure 6-3 and prying were effectively small.

After point (c), unloading and the loading in the reverse direction occurs. The amount of unloading and loading moment force before initial sliding in the reverse direction is M_a. Therefore, the moment at Point (d), M_d, equals (M_c-2M_a). Also, the moment force at Point (e), M_e, equals to (M_c-2M_b). For example for Bam records, M_d equals to 4kN.m (10-2×3=4) and M_e equals to -4kN.m (10-2×7=-4). Purple dashed horizontal lines in Figure 6-15 shows the sliding moment associated with first and second sliding at the beam ends at Points (a) and (b). Also, green dashed horizontal lines in Figure 6-15 shows the sliding moment associated with first and second sliding in the reverse loading at the beam ends at Points (d) and (e).

A bottom flanges force when second sliding initiate (point c) can be calculated by the moment divided by the distance between centre of flange plates, $M/(d+t_{fp})$ = 7kNm/0.102m = 67 kN. The effective friction coefficient , μ, computed as the flange sliding force divided by the sum of the bolt proof loads divided by the number of interfaces (MacRae, 2010), for the M12 Grade 8.8 structural bolts is 67kN / (45kN/bolt x 4bolts x 2interfaces) = 0.19 where 45kN is the proof load.. This is close to the value recommended for design of 0.21 and it is greater than the

minimum dependable value of ϕ0.21 = 0.7 x 0.21 = 0.15 (MacRae et al. 2010). The peak moment of 12 kN.m obtained is associated with an effective friction coefficient of 0.28, which is close to the overstrength value recommended for design of ϕ0.21 = 1.4 x 0.21 = 0.30 (MacRae and Clifton, 2015).

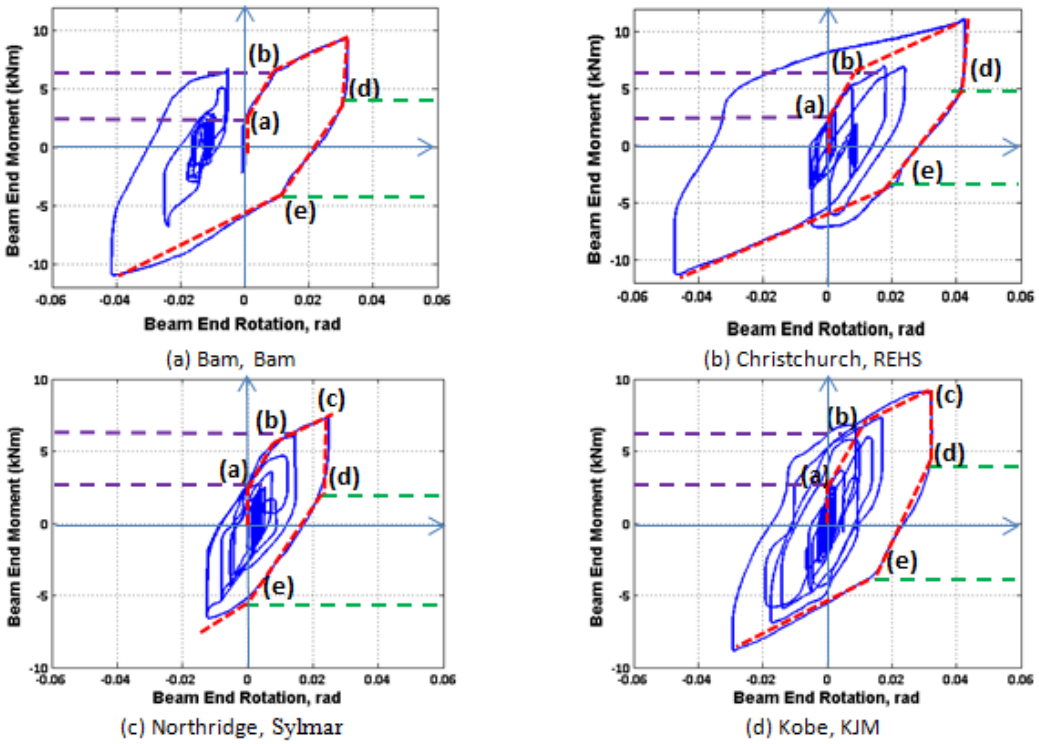

Figure 6-15: Hysteretic behaviour of AFC at beam end under different ground motions with Acc. Scale of 1.0.

Figure 6-16a and 6-16b show the hysteretic behaviour of the AFC at the 1st floor, front frame, north beam end (previously shown in Figure 6-6) subject to the Christchurch (CCCC) record with 50% and 100% acceleration scales. It indicates that the hysteretic behaviour of the AFC at the beam end for 100% scale shaking can be represented by a tri-linear relationship, while for lower shaking levels, only the first 2 stages of this relationship (i.e. a bi-linear relationship) represents the behaviour. It is because two friction surfaces in the connection do not start to slide

at the same time as shown in Figure 6-17. At large displacements, sliding of cap plate occurs. Here cap plate started to slide when beam sliding is more than 1mm which is about beam rotation of 1.0% as shown in Figure 6-17.

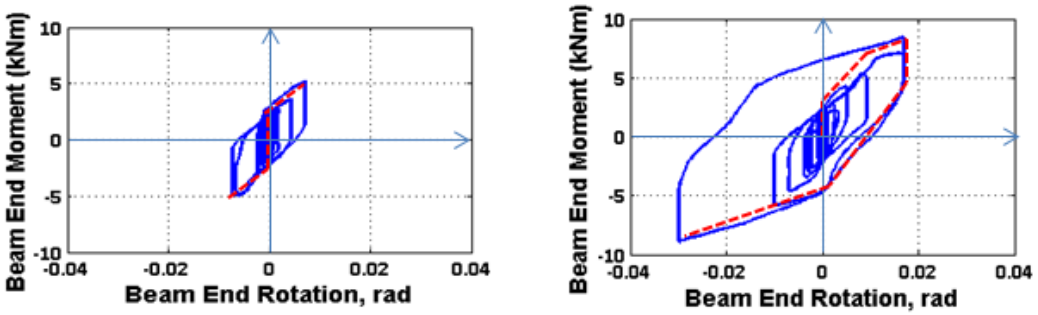

(a) Acc. Scale 50% (b) Acc. Scale 100%

Figure 6-16: Hysteretic behaviour of AFC at beam end under Christchurch (CCCC) record

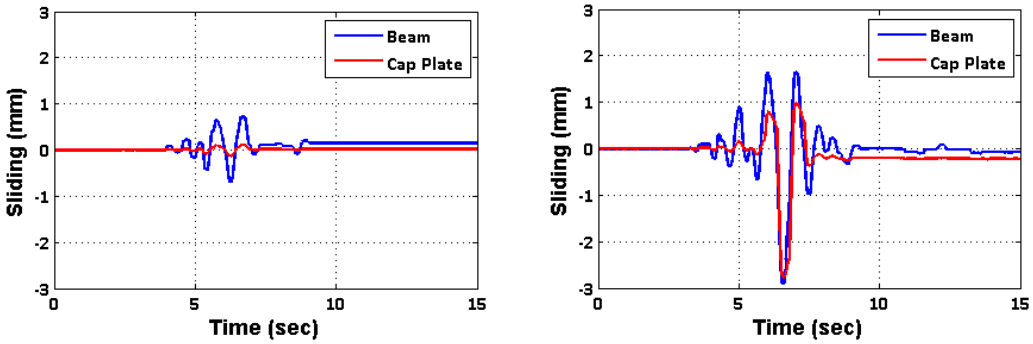

(a) Acc. Scale 50% (b) Acc. Scale 100%

Figure 6-17: Beam and Cap Plate sliding relative to Slotted plate vs time (50% Christchurch (CCCC) record)

Figure 6-18 shows the hysteretic behaviour of the AFC at a base column joint (shown in the Figure 6-6, North end, front frame). In addition, a red line is provided. It is used to represent key feature of behaviour especially for largest displacement cycle behaviour. This is consistent with by Bourzouie et al., 2015a which is essentially bilinear with a high initial rotation sliding stiffness.

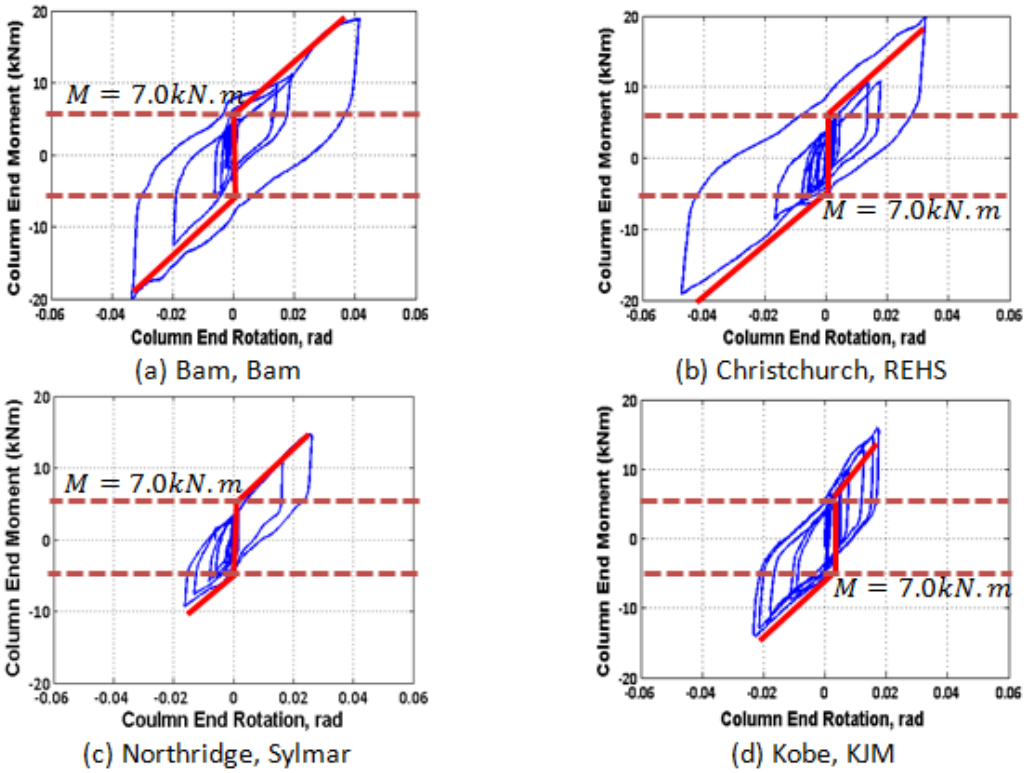

Figure 6-18: Hysteretic behaviour of AFC at column base under different ground motions, Acc. Scale of 1.0.

The moment resistant of the connection results from three components, (i) the moment from axial force (M_{Axial}), (ii) the moment resulting from sliding friction (M_{Slide}), and (iii) the elastic-prying moment (M_{Prying}). The initial column base AFC sliding occurred at a column moment of about 7kN.m. At this stage, the moment resistant results of only M_{Axial}, and M_{Slide} and there is not much prying moment because of small amount of rotation. Based on Eq. 6-2, M_{Axial} is $P \times D_{Axial}$=50×50=2.5kN.m where D_{Axial} is the perpendicular distance from the centre of axial force to the neutral axis and, P, is the peak axial force. The rest of the moment resistant is due to Sliding moment, M_{Slide} , due to friction force which equals to 4.5kN.m.

After initial sliding, the prying effect also increases the column moment demand. For example for 1.5% rotations, column moment is about 10.0kN.m. Here, 2.5kN.m (25%) of this amount is due to the axial force (M_{Axial}), 4.5kN.m (45%) is because of friction (M_{Slide}), and 3.0kN.m (30%) is due to the prying effect (M_{Prying}). After 2% column base rotation, the cap plate sliding also occurred at the base column with an increase in sliding and prying moment forces and this is consistent with Bourzouie (PhD thesis, 2015).

A sliding friction force can be calculated by the friction moment divided by the distance between point of rotation and sliding surface, $M/(d+t_{fp})$ = 4.5kNm/0.105mm = 42kN. The effective friction coefficient at initial sliding using Eq. 6-2 after considering the effect of axial force, computed as the flange sliding force divided by the sum of the bolt proof loads for the M12 Grade 8.8 structural bolts of 45kN, divided by the number of interfaces is = 42kN / (45kN/bolt x 4bolts x 1interfaces) = 0.23. The friction coefficient for the base column connection (shown in the Figure 6-6, North end, front frame) is slightly higher than for the beam end AFC (1st floor, front frame, North end, shown in the Figure 6-6). There are a number of possible reasons for this difference. It may be related to the surface conditions of the shim plates. The shim plates used for base columns were connected to the columns during first days of assembling of the structure which took about three months. However, the shim plates used for end beam were the last part added to structure before starting the tests. Therefore, the humidity condition of the lab could make the plates rusted and change the surface condition of the plates which increased the friction coefficient. It may also be related to the higher sliding displacements on the SHJ rather than at the column

base (where both sides slide a smaller amount each and the bolt angle is reduced leaving a smaller component of axial bolt force in the longitudinal direction of the beams).

6.6.2.5. Bolt Tension Force

Donut load cells were placed between bolt heads and the plates to measure bolt tension during plate sliding. All load cells were calibrated before installing in the connections. Their accuracy was checked by applying compression force and monitored the load cell readings. The load cells were sandwiched between two Grade 350 steel washers to maximize load cell reading accuracy. The nut rotation method, with half a turn after snug tightening according to NZS3404 (2007), was used to tighten bolts. This resulted in a bolt tension force of 45 to 50 kN. This is greater than the proof load of 45kN. Figure 6-19 shows the tension force of the bolts during sliding under Bam, Christchurch (REHS), Northridge (Sylmar) and Kobe (KJM) ground motions (α_a=100%). It shows that bolt tension changed during sliding. However, when the plates return back to their initial position, and the bolts become more vertical, the bolt tension force reduces as shown in Figure 6-19c and 20d (MacRae et al., 2010). This is because increasing bolt tension force increases the bolt elongation and the possibly of yielding. Such a yielded bolt will have permanent elongation and some reduction in tension force, as was observed as shown in Figure 6-19a and 20b. It shows that the maximum reduction in tension force after finishing the sliding, is about 10% (5kN/(45kN=proof load)=11%). This reduction for the case by 5.0% to 6.0%

drifts (Bam and Christchurch (REHS) records with acceleration scale of 100%). For cases by about 4% drift (Northridge and Kobe records with acceleration scale of 100%) there was almost no residual reduction force in tension bolts as shown in Figure 6-19.

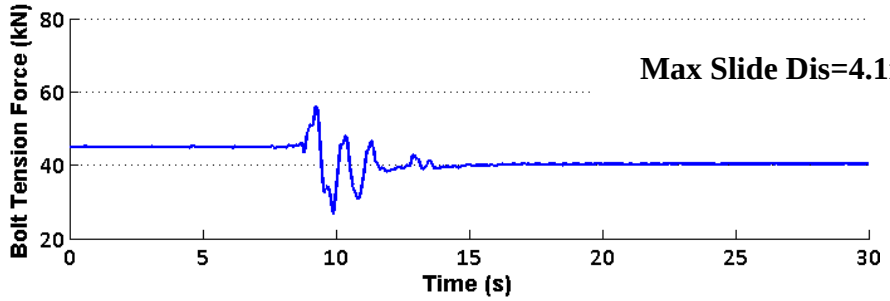

(a) Bam, Bam

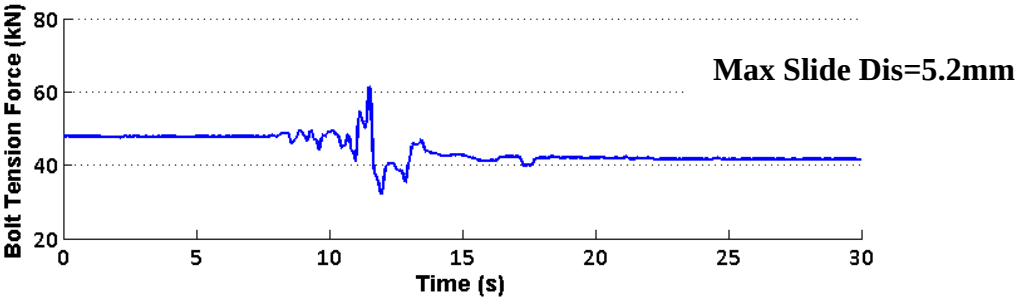

(b) Christchurch, NZ (REHS)

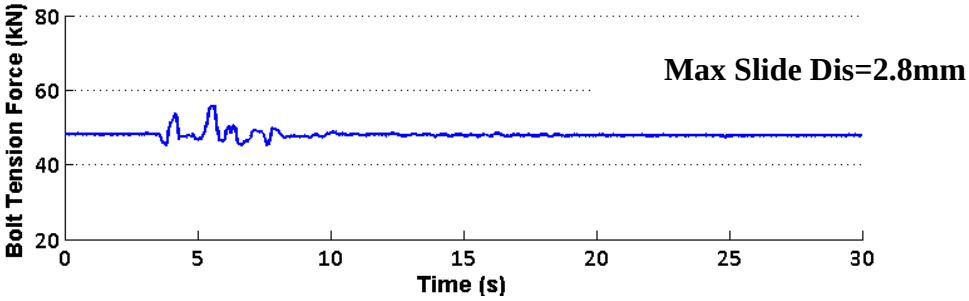

(c) Northridge, Sylmar

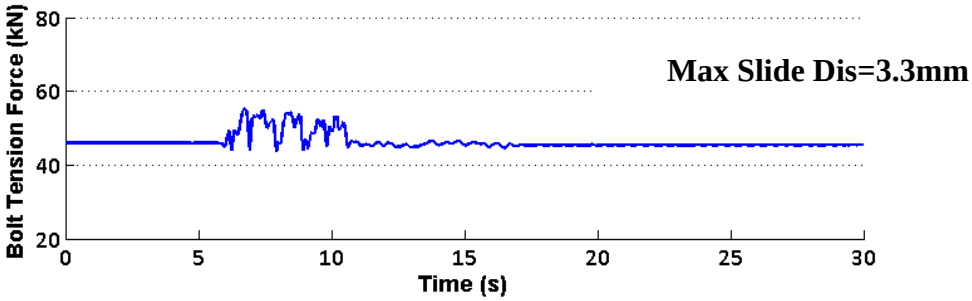

(d) Kobe, KJM

Figure 6-19: Changing of tension force of the bolts during sliding under different ground motions.

6.7. NUMERICAL SIMULATION

A simple two-dimensional model as shown in Figure 6-20a was created using the software OpenSees for simulating the nonlinear response under earthquake excitations. The 2-D model was appropriate as torsional displacements of the frame were less than 0.1% of the peak values. A simple elastic element was used to model the elastically responding 100UC14.8, Grade 300 beams and columns. Zero-length elements were used to capture friction connection moment-rotation behaviour. Lateral and vertical displacements of the both ends of the connections were constrained to the beams and columns. From modal analysis the fundamental period of the structure is 0.46s which is almost has a same value from snap back test of 0.47s as described above in section 6.1.

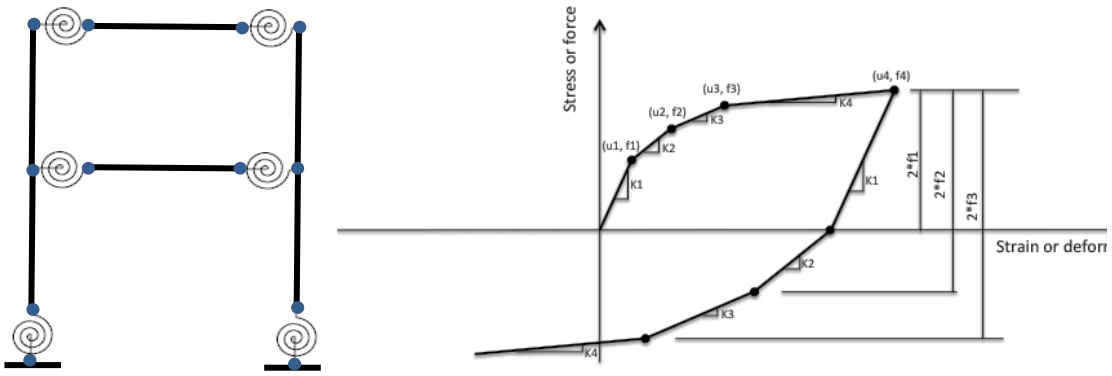

(a) Numerical Model ***(b) MultiLinear Material***

Figure 6-20: Numerical Simulation

6.7.1. **Beam End Connections**

The hysteretic behaviour of the AFC at beam ends is approximated reasonably by a trilinear model following Section 5.2. To model this behaviour *MultiLinear Material* from OpenSees is used as shown in Figure 6-20b. The parameters were provided with following values based on the experimental results. They were Point (a): (M=3kN.m, θ=0.01%), Point (b) : (M=7kN.m, θ=1.0%), and Point (c) : (M=11kN.m, θ=4.0%). As shown in Figure 6-15 Point (a) describes when initial sliding occurrs; Point (b) is when the second sliding occurs, and Point (c) is where the maximum positive rotation is occurred. By specifying these three points in forward direction loading, the model cyclic loading is also defined as shown in Figure 6-20b. This behaviour is consistent with the beam end behaviour described in Section 5.2.

6.7.2. **Base Column Connection**

A bilinear curve is used to approximate the AFC base column hysteretic behaviour in Section 5.2. The OpenSees *Steel02 Material* (Giuffre-Menegotto-Pinto model) is used. Based on the experimental results as shown in Figure 6-18.

The main parameters of the model were; (i) an initial sliding base column moment of 7kN.m; (ii) a base column initial rotational stiffness of 30EI/L to represent rigid fixed base conditions (Eurocode 3, 2005), and (iii) a column post elastic stiffness of 7%. Moreover, the Giuffre-Menegotto-Pinto model parameters controling the transition from elastic to plastic branches were considered to be 18.5 for R_0, 0.928 for cR_1 and 0.15 for cR_2 (Menegotto-Pinto, 1973).

6.7.3. **Numerical Simulation and Experimental Comparison**

The numerical model was provided with initial mass proportional Rayleigh damping with a damping ratio of 3.4% based on the test results were assigned to the first 2 modes of the structure. The ground motions used in the experimental study were applied to the numerical structural model.

Figure 6-21 shows that the first level drift and acceleration time histories, and beam end and base column moment-rotation hysteresis curves, compared well with the test results. The simulated moments in the two final small cycles in Figures 22c and 22d were higher than in the experiments. This may be due bolt tension force loss after big cycle of rotation in the joint. which was not considered in the simulation. This does not have big effect on general response of the structure. Thus, the simulation seemed to capture key peak strength and deformation parameters of the seismic response of the structure considered.

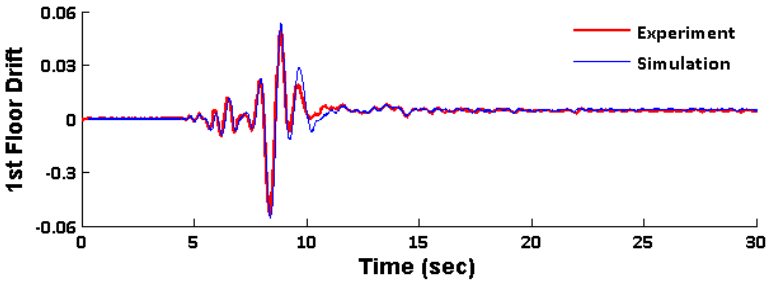

(a) Drift

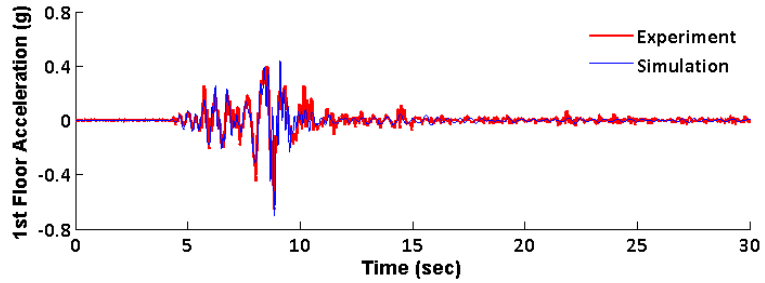

(b) Acceleration

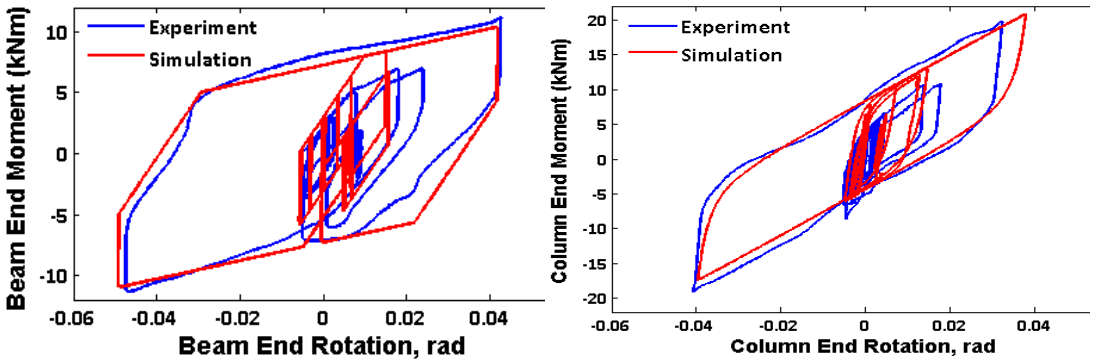

(c) Beam End (d) Column Base

Figure 6-21: Comparing experimental with numerical simulation under Christchurch (REHS) 2011 records (ACC_{scale} = 100%).

Table 6-5 compares simulated and experimental model peak and residual drifts for records with different acceleration scales. The most difference between the simulation and test was about 10%. Residual drifts less than 0.1% are reported as zero in the table.

Table 6-5: Comparing the peak and residual drift response of the simulated and experimental model.

No	Earthquake name	ACC_{scale}	Peak 1st Floor Drift		Peak 2nd Floor Drift		Residual 1st Floor Drift		Residual 2nd Floor Drift	
			Test	Simu	Test	Simu	Test	Simu	Test	Simu
1	Christchurch (CCCC)	50%	1.25%	1.1%	1.29%	1.15%	0	0	0	0
1	Christchurch (CCCC)	75%	2.39%	2.4%	2.63%	2.6%	0	0	0	0
1	Christchurch (CCCC)	100%	3.91%	4.0%	3.99%	4.1%	0.1%	0.12%	0.1%	0.13%
2	Bam, Iran	50%	1.9%	1.7%	2.03%	1.75%	0.17%	0.2%	0.19%	0.25
2	Bam, Iran	75%	3.3%	2.9%	3.5%	3.2%	0.27%	0.3%	0.29%	0.35%
2	Bam, Iran	100%	4.9%	4.7%	5.2%	4.8%	0.69%	0.65%	0.72%	0.7%
3	Northridge (Sylmar)	50%	0.89%	0.95%	0.96%	1.1%	0	0	0	0
3	Northridge (Sylmar)	75%	1.8%	1.65%	1.81%	1.8%	0	0	0	0
3	Northridge (Sylmar)	100%	2.93%	2.8%	3.21%	3.0%	0.11%	0.06%	0.11%	0.085%
4	Kobe (KJM),	50%	2.38%	2.1%	2.62%	2.39%	0	0	0	0
4	Kobe (KJM),	75%	3.2%	2.85%	3.6%	3.3%	0	0	0	0

4	Kobe (KJM),	100%	3.6%	3.3%	4.35%	4.23	0	0	0	0
5	Tabas, Iran	50%	1.47%	1.5%	1.7%	1.6%	0.1%	0.135%	0.12%	0.13%
5	Tabas, Iran	75%	2.4%	2.3%	2.6%	2.5%	0.12%	0.15%	0.16%	0.2%
5	Tabas, Iran	100%	3.7%	3.6%	3.9%	3.7%	0.18%	0.25%	0.24%	0.3%
6	Christchurch (REHS)	50%	2.63%	2.3%	2.71%	2.4%	0	0	0	0
6	Christchurch (REHS)	75%	4.0%	3.6%	4.6%	4.1%	0.18%	0.225%	0.2%	0.256%
6	Christchurch (REHS)	100%	5.5%	5.4%	6.1%	6.0%	0.47%	0.42%	0.54%	0.5%

6.8. OVERALL STRUCTURAL PERFORMANCE

From the ground motions considered, where peak drifts were up to 6%, there was no significant member damage. No column web or flange buckling was observed, and all flanges plates welded to the columns and base plates showed no sign of yielding or paint flaking. After very severe shaking, when there was bolt tension force reduction, new bolts were inserted and tightened before each run. Figure 6-23a shows the condition of AFC bolts after different levels of shaking. Bolts (i) and (ii) had undergone small inelastic cycles, so there is almost no shank damage. However, Bolts (iii) and (iv) underwent a significant number of large inelastic cycles which caused Bolt (iii) plastic deformation and Bolt (iv) fracture just below the bolt head. Figure 6-23b also shows an AFC shim after a number of inelastic cycles. The shims felt smooth with no gouging or visual damage.

Residual displacements were often small, especially when peak drifts were less than 2.5%. When there were residual displacements, usually from higher peak drifts, manual restraightening was carried out and the frame was brought back to its initial straight position. The structural performance was repeatable with peak

and residual displacements errors less than 2.0% for straight structures subject to same record. This is shown for Bam ground motion in Figure 6-22. For these reasons, the overall structural performance was considered to be excellent.

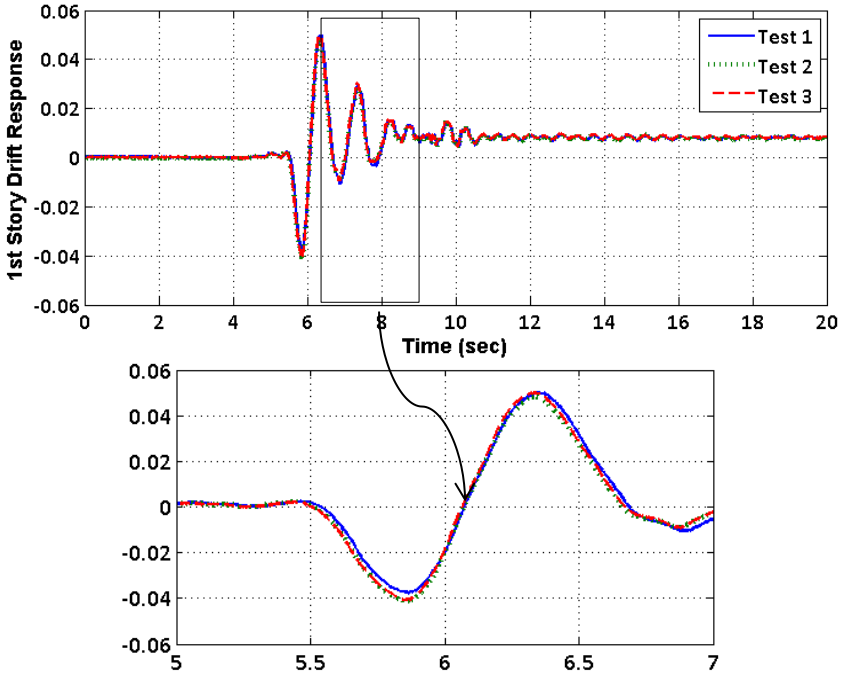

Figure 6-22: Consistent peak and residual drift under repeatable shaking (Bam records, 100%).

(a) Tested bolts (b) Tested shim

Figure 6-23: Beam degraded shim (between beam and flange plate) and proof-loaded bolts after test.

6.9. Conclusion

This chapter describes seismic shake table tests of a half-scale two-storey steel building incorporating asymmetric friction connections (AFCs) at steel column bases and beam-column joints. Based on the experimental results obtained, the following conclusions can be drawn:

1) The structure peak displacement response was consistent with that from the ground motion spectral displacements. Drift concentration of the structure is also calculated to show the structure moved over linearly. Also, the residual displacement is shown to be consistent with residual displacement predictions. For peak drifts up to 6.0%, the residual drift is not more than 0.7%.
2) The hysteresis loop shapes for beam-column and base-column joints indicated tri-linear and bilinear characteristics respectively. The effective friction values were consistent with that recommended by MacRae et al (2015), with measured nominal values of 0.21 and 0.23 for beam ends and column bases respectively. Moreover, there was almost no bolt tension force reduction after sliding for drifts less than 4% for the structure tested. For cases with peak drifts of 6%, there was only 10% strength reduction at the end of the sliding.
3) A computational numerical model was developed and compared well with test results with a tolerance of about 10%.
4) The tests indicated no significant member damage even in drifts as high as 6%. The behaviour was repeatable and could be modelled with a tolerance

of less than 2.0%. Residual displacements were generally small, but even when there were residual displacements, manual restraightening allowed the structure to be fully repaired. Therefore, it can be considered to be a low-damage structure.

6.10. REFERENCES

Yang TS, Popov EP. "Experimental and analytical studies of steel connections and energy dissipators", Report No. UCB/EERC-95/13, Earthquake Engineering Research Centre: Berkeley, California. 1995.

Clifton, G.C. "Development of Perimeter Moment-Resisting Steel Frames Incorporating Semi-Rigid Elastic Joints, New Zealand National Society for Earthquake Engineering Conference,1996. 177-184.

Clifton C. "Semi-rigid joints for moment-resisting steel framed seismic-resisting systems", PhD Thesis, Department of Civil and Environmental Engineering, University of Auckland.2005.

MacRae, G. A., Clifton, G. C., Mackinven, H., Mago, N., Butterworth, J., and Pampanin, S. "The sliding hinge joint moment connection", NZSEE Bull., 2010. 43(3), 202–212.

Borzouie J, MacRae G. A., Chase J. G., Rodgers G. W., and Clifton G. C. "Experimental Studies on Cyclic Performance of Column Base Strong Axis–Aligned Asymmetric Friction Connections", Journal of Structural Engineering, 2015, DOI: 10.1061/(ASCE)ST.1943-541X.0001327.

Chanchí, J. C., MacRae, G. A., Chase, J. G., Rodgers, G. W., and Clifton, C. G. "Behaviour of asymmetrical friction connections using different shim materials", NZSEE Conf., New Zealand Society for Earthquake Engineering, Wellington, New Zealand.2012.

Chanchí, J. C., Xie, R., MacRae, G., Chase, G., Rodgers, G., and Clifton, C. "Low-damage braces using asymmetrical friction connections (AFC)", NZSEE Conf., The New Zealand Society for Earthquake Engineering, Auckland, New Zealand.2014.

Borzouie J, MacRae G. A., Chase J. G., Rodgers G. W., and Clifton G. C. "Experimental studies on cyclic performance of column base weak axis aligned asymmetric friction connection", 2015, Journal of Constructional Steel Research, 112, 252–262.

MacRae, G. A. and Kawashima, K. "Post-earthquake residual displacements of bilinear oscillators", Earthquake Engineering and Structural Dynamics, 1997, 26, 701-716.

MacRae, G. A., Kimura, Y., and Roeder, C. W. "Effect of Column Stiffness on Braced Frame Seismic Behavior", Journal of Structural Engineering, ASCE. 2004, March, 130(3), pp. 381-391.

NZS 1170.5. "Structural Design Actions Part 5: Earthquake Actions New Zealand". Standards New Zealand: Wellington, New Zealand. 2016.

NZS3404, "Steel Structures Standard", Standards New Zealand: Wellington, New Zealand. 2007.

Bradley B. A. and Cubrinovski M. "Near-source strong ground motions observed in the 22 February 2011 Christchurch earthquake", Seismological Research Letter, 2011. 82(6): 853-865.

Campbell, K.W., Bozorgnia, Y. “NGA ground motion model for the geometric horizontal component of PGA, PGV, PGD and 5% damped linear elastic response spectra for periods ranging from 0.01 to 10s”, Earthquake Spectra, 2008, 24 (1), 139-171.

MacRae, G. A., Clifton, G. C. “Research on seismic performance of steel structures”, Steel Innovations 2015 Conference Auckland. 2015.

OpenSees, “Open System for Earthquake Engineering Simulation-Home”, 2015, Page: http://opensees.berkeley.edu/.

Menegotto, M., Pinto P.E. “Methods of analysis of cyclically loaded RC plane frames including changes in geometry and non-elastic behaviour of elements under normal force and bending”, 1973, Preliminary Report IABSE, Vol 13.

Chapter 7: Structural Strengthening/Stiffening with Tension Braces Using Aftershocks – Shaking Table Study

7.1. Introduction

Buildings can have post-earthquake residual deformations. If during an aftershock, or subsequent earthquake, they experience increased displacements, they have a greater probability of collapse and of affecting buildings in their proximity. The likelihood of increased displacement in the direction of residual displacements for general ground motions may be greater than 50% as a results of P-Δ affects and other effects. To mitigate further movement in the direction of residual displacements, structural modification by means of stiffening/strengthening structure in that direction only may be helpful. No study is known to have been performed to discourage buildings from having further displacements in the same direction during aftershocks which could possibly lead to collapse.

It may be seen from the above discussion that there is a need to develop methods to discourage buildings from having increased displacements during aftershocks.

This study seeks to address this need by using the shake table testing and numerical analyses of a half-scale two story steel frame under a sequence of shakes considering different bracing system interventions applied to the structure between shakes. In particular, answers are sought to the following questions:

1) For out-of-straight structure, what is the effect of different structural modifications on the subsequent response?

2) Can the behaviour be modelled?

3) Of the mitigation methods considered which ones work best?

7.2. Literature Review

Dynamic stability concepts indicate that structures with permanent displacements (i) tend to yield toward the origin if they have a positive effective post-elastic stiffness ratio, and (ii) tend to increasing displacements in one direction if they have a negative effective post-elastic stiffness ratio (MacRae, 1994). The post elastic stiffness is affected by the strain hardening behavior, local member degradation effects and global P-Δ effects. Those with fatter hysteresis loops tend to have greater permanent displacements than those with more pinched loops.

For multistory structures, Rad et al. (2015) have shown that undamaged buildings constructed with initial residual displacements tend to increase peak and residual displacement demands in the initial residual displacement direction due to earthquake shaking. Analyses of buildings under September 2010 and February 2011 excitations of the Canterbury Earthquake Sequence (Rad et al., 2015b) showed that residual inter-story drift response of the buildings is also increased in subsequent earthquake events. For example, the February event produced larger residual drifts after the September earthquake than when the February event was been applied alone. However, residual displacements do not always increase with

subsequent shaking as shown by the case of Pacific Tower in Christchurch where the residual displacement decreased from 60mm after the 2010 September event to 30mm after the 2011 February event (MacRae et al., 2015 & Clifton et al. 2011).

Still there is concern about the tendency for structures to have further displacements, or even collapse in subsequent earthquake events. For example, the 43m Gallery Apartment building next to the Christchurch Art Gallery (which was the civil defence headquarters following the Christchurch earthquakes) was damaged and leaning. It was quickly removed to mitigate risk to the Art Gallery. Also, buildings such as the Hotel Grand Chancellor (24 stories) and Park Terrace apartments were damaged and structures in their proximity were not permitted to be used until these two structures had been demolished.

The issues above do not relate only to structures which have suffered strength degradation. Some structures, such as those using friction connections and others that do not have strong self-centring characteristics, may be out-of-straight as a result of post-earthquake residual deformations.

There are different types of tension-only bracing systems that can be used to indicate the likelihood of further deformation in one direction. One is a simple steel slender rod bracing that yields in tension and buckles elastically in compression. In this tension-only bracing system, the plastic deformation on prior cycles will increase the unstressed member length and result in a dead-zone with take-up on subsequent cycles which is known as slackness characteristic as shown in Figure 7-1a. Another is a ratcheting brace (RB) which has been conceived to

address the slackness issues as shown in Figure 7-1b. This concept was originally referred to as a Grip ‘n’ Grab (GnG) device and was conceived by MacRae primarily for rocking walls and was modelled in a rocking system simulation (Gunning and Weston 2013). Then, it was further developed and tested by Cook et al. (2015). Here, during tensile loading, teeth grip the device and tensile force is applied to the specimen. Then, after loading in the compression direction, where it carries almost no force, there may be a region of no force in the positive direction until the teeth grip the device.

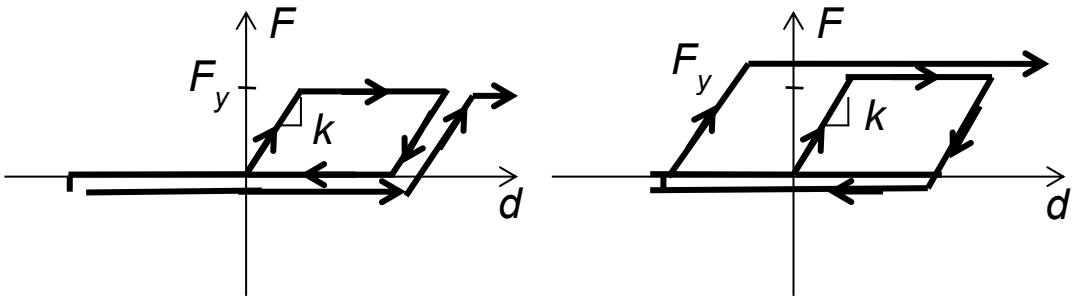

(a) Buckling Brace (b) Ratcheting Brace

Figure 7-1: Hysteretic models for braces

7.3. Test specimen

The test specimen is composed of two steel frames (yellow frame) with AFC connections at the base column and beam ends which was explained in Chapter 6, Section 6.3 and shown in Figure 6-6 and Figure 6-7.

Here, before the second shake the structure is fitted with two different tension-only braces in first story. One is a buckling brace as shown in Figure 7-2a, which has a slackness characteristic. The other one is ratcheting brace which does not

have slackness characteristic and takes up a tension force from near its last displacement as shown in Figure 7-2b. Both types of the brace have the same yield strength and stiffness in tension. Steel rods used in both braces were reinforcing bars with diameters of 16 and 12mm and yield strengths of 95 and 65kN. The hysteric characteristic of the two braces is shown in Figure 7-1.

(a) Buckling Brace

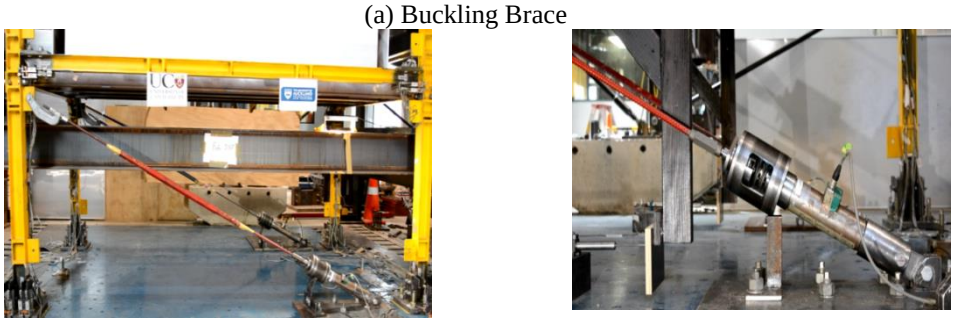

(b) Ratcheting Brace

Figure 7-2: Test Specimen

Moreover, since adding tension-only braces to the structure may causes over-straightening and significant residual drifts in the opposite direction, gapping braces (GB) were also considered in this study. This involved a ratcheting brace in conjunction with a buckling brace with a displacement gap in the other direction as shown in Figure 7-3 to prevent over straightening and help to re-centre the structure. The amount of gap is decided based on the amount of residual drift and it can be controlled by the nut end of the brace.

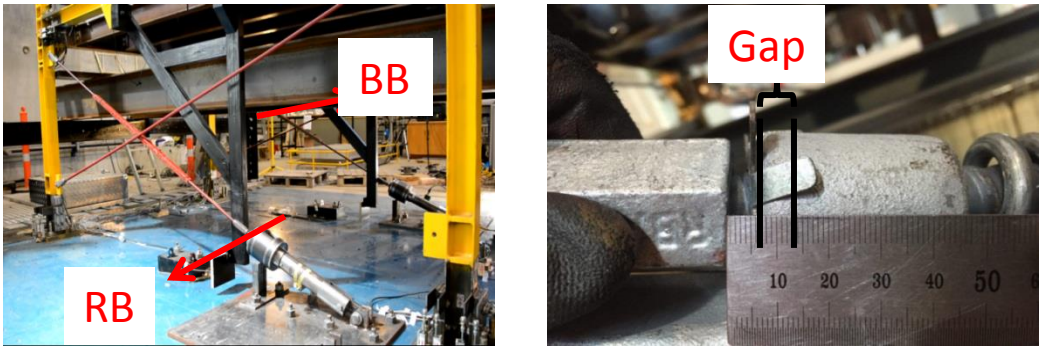

Figure 7-3: Gap brace system

7.4. Instrumentation

The instrumentation of the test frame consisted of a combination of string pots, accelerometers, and load cells which was explained in Chapter 6, Section 6.4 and Figure 6-8. Here, load cells were also used as shown in Figure 7-4 for each ratcheting device to measure the amount of the force going to the brace. Moreover, a strain gauge was attached for each steel rod to measure the strain in each brace.

Figure 7-4: Load Cell for Ratcheting Device

7.5. Test Protocols

The testing input was a set of 4 earthquakes ground motions selected from both NZ local earthquake events and the NGA database as shown in Table 6-3. Four different ground motions with different scales applied to the structure. The time-step of each ground motion was reduced by a factor of 0.707 to fulfil similitude requirements and to ensure similar peak acceleration. Figure 7-5 compares the NZ code (NZ1170.5) spectra with spectral acceleration of ground motions.

Table 7-1: Ground motions

No	EQ name	Station	Orientation	Date	M_w	PGA (g)	PGV (mm/s)	PGD(mm)
1	Christchurch,NZ	REHS	N-S	22/02/2011 12:51pm	6.2	0.71	587	143.8
2	Northridge, US	Sylmar	N-S	17/01/1994	6.7	1.02	467.6	110.9
3	Tabas, Iran	Tabas	N-S	16/09/1978	7.4	0.85	694.5	175.7
4	Bam, Iran	Bam	N-S	26/12/2003	6.6	0.81	868.84	166.7

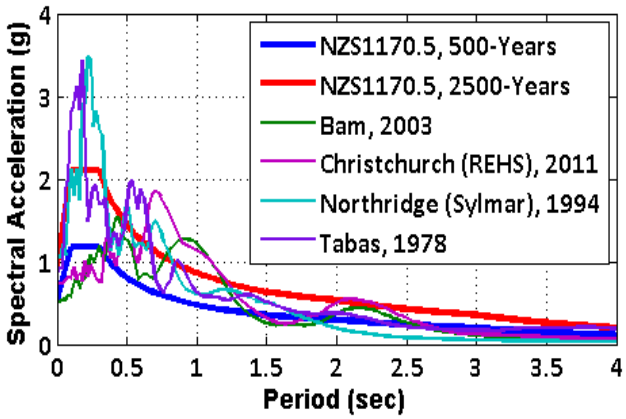

Figure 7-5: Spectral Acceleration of ground motions compared with NZ Code Spectra (NZ1170.5), (3.4% damping, Z=0.4, Soil C, S_p=1.0), Time scale=0.7.

7.6. Structural Response

7.6.1. *Peak and Residual Drift Response of the Frame with Brace*

Table 7-2 and Table 7-3 show the drift responses of the different storey of the structure under second shakes with and without braces. The Bam ground motion in the same direction as the 1st shake with 3 different ground motions were applied with acceleration scale of 1.0 or 0.5. Tests were not completed for some cases due to the lab constraints, so some cells in the table are blank. Residual drift (RD) is defined as a drift at the end of the 2nd shake and peak drift (PD) is defined as a maximum drift under the sequence of shakes (considering both 1st and 2nd shakes). Here, because the sequence of shakes did not increase the peak drift of the structure for most of the cases (except 100% Christchurch (REHS) record), the peak drift in Table 7-2 and Table 7-3 is same for different records and brace configuration. Table 7-2 and Table 7-3 show that when the frame with no brace (NB) was subjected to additional shaking with the same record the residual displacement decreased by -15% on average for the records used. Use of a buckling brace (BB) changed the residual drift -75% and did not push the frame in the opposite direction. Application of a ratcheting brace (RB) caused a residual displacement change of -260% implying that it caused significant residual displacement in the opposite direction. A gapping brace (GB) also changed the residual displacement by -150%.

Table 7-2: First story total peak and total residual drift response of the structure under sequence of shakes (First shake was 100% scale of Bam record with PD 0f 4.9% and RD of 0.7%).

2nd Ground Motions	Acceleration Scale (α_a)	1st Floor							
		No Brace		With BB16mm		With RB16mm		With GB16mm	
		PD*	RD*	PD	RD	PD	RD	PD	RD
Bam	1	4.9%	0.75%	4.9%	0.11%	4.9%	-2.8%	4.9%	-0.2%
	0.5	4.9%	0.7%	4.9%	0.63%	4.9%	-0.5%	4.9%	-0.1%
Christchurch (REHS)	1	5.5%	0.46%	5.5%	-0.8%	*-	-	-	-
	0.5	4.9%	0.55%	4.9%	0.35%	4.9%	-0.9%	4.9%	-0.68%
Northridge (Sylmar)	1	4.9%	0.36%	4.9%	0.35%	-	-	-	-
	0.5	4.9%	0.7%	4.9%	0.6%	4.9%	-0.2%	4.9%	-0.03%
Tabas	1	4.9%	0.6%	4.9%	0.3%	-	-	-	-
	0.5	4.9%	0.66%	4.9%	0.49%	4.9%	-1.5%	4.9%	-0.7%

* PD=Peak Drift, RD=Residual Drift, '-'=no test

Table 7-3: Second story total peak and total residual drift response of the structure under sequence of shakes (First shake was 100% scale of Bam record with PD 0f 5.2% and RD of 0.75%).

2nd Ground Motions	Acceleration Scale	2nd Floor							
		No Brace		With BB16mm		With RB16mm		With GB16mm	
		PD*	RD*	PD	RD	PD	RD	PD	RD
Bam	1	5.2%	0.8%	5.2%	0.2%	5.2%	-3.5%	5.2%	-0.26%
	0.5	5.2%	0.75%	5.2%	0.69%	5.2%	-0.6%	5.2%	-0.16%
Christchurch (REHS)	1	6.2%	0.42%	6.2%	-0.85%	*-	-	-	-
	0.5	5.2%	0.49%	5.2%	0.28%	5.2%	-1.0%	5.2%	-0.75%
Northridge (Sylmar)	1	5.2%	0.32%	5.2%	0.3%	-	-	-	-
	0.5	5.2%	0.75%	5.2%	0.67%	5.2%	-0.26%	5.2%	-0.05%
Tabas	1	5.2%	0.58%	5.2%	0.31%	-	-	-	-
	0.5	5.2%	0.69%	5.2%	0.57%	5.2%	-2.1%	5.2%	-0.78%

7.6.1.1. Drift Response using Buckling Brace

Figure 7-6 shows the story residual drift response under the sequence of shakes with or without a 16mm buckling brace which increases the computed storey stiffness by about 2.5 times. It firstly shows that first without adding braces secondary shakes changed the residual displacement by -15% on average. The negative value implies that it was decreased on average for these records.

Moreover, by adding a 16mm buckling brace at the first floor, the drift response of the structure was reduced by 75% on average. This is seen by the fact that while peak drifts are the same as in the first shake, the residual displacements are generally significantly reduced. Sometimes they are negative (e.g. Figure 7-6b) indicating movement in the opposite direction. This is also can be seen in the time history drift response of the structure as shown in Figure 6-14. It can be seen that the structure started to oscillate with initial residual drift of 0.7% from first shake (Bam record). Adding brace decreased the peak and residual drift during aftershocks.

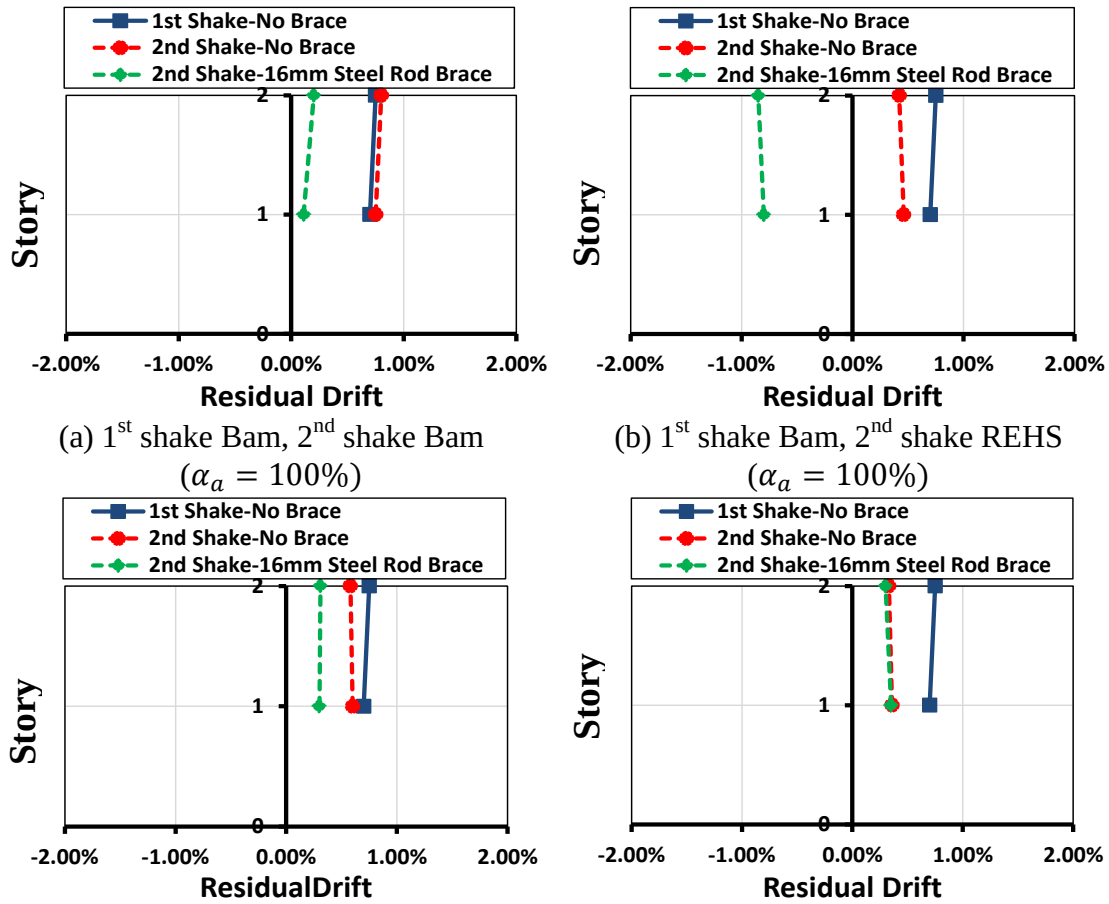

(a) 1st shake Bam, 2nd shake Bam ($\alpha_a = 100\%$)

(b) 1st shake Bam, 2nd shake REHS ($\alpha_a = 100\%$)

(c) 1st shake Bam, 2nd shake Tabas ($\alpha_a = 100\%$)

(d) 1st shake Bam, 2nd shake Northridge ($\alpha_a = 100\%$)

Figure 7-6: Residual drift response of the structure under sequence of shakes with and without having 16mm buckling brace

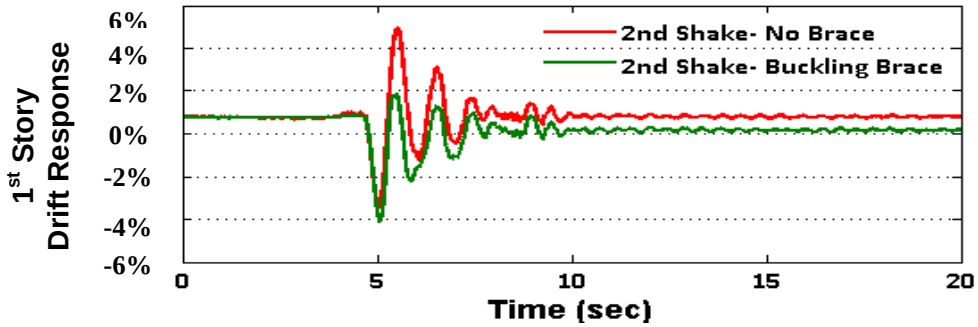

(a) Bam ($\alpha_a = 100\%$)

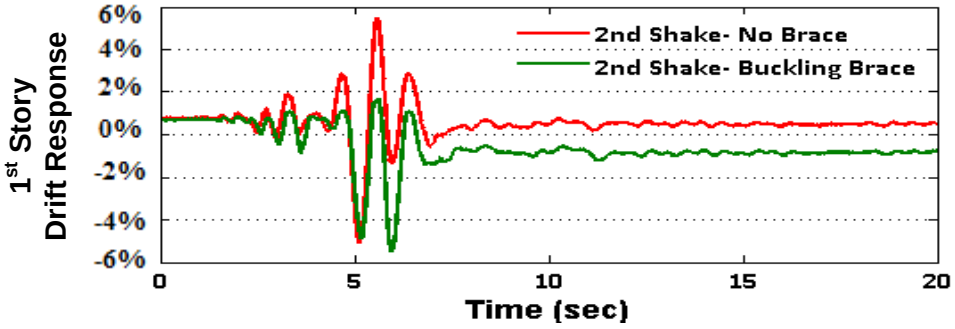

(b) Christchurch (REHS) ($\alpha_a = 100\%$)

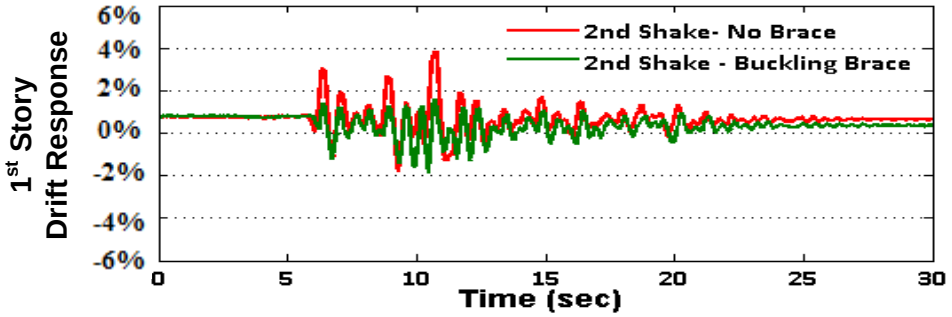

(c) Tabas ($\alpha_a = 100\%$)

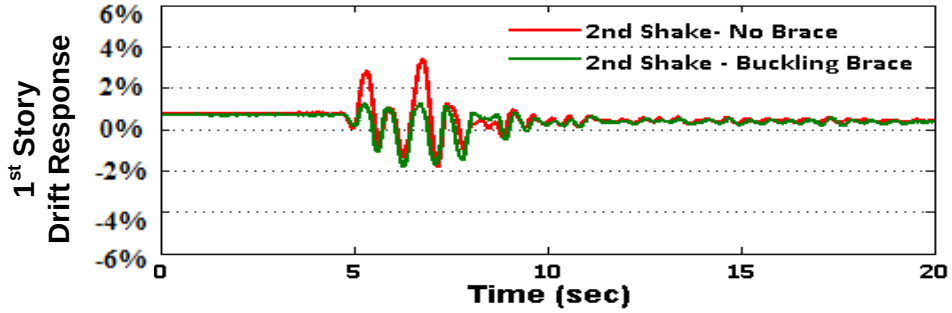

(d) Northridge (Sylmar) ($\alpha_a = 100\%$)

Figure 7-7: Comparing 1st story drift response under 2nd shake with or without having 16mm buckling brace.

Figure 7-8 shows the hysteretic behaviour of the first storey 16mm buckling brace under different ground motions. The force was measured from the load cell at the end of the brace. As compression force applied to the brace, it buckled easily with very small force ($F_{buckling} = 0.65\ kN$), but as it deformed during compression, some compression stiffness can be seen in hysteresis loop. The brace has a very small stiffness in compression compared to tension and it did not yield in tension. Sometimes the force-displacement of brace in tension during forward and backward loading is not in the same line. This is because of the limitation of string pot during very high speed loading. The slackness characteristic of the brace also shows that when the brace goes to compression, it returns to zero position to reload again. It also shows that for low-intensity ground motions such as Northridge record (Figure 7-8d) as displacement response is not high, the brace does not work much. Therefore, adding buckling brace does not change the residual response of the structure much under 2nd shake as shown in Figure 6-14d.

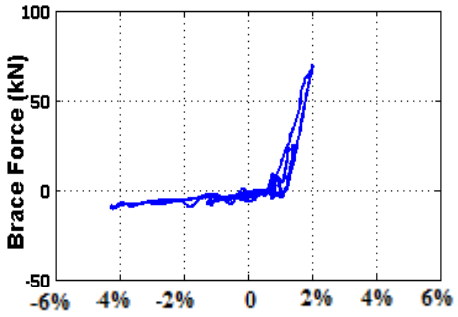

(a) Bam ($\alpha_a = 100\%$).

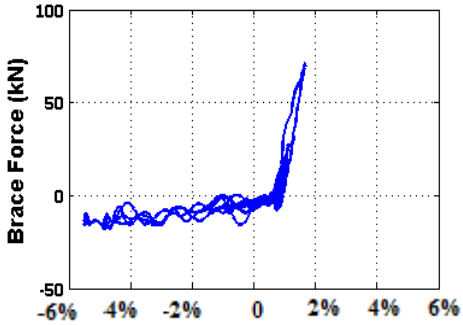

(b) REHS ($\alpha_a = 100\%$).

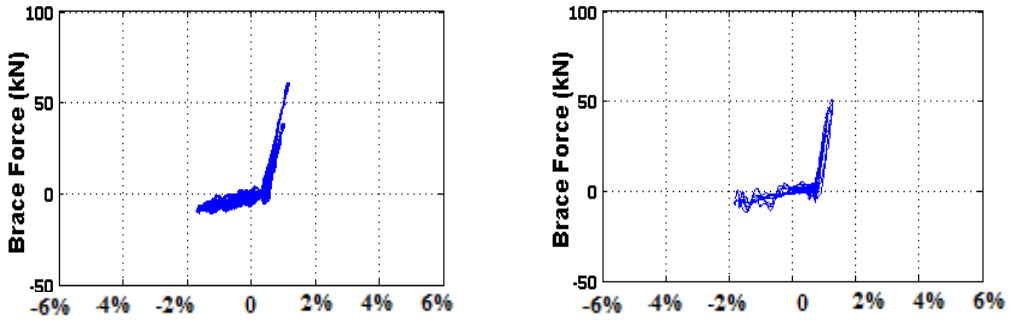

(c) Tabas (α_a = 100%). **(d) Northridge** (α_a = 100%).

Figure 7-8: Hysteretic behaviour of 16mm buckling brace under 2nd shake

Figure 7-9 compares the base shear verses roof drift response of the structure with and without having 16mm buckling brace at first story in tension in positive displacement under different ground motion records. The base shear of the structure was estimated as the sum of the floor accelerations multiplied by their corresponding masses. It shows that the buckling brace causes a higher base shear in the positive direction and reduced roof drift response. Based on the dynamic stability concept (e.g. MacRae 1994, Rad et al. 2015), the structures would require a larger shear force in the positive direction to cause yielding compared to the negative direction. Therefore, adding buckling braces can straighten the structure and reduce the residual drift in positive direction during the 2nd shake.

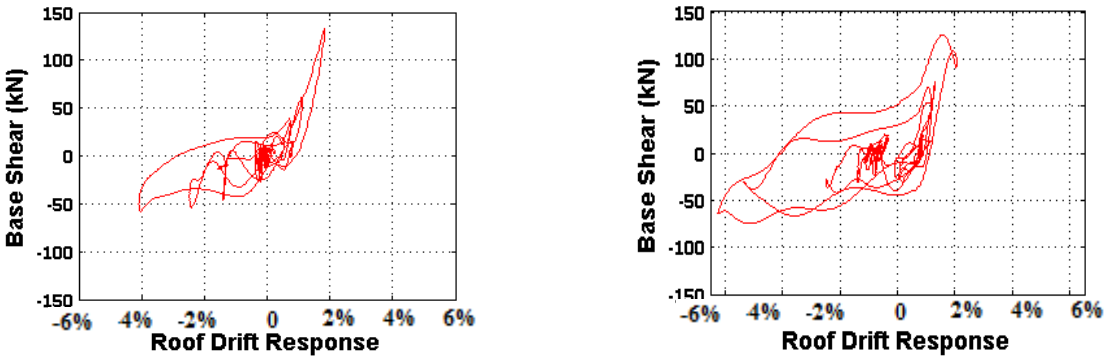

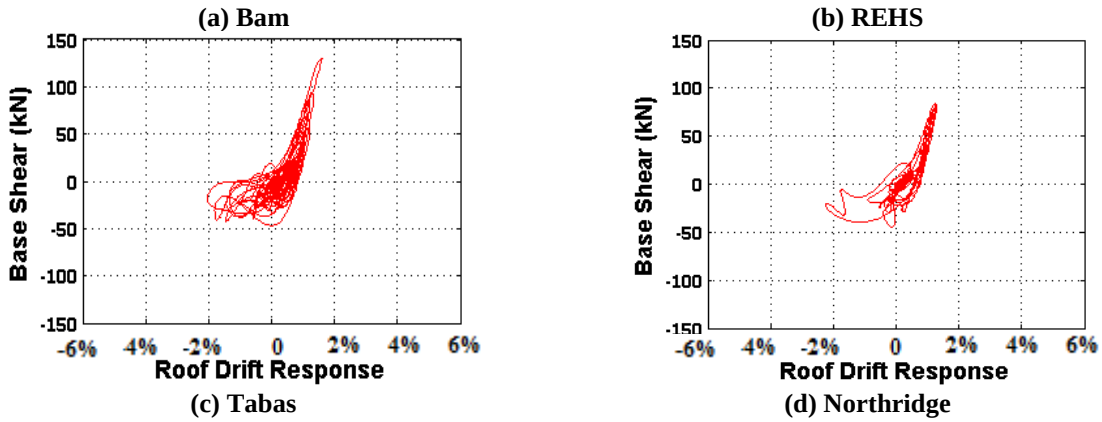

Figure 7-9: Comparing base shear-roof drift response of the structure with and without 16mm buckling brace under 2nd shakes ($\alpha_a = 100\%$)

Figure 7-10 also shows that by decreasing the acceleration intensity of 2nd shake, the residual drift reduction from adding the 16mm buckling brace is decreased. This is because the displacement demands are reduced in the negative direction.

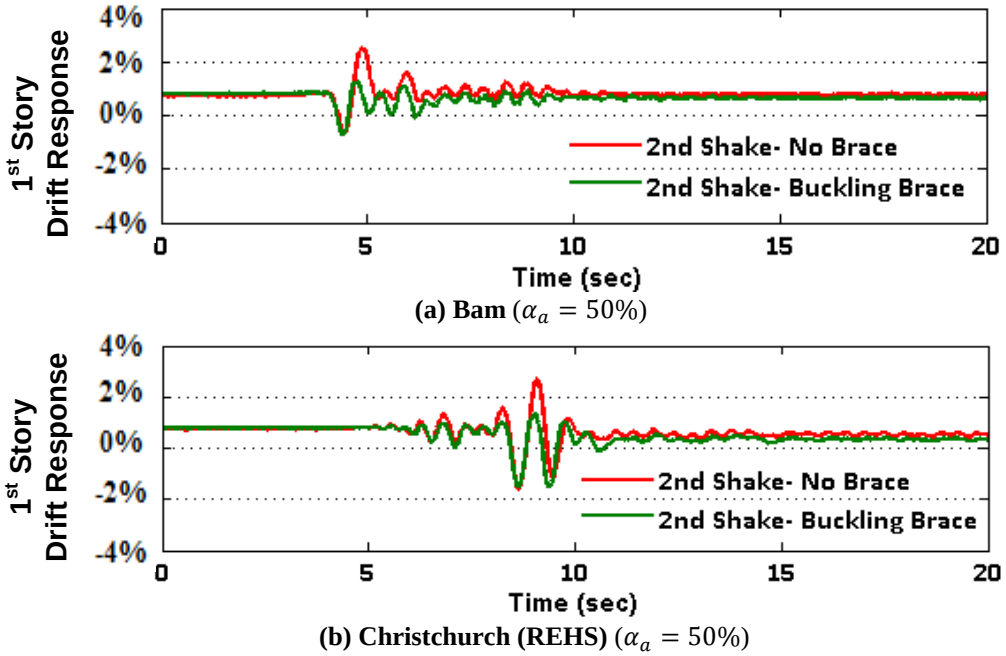

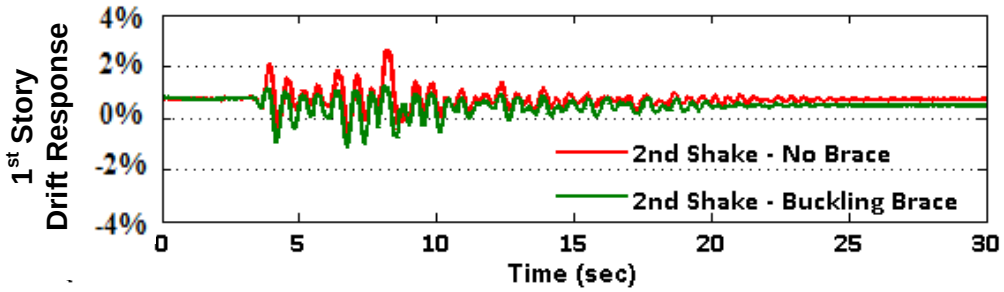

(c) Tabas ($\alpha_a = 50\%$)

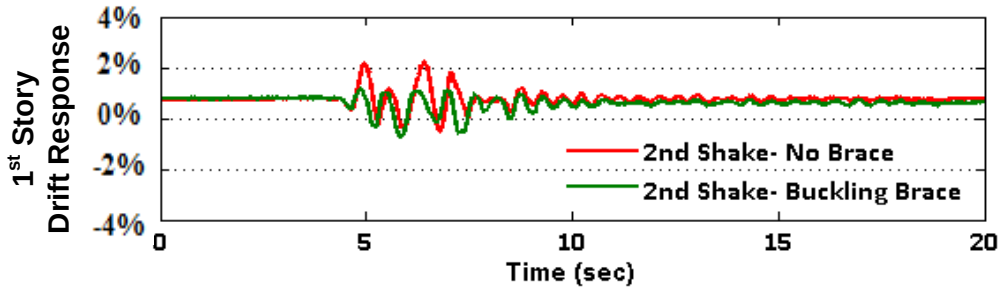

(d) Northridge (Sylmar) ($\alpha_a = 50\%$)

Figure 7-10: Comparing drift response of the structure under 2nd shakes with or without having 16mm buckling braces.

7.6.1.2. Drift Response using Ratcheting Brace

The Bam ground motion is again applied to the structure as a 1st shake to have high residual drift (0.7%) then it is applied again with the same direction and intensity as a 2nd shake. Figure 7-11a shows the first floor time history drift response of the structure under the 2nd shake with or without adding 16 and 12mm ratcheting brace (RB) between shaking which increases the computed storey stiffness by about 2.5 and 2.0 times respectively. It shows that with RB on first storey alone, the residual drift response is reduced significantly and it caused significant residual drifts in the opposite direction. It is because when the brace goes to compression (positive drift here), the rod can freely move inside of the RB, but as it extends and comes back to the zero position, the device stands working in tension again when the teeth are engaged as shown in Figure 7-1. This

makes it difficult for the frame to straighten as it does not have a slackness characteristic.

If the steel rod yields and has plastic deformation, it may allow the structure to move toward zero position. This can be seen using 12mm steel rod. This 12mm rod has less strength and stiffness, so it yields sooner than the 16mm rod and has more plastic deformation as shown in Figure 7-11c. Therefore, it moved more toward zero position and the structure had less residual drift with the 12mm RB than with the 16mm RB. Figure 7-11b, and c shows that when the RB goes in tension, the teeth are engaged and it soon carries load, making it difficult for it to return to zero residual displacement. It also shows that the brace compressive resistance is small.

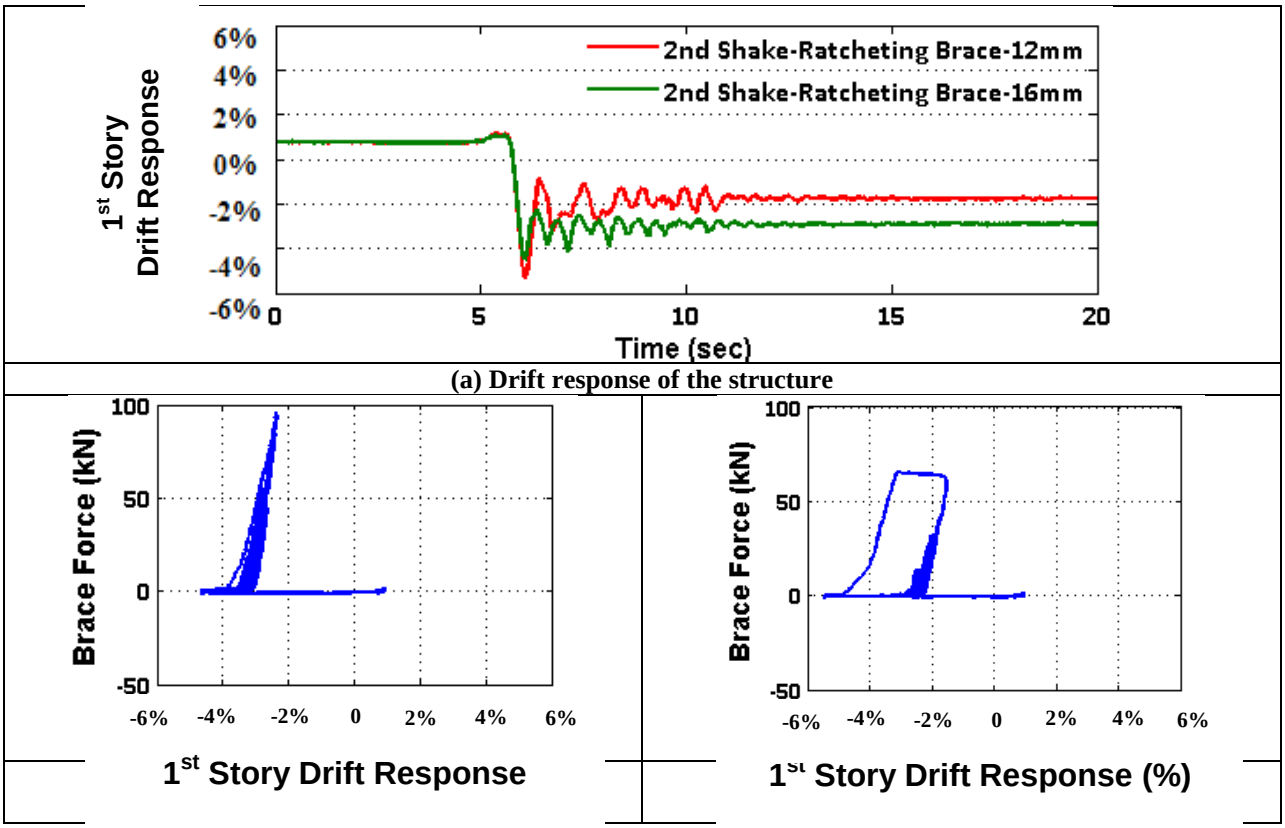

Figure 7-11: Comparing response of the structure with having 16 and 12mm RB under 2nd shake (Bam, $\alpha_a = 100\%$).

As shown in Figure 7-11a, the RB has a higher tendency to cause deformation in only one direction than other brace configurations with similar stiffness and strength because of the ratcheting mechanism. Therefore, because of high residual drift using high intensity ground motions, for the rest of the tests, low scale ground motions were used as a 2nd shake. Figure 7-12 shows that for 2nd shakes with lower acceleration intensity, adding RB on first floor still causes residual drifts in the opposite direction, but it is much less than for records with 100% acceleration intensity. This is because low intensity ground motions push the structure and the brace less in compression. Therefore, the steel rod deformation is less than the tooth pitch. It also shows that under low intensity 2nd shakes, the 16mm and 12mm steel rods had a similar effect on residual drift. However, as the 12mm rod has less strength and stiffness, when it goes in tension, the structure has more displacement towards positive direction as shown in Figure 7-12. The different between this one with Figure 7-11 is the intensity of 2nd shake. Here as the 2nd shake has low intensity, the brace does not have high plastic deformation demand as shown in Figure 7-13, so it does not return the structure toward zero position. This indicates that the strength/stiffness of the brace and intensity of the 2nd shake may affect the residual drift of the structure.

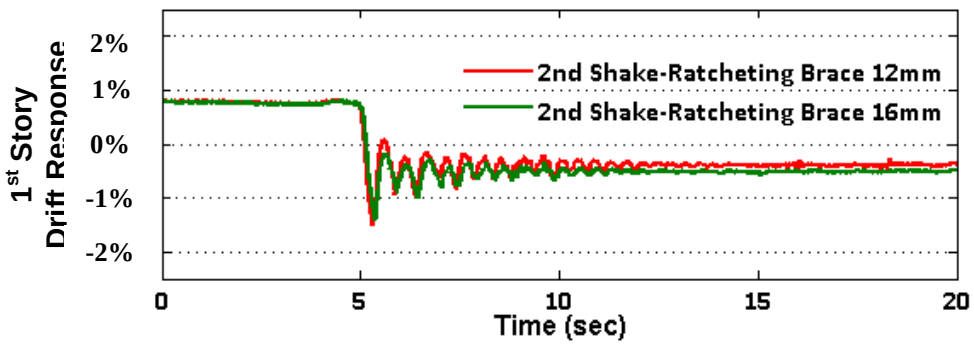

(a) Bam ($\alpha_a = 50\%$)

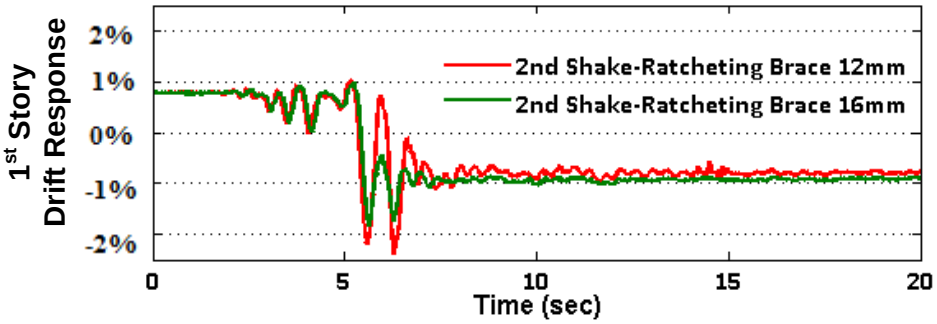

(b) REHS ($\alpha_a = 50\%$)

Figure 7-12: Comparing the drift response of the structure using 12mm and 16mm RB under 2nd shake.

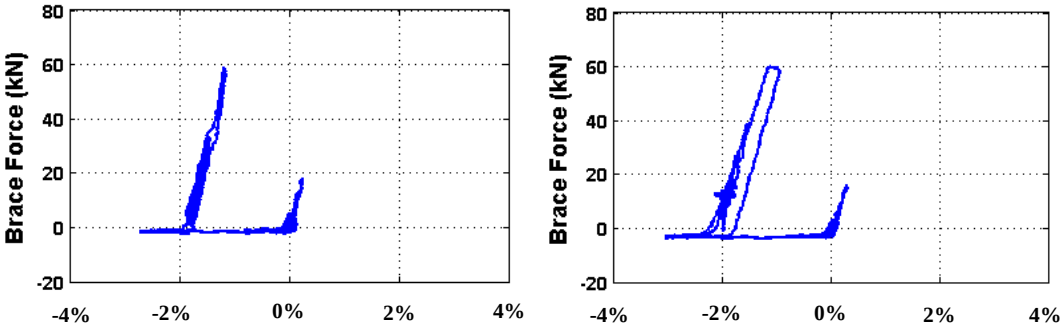

Figure 7-13: Hysteretic Response of the RB under REHS record ($\alpha_a = 50\%$)

7.6.1.3. Drift Response using Gapping Brace

To prevent over-straightening, a gapping braces (GB) may be used to limit the displacement in the negative direction. Gapping braces have consist of a ratcheting brace carries tension in the positive direction in conjunction with a buckling brace with a displacement gap carries tension in the negative direction. Figure 7-14 compares the first story drift response of a structure with 16mm

gapping braces (GB) and ratcheting braces (RB) in the tension direction only. It shows that having gapping braces had lower residual displacements in this case. This is because the gapping braces do not allow the structure to move a lot in the negative direction.

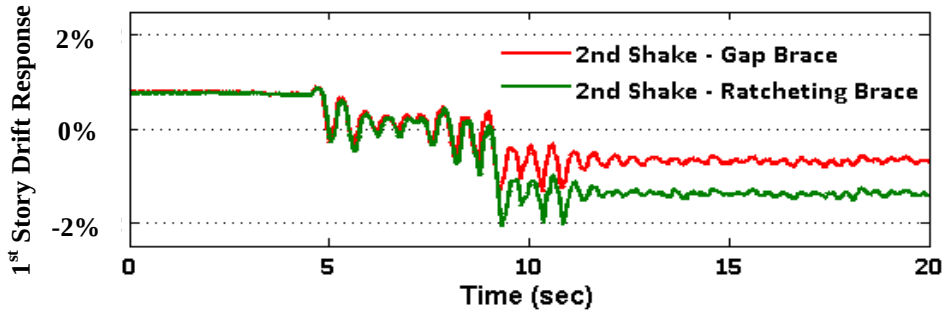

(b) Tabas ($\alpha_a = 50\%$)

Figure 7-14: Comparing drift response of the structure with 16mm ratcheting braces (RB) and gapping braces (GB) under 2nd shake.

Figure 7-15 compares the drift response of the structure with 12mm RBs and GBs. The 12mm brace has more plastic deformation, so it moved more toward the zero position and the structure had less residual drift compared to the 16mm brace. The GBs also do not allow the structure to move more in opposite direction.

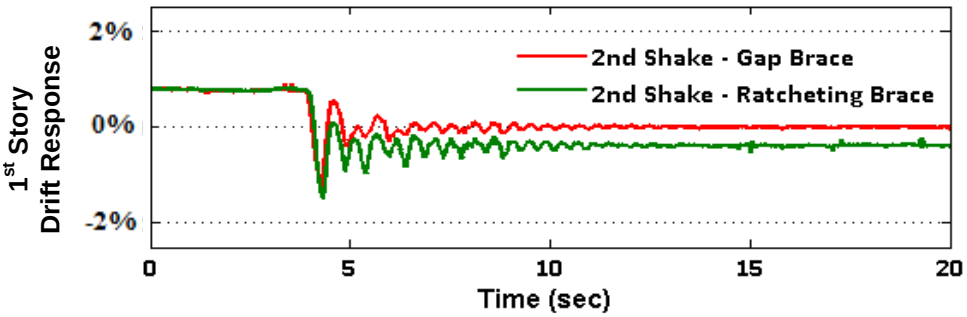

(a) Bam ($\alpha_a = 50\%$)

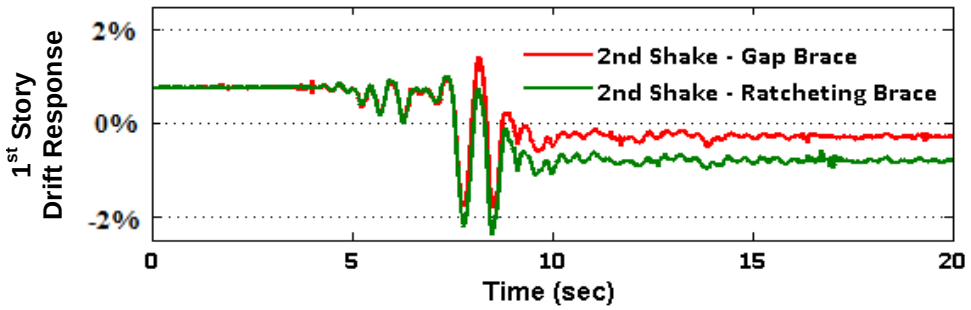

(b) REHS ($\alpha_a = 50\%$)

Figure 7-15: Comparing drift response of the structure with 12mm ratcheting brace (RB) and gapping brace (GB) under 2nd shakes.

7.7. Numerical Simulation

As torsional displacements of the frame were negligible (<0.1%), to investigate the seismic behaviour of the structures, a simple two-dimensional model as shown in Figure 6-20 was created using the software OpenSees for simulating the nonlinear response under earthquake excitations. As beams and columns remain elastic during the tests, simple elastic element was used to model the beams and columns (with a section property of 100UC14.8, Grade 300). Zero-length element was used to capture the moment-rotation behaviour of the friction connections. For defining braces, two types of tension-only element were used. The first was a buckling brace with slackness and the other one was ratcheting brace based on the Figure 7-1. As shown in Figure 7-2 the brace was not connected to the corner of the column because of the construction difficulties and it was connected to the base plate beside the column base which it was also shown in Figure 7-3. Beam

ends and column bases connection modelling was explained in Chapter 6, Section 6.7.

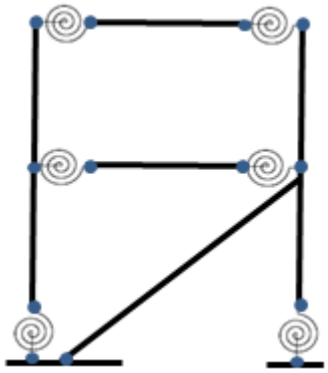

Figure 7-16: Numerical Model

7.7.1. *Comparison of Numerical Simulation and Experimental Results*

To verify the proposed numerical methods for evaluating the seismic performance of the tested steel frame with two different tension-only bracing systems, a series of nonlinear dynamic time history analyses were conducted. Figure 7-17 shows the time histories first floor drift response of the structure with 16mm buckling brace (BB) and 12mm ratcheting brace (RB) respectively. The simulation results presented a sound agreement with the test results. Figure 7-18 also compares the experimental and numerical simulation of the brace hysteresis behaviour for both bracing system respectively. It shows that for the RB, when was loaded in tension a drift of about -4.5%, there is small amount of slack in the device that has not

been numerically simulated. However, it does not significantly affect the general response of the structure.

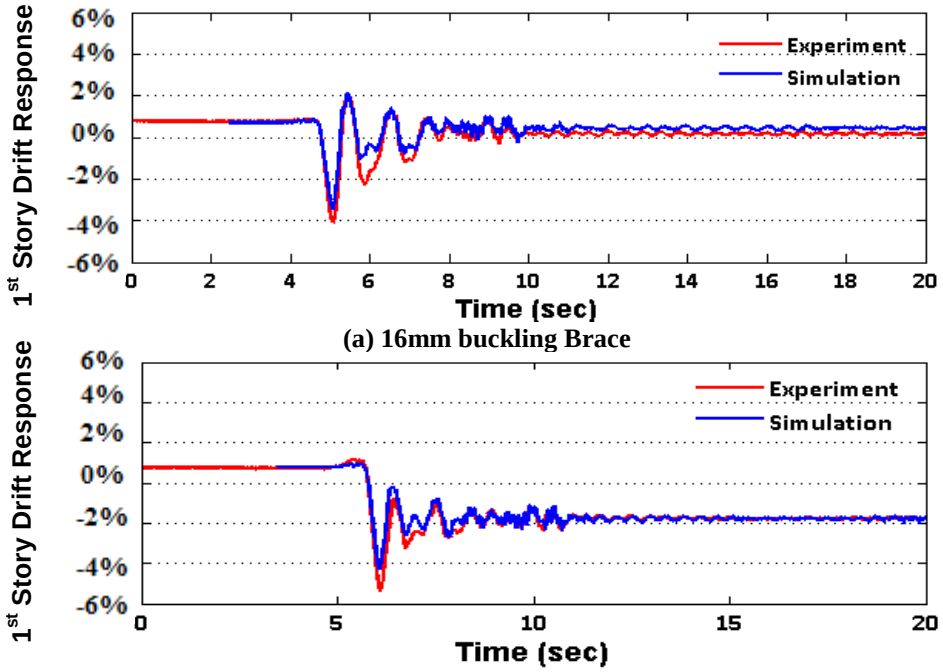

(a) 16mm buckling Brace

(b) 12mm RB

Figure 7-17:Comparing experimental and numerical simulation of drift response of the structure under Bam ground motions (Acc Scale of 100%)

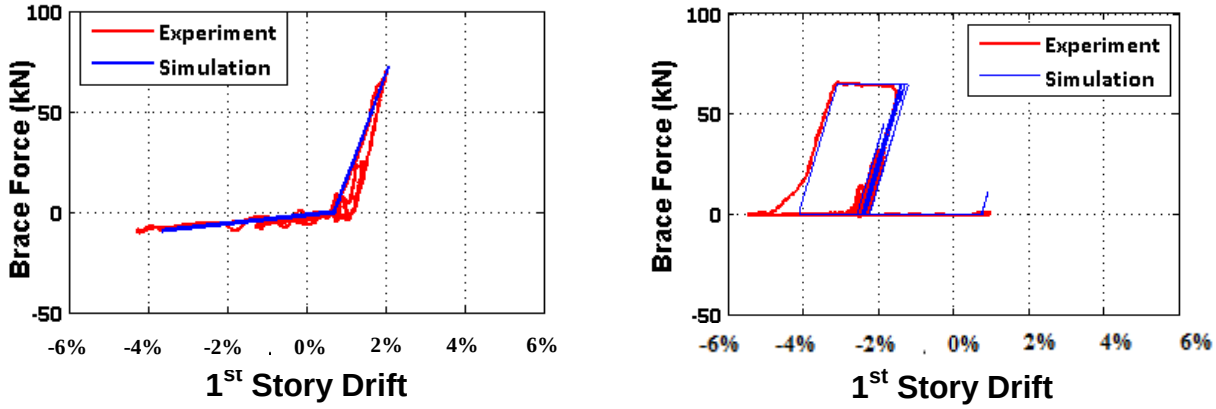

(a) 16mm buckling Brace

(b) 12mm ratcheting brace

Figure 7-18: Comparing experimental and numerical simulation of hysteretic response of the structure under Bam ground motions (Acc Scale of 100%)

7.8. Conclusion

Structural strengthening/stiffening of a tested frame having residual drifts with different tension bracing systems carried out to discourage buildings from having further displacements in the same direction during aftershocks. The residual drift of the building after the first shake and then after additional shakes with different braces was investigated. Based on the experimental results obtained, the following conclusions can be drawn:

1) When the frame without brace (NB) was subjected to additional shaking the residual displacement sometimes increased and sometimes decreased. For this particular series of tests it decreased by -15% on average. The buckling brace (BB) reduced the residual drift by 75% on average and did not push the frame in the opposite direction. The ratcheting brace (RB) was very effective of straightening the structure with a residual displacement change of -260% on average (This means the final residual displacement has a magnitude of 2.6 times the initial value, but it is in the opposite direction). It implies that it caused significant residual displacement in the opposite direction. The GB was also effective by changing the residual drift by -150% on average.
2) The buckling brace (BB) or gapping/ratcheting brace (GB/BB) combination limited further drift in the same direction and do not push the frame much in the opposite direction.
3) Numerical models were able to capture the responses well.

7.9. References

Borzouie J, MacRae G. A., Chase J. G., Rodgers G. W., and Clifton G. C., "Experimental Studies on Cyclic Performance of Column Base Strong Axis–Aligned Asymmetric Friction Connections", Journal of Structural Engineering, 2015, DOI: 10.1061/(ASCE)ST.1943-541X.0001327.

Borzouie J, MacRae G. A., Chase J. G., Rodgers G. W., and Clifton G. C., "Experimental studies on cyclic performance of column base weak axis aligned asymmetric friction connection", Journal of Constructional Steel Research, 2015, 112, 252–262.

Clifton C. "Semi-rigid joints for moment-resisting steel framed seismic-resisting systems", PhD Thesis, Department of Civil and Environmental Engineering, University of Auckland.2005.

Clifton, C., Bruneau, M., MacRae, G., Leon,L., and Fussell, A., "Steel building damage from the Christchurch earthquake series of 2010 and 2011", Bulletin of the New Zealand Society for Earthquake Engineering, 2011, 44(4), 297-318

Cook J., Rodgers G.W., MacRae G.A. & Chase J.G. "Development of a ratcheting, tension-only fuse mechanism for seismic energy dissipation", NZSEE Conference, New Zealand. 2015.

Gunning, M. & Weston, D. "Assessment of Design Methodologies for Rocking Systems", ENCI493 Report, Supervised by MacRae, G.A., Department of Civil and Natural Resources Engineering, University of Canter-bury, Christchurch, New Zealand. 2013.

MacRae GA. "P-Δ effects on single-degree-of-freedom structures in earthquakes". Journal of Earthquake Spectra, 1994; 10(3):539–568.

MacRae G., Clifton G. C., Bruneau M., Kanvinde A. and Gardiner S., " Lessons from steel structures in Christchurch earthquakes", 8th International Conference on Behavior of Steel Structures in Seismic Areas Shanghai, China. 2015.

OpenSees, "Open System for Earthquake Engineering Simulation-Home", Page: http://opensees.berkeley.edu/.2015.

Rad A. A., MacRae G. A., Yeow T. Z. and Bull D. K., "Seismic behavior of steel buildings with out-of-plumb", Earthquake Engineering & Structural Dynamics, 2015, DOI: 10.1002/eqe.2598.

Rad A. A., MacRae G. A., Yeow T. Z. and Bull D. K., "Earthquake sequence effect on steel building", 8th International Conference on Behavior of Steel Structures in Seismic Areas Shanghai, China.2015.

Chapter 8: Conclusions

This thesis explores the numerical and experimental studies on performance of steel low damage buildings with ratcheting tendency under seismic demands. It was found that:

1) The peak inter-story drift and the ratio of residual-to-peak interstory drift response obtained from numerical time history analysis generally increased for steel structures with greater out-of-plumb and with higher lateral force reduction factor. For very high out-of-plumb, the ratio of residual-to-maximum possible peak drift tend to unity, indicating that the buildings were yielding predominantly in one direction. Based on the results obtained, a procedure is developed to estimate the peak and residual inter-story drift of the structures with out-of-plumb.

2) Canterbury earthquake sequence aftershocks increased the peak and residual drift responses. This was most significant with increasing force design reduction factor (R) and design drift. The structures tended to ratchet in one direction.

3) Elastic structures with different stiffnesses in opposite horizontal directions had decreased peak relative displacement in the stiffer direction. The likely displacement in a direction could be estimated from the displacement in the opposite direction by using energy considerations irrespective of the level of damping or period. Also, the peak displacement

in the negative direction was predicted by the spectral displacement associated with the period in that direction. Using these findings, a simple design approach is developed to show how peak displacements can be estimated for unbalanced stiffness elastic structures.

4) For yielding structures with unbalanced stiffness/strength, when stiffness and strength are increased together, the inelastic displacement in each direction could be estimated from the elastic response in that direction using standard modifications for inelasticity. The residual displacement decreased in the stiffer direction. However, the absolute residual drift, which occurred in the flexible direction, did not decrease, but remained relatively constant.

5) Shaking table testing of a half-scale two-story steel moment frame with asymmetric friction connections (AFCs) at the column bases and at the beam ends shows that the behaviour of the test frame to ground motions was consistent with standard methods to estimate peak displacements, and residual displacements. Residual drifts were less than 0.2% for peak inter-storey drifts up to 3%, and less than 0.7% for peak inter-storey drifts of 6.0% indicating desirable seismic performance. When beam ends and the base-column joints were modelled by appropriate trilinear and bilinear hysteresis loops respectively the response with time matched the numerical simulations well. The overall structural performance occurred without any significant member damage. Therefore, these may be considered to be low-damage structures.

6) Structural strengthening/stiffening of a tested frame having residual drifts with different bracing systems showed that adding buckling braces (BB) decreased the residual drift by 75% and did not push the frame in the opposite direction. The ratcheting brace (RB) caused significant residual displacement in the opposite direction changing the residual displacement by -260%. The gapping brace (GB) also changed the residual displacement by -150%. It was found that inserting the buckling brace (BB), or gab/buckling brace (GB/BB) combination, had the desirable characteristics during aftershocks of limiting further drift in the same direction without pushing the frame in the opposite direction.

Chapter 9: Future Work

The research within this thesis provided significant insight into the seismic ratcheting of structure. Several areas that have potential for further studies have been identified as a result of this work, and these are detailed within this chapter.

9.1: Seismic Response of Nonlinear Steel Structures with Unbalanced Stiffness/Strengths in Multi Storey Buildings

This thesis evaluates the nonlinear seismic performance of single storey steel Buildings. However, evaluating structures with higher periods and modes play a significant role in seismic evaluating of structures. Hence, there is a need to do more study on the seismic performance of MDOF system with unbalanced stiffness/strength.

9.2: Seismic Strengthening/Stiffening of Steel Structures with Tension Braces in Multi degree of freedom system

Determining the optimal configuration and location of tension braces in multi-degree freedom (MDOF) structures is important in strengthening/stiffening structures. Higher mode effect should consider for the MDOF system. Moreover, effect of initial residual deformation need to be considered. Therefore, there is a

need to do more study on the seismic strengthening/stiffening of MDOF system with tension braces.

9.3: Seismic Ratcheting of Concrete Structures

This thesis only studies the seismic ratcheting of steel structures, but concrete structures such as concrete moment frame and walls have different hysteretic characteristics and have different responses during earthquake excitation. Therefore, there is a need to evaluate seismic ratcheting in concrete structures.

9.4: Effect of Different Tension Braces on Seismic Ratcheting of Structures

The presented experimental shake table tests in this thesis showed that different tension braces have different effect on displacement response of the structures. Therefore, there is a need to do numerical studies with different tension braces to quantify the displacement response of the structures with different braces. Single and multi-degree of freedom structures need to be considered with different design parameters in steel and concrete buildings.

9.5: Implementation in the Field

The final step for any useful research is implementing by consultant and practitioners. The presented research in this thesis, provided all the basic tools

needed for considering ratcheting into a design. Future research topics may result from discussions with consultant and practitioners for retrofitting structures with tension braces after earthquakes. A few consultant engineers have used tension braces in their projects in New Zealand after Canterbury 2011 earthquake, and their interest has been expressed in different stages of this research. Ongoing work will hopefully result in implementation of the ratcheting effect in both new building designs and retrofit applications.

Appendix A: Published Papers

A. Journal Papers

1) Rad. A. A., MacRae G.A., Yeow T. Z., Bull D., (2015), Seismic behavior of steel buildings with out-of-plumb, EARTHQUAKE ENGINEERING & STRUCTURAL DYNAMICS, DOI: 10.1002/eqe.2598.

2) Rad. A. A. and MacRae G.A., (2017), Seismic Response of Elastic Single Story Structures, EARTHQUAKE ENGINEERING & STRUCTURAL DYNAMICS, Under Review.

3) Rad. A. A. and MacRae G.A., (2017), Seismic Response of Nonlinear Single Story Steel Structures with Unbalanced Stiffness/Strengths, Submitted to EARTHQUAKE ENGINEERING & STRUCTURAL DYNAMICS.

B. Conference Papers

1) Rad A. A., MacRae G.A., Yeow T. Z. and Bull D. K. (2014) "Seismic response of out-of-plumb buildings", Second European Conference of Earthquake Engineering and Seismology, Istanbul, Turkey.

2) Rad A. A., MacRae G.A., Yeow T. Z. and Bull D. K. (2015) "Earthquake sequence effect on steel building", 8th International Conference on Behavior of Steel Structures in Seismic Areas Shanghai, China,

3) Rad. A. A. and MacRae G.A., (2017), Dynamically Straightening of Low-Damage Steel Buildings after Earthquake, 16th World Conference on Earthquake, 16WCEE 2017, Santiago, Chile.

4) Rad. A. A. and MacRae G.A., Hazaveh N., Ma Q. (2018), Shake Table Testing of a Low Damage Steel Building with Asymmetric Friction Connections (AFC), The 9th International Conference on the Behaviour of Steel Structures in Seismic Areas, STESSA, Christchurch, New Zealand.

5) Rad. A. A. and MacRae G.A. (2018), Seismic Response of Steel Structures with Unbalanced Stiffness/Strength - Numerical and Shake Table Study, NZSEE Conference, Auckland, New Zealand.

Appendix B: Residual Displacement

B.1. Studies related to SDOF systems:

Several studies have been done on the evaluation of residual deformation demands in single-degree-of-freedom (SDOF) systems. MacRae and Kawashima (1993) pointed out that the post-yield stiffness ratio (i.e. ratio of post-yield stiffness to initial elastic stiffness) of bilinear SDOF systems has a significant influence on the amplitude of residual displacements as shown in Figure B-1. They showed that the oscillators with positive stiffness ratios generally have small residual displacements, while those with negative stiffness ratios have larger residual displacements.

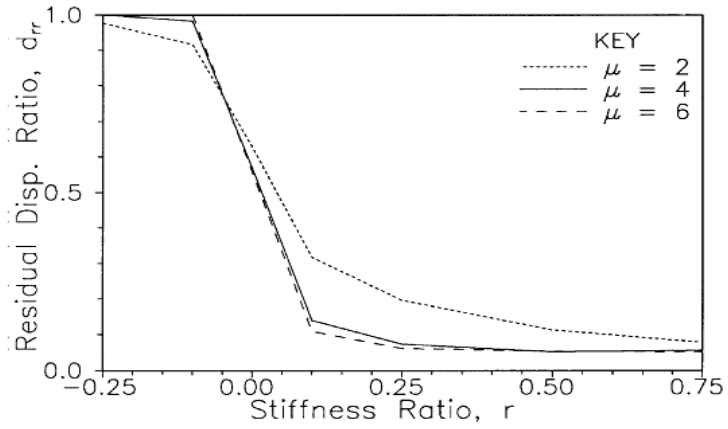

Figure B-1: Effect of stiffness ratio on average residual displacement ratio (MacRae, 1993).

Residual displacement prediction methods have been developed by MacRae and Kawashima (1997) for elasto- plastic single-degree-of-freedom (SDOF) oscillators with specified ductilities of 2, 4 and 6, post elastic stiffness ratios ranging from 0.25 to 1 and fundamental periods from 0 to 3s. It was shown that the ratio of the residual displacement to the maximum possible residual

displacement is almost totally dependent on the post-elastic stiffness ratio of the force-displacement hysteretic curve. The oscillators with positive stiffness ratios generally have small residual displacements, while those with negative stiffness ratios have larger residual displacements. The residual displacement, D_r, was calculated by Eq. B-1 where D_{mr} is the maximum possible residual displacement based on slow unloading from the peak displacement and D_{rr} is a non-dimensional residual displacement ratio which has values ranging from zero to unity. D_{mr} was calculated by Eq. B-2 where μ is ductility, r is post elastic stiffness ratio and D_y is yield displacement.

$$D_r = D_{rr} \times D_{mr} \tag{B-1}$$

$$D_{mr} = \begin{cases} (\mu - 1)(1 - r)D_y & r(\mu - 1) < 1 \\ \frac{(1-r)}{r} D_y & r(\mu - 1) \geq 1 \end{cases} \tag{B-2}$$

Also, a "Hysteresis Centre Curve" (HCC) concept was developed to describe the dynamic stability of a general hysteresis loop as shown in Figure B-2. This allowed P-Δ effects to be understood (MacRae, 1994) and it has been used to characterise the behaviour of cantilever bridge columns (MacRae and Kawashima, 1990; Yeow et al. 2013). The work resulted in design recommendations for RC structures in the Japanese Bridge Code (1997).

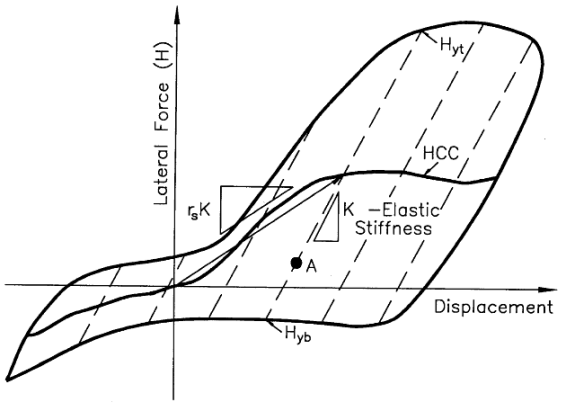

Figure B-2: General shaped stable hysteresis curve (MacRae, 1993)

Christopoulos et al. (2003) considered three different hysteretic behaviours (i.e. Elasto-Plastic (EP), Takeda (TK) and Flag-Shaped (FS) as shown in Figure B-3 to characterise residual displacements. An example of a time history analysis under 150% of the scaled Loma Prieta record is shown in **Error! Reference source not found.**b for three different hysteretic models. The residual displacements, shown both on the time-trace and in the individual hysteresis loops of each system, are 44.4 mm, 17.6 mm and 0.0 mm for the EP, TK and FS systems respectively.

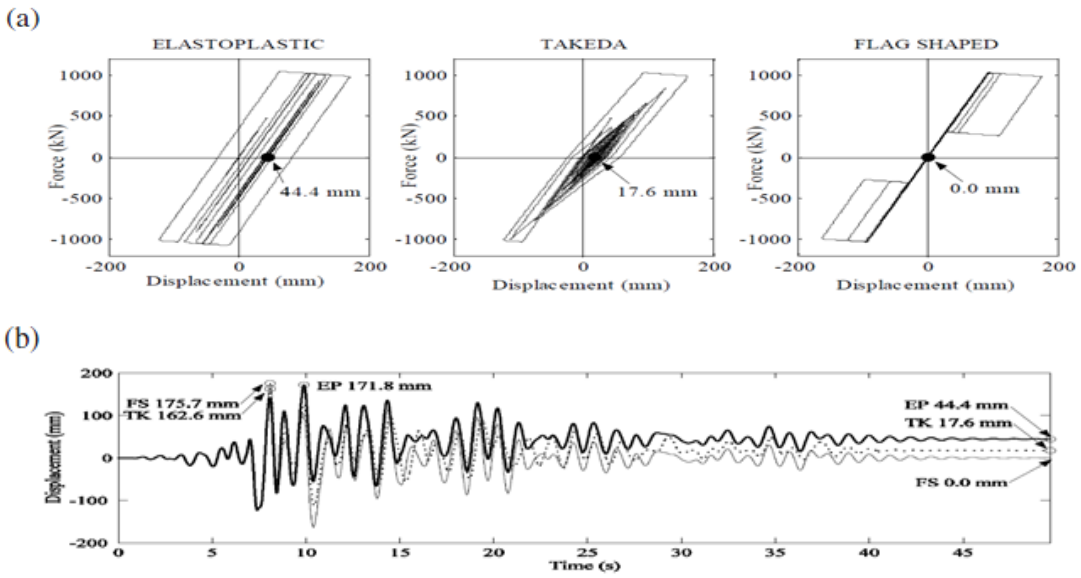

Figure B-3: Response of three hysteretic systems to 150% of the scaled Loma Prieta record (Christopoulos et al. (2003).

Ruiz-Garcia and Miranda (2006a) presented a comprehensive statistically study to investigate residual displacement demands of SDOF systems, they normalized the residual displacement demand, Δ_r, with respect to the peak elastic displacement demand, S_d, of a SDOF system. They evaluate the influence of period of vibration, level of relative lateral strength, site conditions, earthquake magnitude, and distance to the source. They point out that for structures in the short period spectral region (e.g. T<0.5 s), the ratio of residual displacement to maximum elastic displacement demand is strongly dependent on the period of vibration and the lateral strength ratio as shown in Figure B-4. For periods longer than 1.0 s, mean residual deformation ratios are not very sensitive to changes in the period of vibration and they primarily depend on the lateral strength ratio.

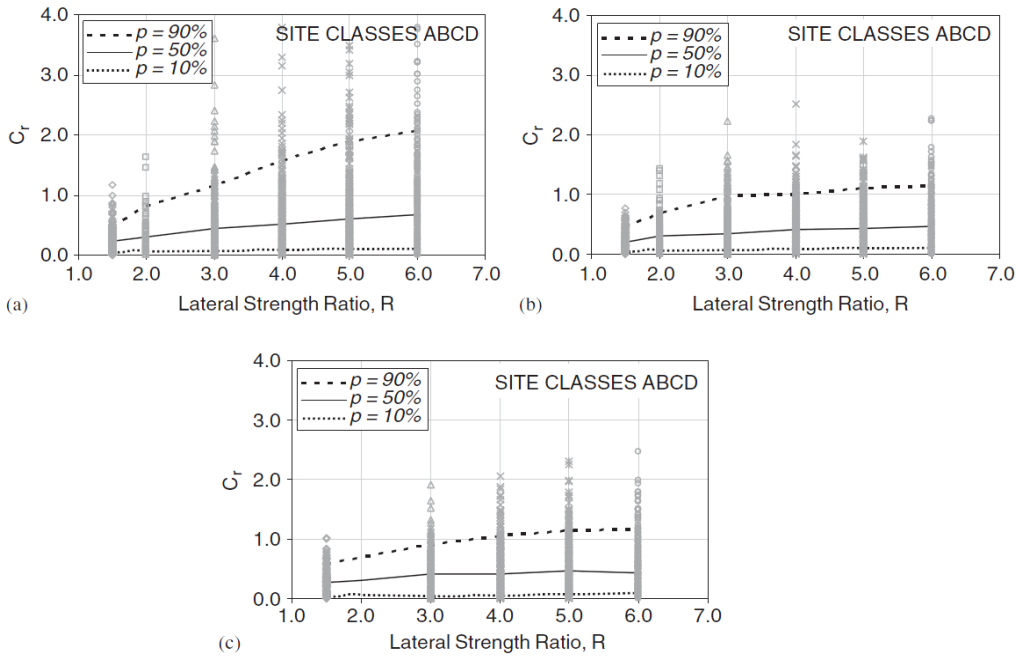

Figure B-4: Effect of lateral strength ratio on residual displacement ratios for Elasto-plastic systems: (a) T =0:5 s; (b) T =1:0 s; and (c) T =2:0 s (Ruiz-Garcia and Miranda, 2006a)

Moreover, they found that earthquake magnitude has smaller effect on strong systems (e.g. R<3) than in weak systems (e.g. R>3) in the short- and medium-

period range. The results of their studies indicated that increasing magnitude does not necessarily lead to larger residual displacement ratios. Ruiz-Garcia and Miranda (2006a) also suggested that the effect of local firm soil conditions may need to be considered when estimating residual displacement demands. In general, they found that neglecting the effect of site conditions, cause overestimate or underestimate the residual displacement demands.

B.2. Studies related to MDOF systems:

Gupta and Krawinkler (1999) reported residual drift demands of three steel moment-resisting frames (SMRF) in three different seismic areas in the U.S. The authors noted that the amplitude of residual drift demands increased as the intensity of the ground motions increased.

Later, Pampanin et al. (2003) evaluated residual drift demands of four framed building models having 4, 8, 12, and 20 stories. The authors noted that mean residual drift demands are very sensitive to the hysteretic modelling of the structural components.

Moreover, Medina and Krawinkler (2003) studied the median residual drift demands of regular one-bay generic building frame models. They noted that dispersion of residual drift demand is large and non-uniform along the height as shown in Figure B-5.

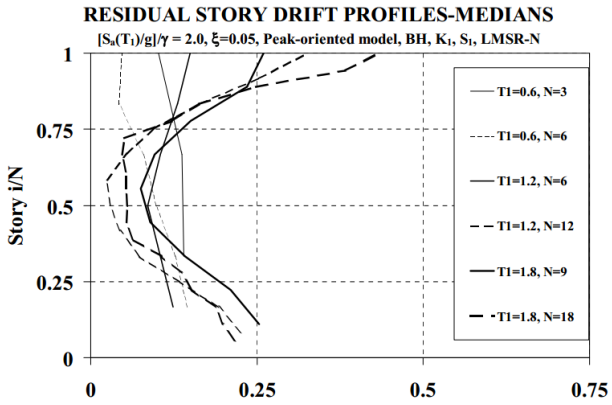

Figure B-5: Normalized residual story drifts (Medina and Krawinkler (2003))

Ruiz-Garcia and Miranda (2006b) presented statistical studies to evaluate central tendency and dispersion of residual deformation demands in MDOF systems. The authors studied the influence of ground motion intensity, number of stories, period of vibration, frame mechanism, system over strength, and hysteretic behaviour on central tendency of residual drift demands. They found that for both rigid and flexible building models the distribution of residual inter-storey drift demand (RIDR) along the height changes as the number of stories increases and it tends to concentrate at specific stories, which is more evident for flexible frame models as shown in Figure B-6 and Figure B-7.

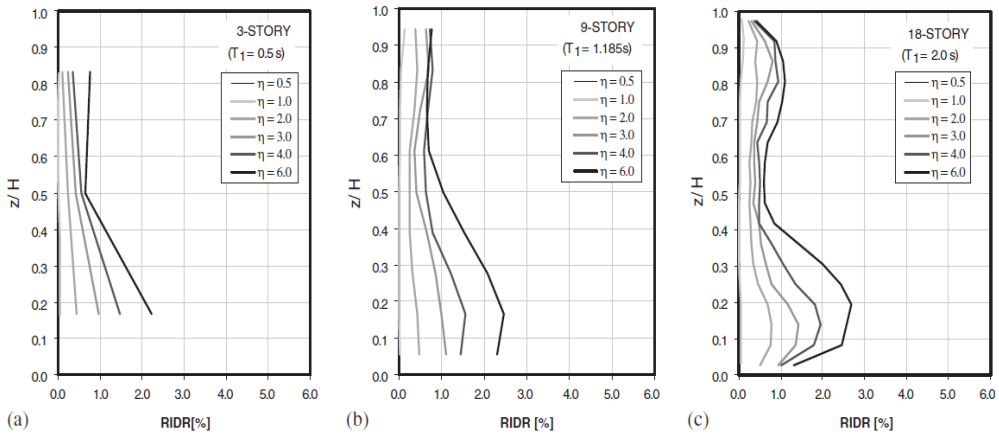

Figure B-6: Effect of number of stories on residual drift demands with different number of stories: (a) N =3; (b) N =9; and (c) N =18 (Ruiz-Garcia and Miranda, 2006b).

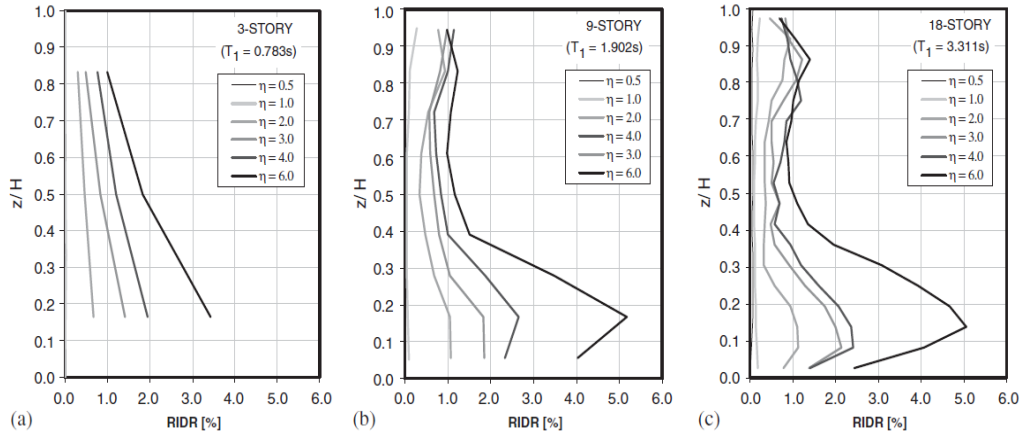

Figure B-7: Effect of number of stories on residual drift demands for generic flexible frames with different number of stories: (a) N =3; (b) N =9; and (c) N =18(Ruiz-Garcia and Miranda, 2006b).

Moreover, regarding frame mechanism their analyses showed that FH (Full Hinge) and CH (Column Hinge) mechanism leads to a concentration of RIDR at the bottom stories as the relative intensity increases, while the ideal BH (Beam Hinge) mechanism tends to develop a more uniform distribution of RIDR along the height as shown in Figure B-8. In addition, it can also be observed that CH and FH mechanisms lead to a secondary residual drift concentration on the upper stories for large levels of ground motion intensity, which might be a consequence of higher-mode effects. However, this feature is not observed in the BH mechanism. Moreover, it can be seen that CH mechanism leads to larger RIDR max than those experienced in buildings with FH and BH frame mechanisms as the ground motion intensity increases, which is a consequence of residual drift concentration in the lowest storey.

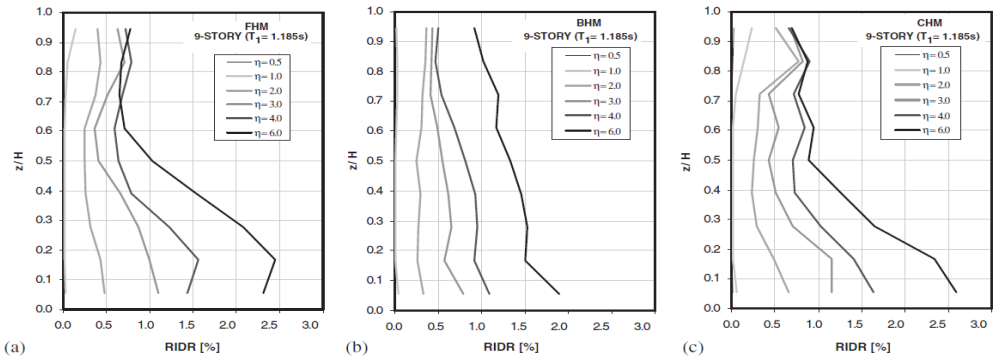

Figure B-8: Effect of the type of mechanism on the heightwise distribution of RIDR for building model (T_1 =1.185s) (a) FH mechanism; (b) BH mechanism; and (c) CH mechanism (Ruiz-Garcia and Miranda, 2006b).

Furthermore, the results of their study regarding over strength indicated that the presence of over strength in the frame model leads to smaller residual drift demands than in the absence of over strength as shown in Figure B-9. Moreover, consideration of over strength non-uniformly distributed along the height leads to a more uniform distribution of residual drift demands along the stories and, in consequence, avoiding residual drift concentration.

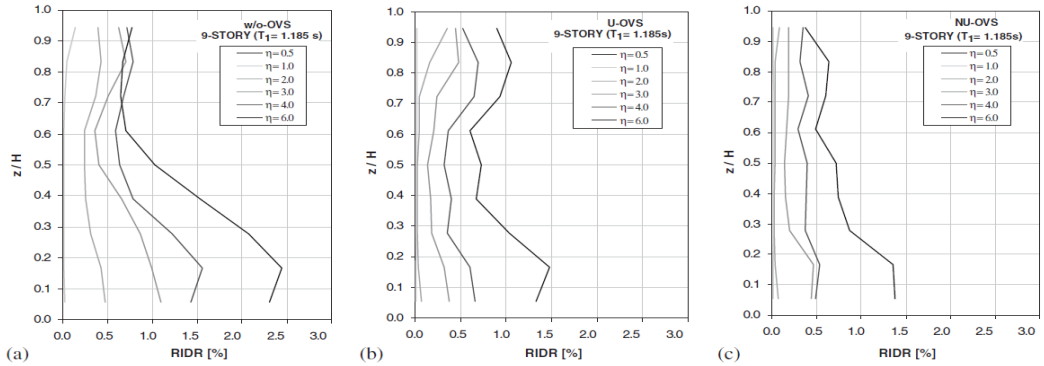

Figure B-9: Height wise distribution of median RIDR building model: (a) without over strength; (b) assuming uniform over strength; and (c) assuming non-uniform over strength (Ruiz-Garcia and Miranda, 2006b).

Appendix C: MATLAB Codes for RUAUMOKO

C.1 Matlab Function to design CISDR model

```
function [hfl wfl K Vfinal T ISDR Cdt1 Cdt2
Ct]=CISDR_Design_fn(nbs,h,mass,tr,R,mu)
%Storey heights between floor levels (m).
h_fl=[];
for i=1:nbs
h_fl(i)=h;
end
hfl=h_fl;
%Height of each floor from the ground level (m).
hfg=cumsum(hfl);
%Target interstorey drift ratios.
t_ratio=[];
for i=1:nbs
t_ratio(i)=(tr/100);
end
tratio=t_ratio;
%Mass at every floor (kg).
m_fl=[];
for i=1:nbs
m_fl(i)=mass;
end
mfl=m_fl;
%Mass matrix (kg).
m_mat=[];
for i=1:nbs
m_mat(i,i)=mfl(i);
end
mmat=m_mat;
%Weight of each floor (N).
wfl=mfl*9.81;
%Total seismic weight of the structure (N).
wfl_g=cumsum(wfl);
wst=wfl_g(nbs);
%Product of weight and height of each floor from G.L. (N-m)
wh=wfl.*hfg;
wh_st=cumsum(wh);
whst=wh_st(nbs); %Total
%Lateral stiffness of each storey (N/m).
kiter=[];
for i=1:nbs
    kiter(i)=1000000; %Initial assumption
end
% for i=1:nbs
%     kiter(i)=1; %Initial assumption
% end
%Calculation of deflection scale factor, kd (Table 6.1 in NZS 1170.5).
if (nbs==1)
kd=1;
elseif (nbs==2)
kd=0.97;
elseif (nbs==3)
kd=0.94;
elseif (nbs==4)
kd=0.91;
elseif (nbs==5)
kd=0.88;
else
```

```
kd=0.85;
end
%Calculation of drift modification factor, kdm (Table 1.1 in NZS 1170.5).
tsh=hfg(nbs); %Total height of the structure, in m.
if (tsh<15)
kdm=1.2;
elseif (tsh>=15&tsh<=30)
kdm=1.2+0.02*(tsh-15);
else
kdm=1.5;
end
check=1;
tol=1e-6;
cpt=0;
%********************** Iteration begins from here
**********************
while ((check>tol)&(cpt<5000))
cpt=cpt+1;
K=kiter;
%Formation of structural stiffness matrix (N/m).
k_mat=[];
for i=1:(nbs-1)
k_mat(i,i)=K(i)+K(i+1);
k_mat(i,i+1)=-K(i+1);
k_mat(i+1,i)=-K(i+1);
end
k_mat(nbs,nbs)=K(nbs);
kmat=k_mat;
%Calculation of fundamental natural period of the structure (s).
e_value=eig(kmat,mmat);
evalue=sqrt(e_value);
omega=min(evalue); %fundamental natural circular frequency in rad/sec.
funda_freq=omega/(2*pi); %fundamental natural frequency in Hz or cps.
T=(1/funda_freq); %fundamental natural period in s.
%Call the function to calculate the horizontal design action coefficient
[Cdt Cdt1 Cdt2 Ct]=NZS11705_CdT_fn(T,R,mu);
%Calculation of horizontal seismic base shear, N (Clause 6.2.1.2).
Vb=Cdt*wst;
%Equivalent static horizontal force at each level, N (Clause 6.2.1.3)
%floor level in N (clause 6.2.1.3)).
F_eq=[];
for i=1:(nbs-1)
F_eq(i)=0.92*Vb*(wh(i)/whst);
end
F_eq(nbs)=(0.08*Vb)+0.92*Vb*(wh(nbs)/whst);
Feq=F_eq;
Feq_tot=cumsum(Feq);
Feq_base=Feq_tot(nbs); %Total force acting at the base, N (=Vb).
%Shear force at each level (N).
veq1=fliplr(Feq);
veq2=cumsum(veq1);
Veq=fliplr(veq2);
%Interstorey drift at every storey, m (without P-Delta effects).
del_di=(Veq./K);
%Displacement of each floor, m (Clause 6.5.4.2 - Step 1).
dieqsm=cumsum(del_di);
%Modified floor displacements, m (Clause 6.2.3 & 6.5.4.2 - Step 2).
m_dieqsm=(kd*mu*dieqsm);
%Ultimate storey inter-storey drifts, m (without P-Delta effects).
udel_d_i=[];
for i=2:nbs
udel_d_i(i)=m_dieqsm(i)-m_dieqsm(i-1);
end
udel_d_i(1)=m_dieqsm(1);
udel_di=udel_d_i;
```

```
%P-Delta storey shears, N (Clause 6.5.4.2, Step 3).
w_pd1=fliplr(wfl);
w_pd2=cumsum(w_pd1);
w_pd=fliplr(w_pd2);
Vpd=((w_pd.*udel_di)./hfl);
%P-Delta forces, N (Clause 6.5.4.2, Step 3).
F_pd=[];
for i=1:(nbs-1)
F_pd(i)=Vpd(i)-Vpd(i+1);
end
F_pd(nbs)=Vpd(nbs);
Fpd=F_pd;
%P-Delta interstorey drifts, m (Clause 6.5.4.2, Step 3).
del_dipd=(Vpd./K);
%P-Delta displacements, m (Clause 6.5.4.2, Step 3).
dipd=cumsum(del_dipd);
%Calculation of beta factor used in Step 4 of Clause 6.5.4.2
% if (T<2)
% kbeta=1;
% elseif (T>=2&T<=4)
% kbeta=(6-T)/4;
% else
% kbeta=0.5;
% end
% if (mu<=3.5)
% beta=max((2*mu*kbeta)/3.5,1);
% else
% beta=max(2*kbeta,1);
% end
beta=2;
%Final force at each level (incl. P-Delta effects), N -(Clause 6.5.4.2,
%Step 5).
Ffinal=(Feq+Fpd*beta);
%Final shear force at each level, N (incl. P-Delta effects).
Vfinal=(Veq+Vpd*beta);
%Final floor displacements (incl. P-Delta effects), m -(Clause 6.5.4.2,
%Steps 5 & 6).
Difinal=mu*kd*dieqsm+dipd*beta;
%Final interstorey drifts, m (Clause 6.5.4.2, Steps 5 & 6).
deld_final=[];
for i=2:nbs
deld_final(i)=kdm*(Difinal(i)-Difinal(i-1));
end
deld_final(1)=kdm*(Difinal(1));
Deldifinal=deld_final;
%Interstorey drift ratios.
ISDR=(Deldifinal./hfl);
%Error calculator.
Delratio=((tratio-ISDR)./tratio);
abdelratio=abs(Delratio);
check=max(abdelratio);
%Adjusting storey stiffnesses.
for i=1:nbs
kiter(i)=K(i)*(ISDR(i)/tratio(i));
end
end
%********************* Iteration ends here ****************
%================================= END OF FUNCTION% ===============
```

C2. Matlab Function to Calculate Earthquake Record Scale Factor

```
function [EQdur DELTAT Slfactor] = EQ_ScaleFact_fn(Ct_mu1,T,EQFlName)
%=========================================================================
% EQ_ScaleFact_fn calculates the earthquake record scale factor.
% Inputs:
% Ct_mu1 : NZS 1170.5 Elastic site hazard spectrum for horizontal
loading (Clause 3.1.1 with μ = 1, Sp = 1)
% T : Fundamental natural period of the structure (s)
% EQFlName : Earthquake record file name
% Outputs:
% EQdur : Duration of the earthquake (s)
% DELTAT : Excitation data interval (s)
% Slfactor : Scale factor applied to the time-history input
% Notes: The central difference numerical method in Table D-1 is used for
%creating this code. A damping ratio of 5%, and a time-step size of
0.001s,
%is assumed for all calculations here. The above outputs are used in the
%function: ROMKO_INPfl_fn. The input parameter, Ct_mu1, can be obtained
%through the function NZS11705_CdT_fn (provided in Section B.3.3) with
the
%appropriate defined parameters.
%=========================================================================
%============================== START OF FUNCTION ======================
Sadesign=Ct_mu1;
alldata=xlsread(EQFlName);
timesp=alldata(:,2); %Time steps column in the Eq. file.
DELTAT=timesp(2)-timesp(1); %Record time interval (s).
EQdur=timesp(size(timesp,1)); %Earthquake duration (s).
gaccln=alldata(:,3)/100; %Accln. column in the Eq. file (m/s2).
tmstep=0.001; %Time-step for Central Diff. method (s).
Melast=1; %Lumped mass of the SDOF system (kg).
Kelast=((2*pi)/T)^2*Melast; %Lateral stiffness of SDOF system (N/m).
dcoeff=(5/100)*2*(sqrt(Kelast*Melast)); %Damping co-efficient (N-s/m).
%Calculation of Unscaled spectral acceleration.
kstar=((Melast/(tmstep)^2)+(dcoeff/(2*tmstep))); %Step 1.3 in Table D-1.
aconst=((Melast/(tmstep)^2)-(dcoeff/(2*tmstep))); %Step 1.4 in Table D-1.
bconst=(Kelast-((2*Melast)/(tmstep)^2)); %Step 1.5 in Table D-1.
mug=-Melast*gaccln;
```

C.3 Matlab Function to Calculate the horizontal design action coefficient

```
function [Cdt Cdt1 Cdt2 Ct] = NZS11705_CdT_fn(T,R,mu)
%Hazard Factor (Clause 3.1.4).
Z=0.3; %e.g. Christchurch
%Calculation of Spectral Shape Factor for Soil Class C (Table 3.1
in
%NZS1170.5, 2004).
if (T<=0.4)
Cht=2.36;
elseif (T<=1.5)
Cht=(2*(0.5/T)^0.75);
elseif (T<=3)
Cht=(1.32/T);
else
Cht=3.96/(T^2);
end
```

```
%Calculation of Spectral Shape Factor for Soil Class A (Table 3.1
in NZS1170.5, 2004).
% if (T<=0.4)
% Cht=1.89;
% elseif (T<=1.5)
% Cht=(1.6*(0.5/T)^0.75);
% elseif (T<=3)
% Cht=(1.05/T);
% else
% Cht=3.15/(T^2);
% end
%Calculation of Near-fault factor (Clause 3.1.6.1).
if (R<=0.75)
Ntd=1;
elseif (T<=1.5)
Ntd=1;
%Calculation of Maximum near-fault factor (Table 3.7 in NZS1170.5,
2004).
elseif (T<=2)
Ntd=(1+0.12*(T-1.5)/0.5);
elseif (T<=3)
Ntd=(1.12+0.24*(T-2));
elseif (T<=4)
Ntd=(1.36+0.24*(T-3));
elseif (T<5)
Ntd=(1.6+0.12*(T-4));
else
Ntd=1.72;
end
%Elastic site hazard spectrum for horizontal loading (Clause
3.1.1).
Ct=Cht*Ntd*min(0.7,Z*R);
%Calculation of Horizontal design action coefficient (Clause
5.2.1.1).
%Calculation of inelastic spectrum scaling factor:
if (T>=0.7)
kmu=mu;
else
kmu=((mu-1)*max(T,0.4)/0.7)+1;
end
%Calculation of Structural performance factor (Clause 4.4).
% if (mu>=1&mu<=2)
% Sp=(1.3-0.3*mu);
% else
% Sp=0.7;
% end
Sp = 1;
%Horizontal design action coefficient.
Cdt1=(Ct*Sp)/kmu; %Equation 5.2(1) in NZS 1170.5.
Cdt2=max(((Z/20)+0.02)*R,0.03*R); %Equation 5.2(2) in NZS 1170.5.
Cdt=max(Cdt1,Cdt2);

%================================ END OF FUNCTION%===============
```

C.4 Matlab Function to Generate Ruaumoko Input File

```
function
[filename]=ROMKO_INPfl_fn_theta(nbs,hfl,wfl,K,V,eqfilelink,EQdur,D
ELTAT,Slfactor,theta,Dir)
% ROMKO_INPfl_fn creates the Ruaumoko input file for a regular
structure.
% Inputs:
% nbs : Number of storeys in the structure
% hfl : Storey heights between floors (m)
% wfl : Weight at every floor level (N)
% K : Storey lateral stiffness (N/m)
% V : Storey strengths (N) (according to Section 2.6)
% eqfilelink : Link to the directory containing the earthquake
file
% EQdur : Duration of the earthquake (s)
% DELTAT : Excitation data interval (s)
% Slfactor : Scale factor applied to the time-history input
% ----------------------------------------------------------------
% Ruaumoko input file name.
filename = 'ROMKO.txt';
% Description of the analysis.
dlmwrite(filename,'Regular
Structure','delimiter','','newline','pc');
% Principal analysis options.
%[IPANAL,IFMT,IPLAS,IPCONM,ICTYPE,IPVERT,INLGEO,IPNF,IZERO,ORTHO,I
MODE]
dlmwrite(filename,' ','-append','delimiter','','newline','pc');
line2=[2,0,1,0,2,0,1,0,0,0,0];
dlmwrite(filename,line2,'-append','delimiter',' ','newline','pc');
% Frame control parameters.
% [NNP,NMEM,NTYPE,M,MODE1,MODE2,GRAV,C1,C2,DT,TIME,FACTOR]
line3=[(nbs+1)*3,(nbs*4),(nbs*2+2),nbs,1,nbs,9.81,5,5,0.001,EQdur,
Slfactor];
dlmwrite(filename,line3,'-append','delimiter',' ','newline','pc');
% Output intervals and plotting control parameters.
[KP,KPA,KPLOT,JOUT,DSTORT,DFACT,XMAX,YMAX,NLEVEL,NUP,IRESID,KDUMP]
line4=[0,1,10,0,1,1,1,1,(nbs+1),2,1,0];
dlmwrite(filename,line4,'-append','delimiter',' ','newline','pc');
% Iteration control and wave velocities.
% [MAXIT,MAXCIT,FTEST,WAVEX,WAVEY,THETA,DXMAX,DYMAX,D,OMEGA,F]
line5=[10,5,0.0001,0,0,0,0,0,0,0,0];
dlmwrite(filename,line5,'-append','delimiter',' ','newline','pc');
% Nodal point input.
dlmwrite(filename,' ','-append','delimiter','','newline','pc');
dlmwrite(filename,'NODES 1','-
append','delimiter','','newline','pc');
% Node information.
nodenum=[];
xnode=[];
ynode1=[];
uxnode=[];
uynode=[];
uznode=[];
kup1=[];
kup2=[];
kup3=[];
nodeflag=[];
```

```
H=hfl;
h=H(1); % Height of one regular floor, in m.
xnode(1)=0;
for i=1:(nbs)
xnode(i+1)=0+theta*i*h;
end
for i=1:(nbs+1)
nodenum(i)=i;
ynode(i)=i*h-h;
uxnode(i)=0;
uynode(i)=0;
uznode(i)=1;
kup1(i)=0;
kup2(i)=0;
kup3(i)=0;
nodeflag(i)=1;
% end
end
uxnode(1)=1;
uynode(1)=1;
%-----------------------------------------------------------------
xnode(2+nbs)=1;
for i=(nbs+2):(nbs*2+1)
xnode(i+1)=1+theta*(i-nbs-1)*h;
end
for i=(nbs+2):(nbs*2+2)
ynode(i)=h*(i-(nbs+2));
nodenum(i)=i;
uxnode(i)=0;
uynode(i)=0;
uznode(i)=0;
kup1(i)=(i+1)-(nbs+2);
kup2(i)=0;
kup3(i)=0;
nodeflag(i)=1;
end
uxnode(nbs+2)=1;
uynode(nbs+2)=1;
kup1(nbs+2)=0;
% ynode=[Ynode,Ynode];
%-----------------------------------------------------------------
xnode(3+2*nbs)=2;
for i=(2*nbs+3):(3*nbs+2)
xnode(i+1)=2+theta*(i-2*nbs-2)*h;
end
for i=(2*nbs+3):(3*nbs+3)
ynode(i)=h*(i-(2*nbs+3));
nodenum(i)=i;
uxnode(i)=0;
uynode(i)=0;
uznode(i)=0;
kup1(i)=(i+1)-(nbs+2);
kup2(i)=0;
kup3(i)=0;
nodeflag(i)=1;
end
uxnode(3+2*nbs)=1;
uynode(3+2*nbs)=1;
kup1(3+2*nbs)=0;
```

```
% [N,X(N),Y(N),NF1,NF2,NF3,KUP1,KUP2,KUP3,IOUT]
line6b=[nodenum',xnode',ynode',uxnode',uynode',uznode',kup1',kup2'
,kup3',nodeflag'];
dlmwrite(filename,line6b,'-
append','delimiter','\t','newline','pc')
% Interstorey drift input.
dlmwrite(filename,' ','-append','delimiter','','newline','pc');
dlmwrite(filename,'DRIFT','-
append','delimiter','','newline','pc');
nodedrift=[]; % N1, N2…Ntop
for i=1:((nbs+1)*2)
nodedrift(i)=i;
end
dlmwrite(filename,nodedrift,'-append','delimiter','
','newline','pc');
% Member topology or geometry.
dlmwrite(filename,' ','-append','delimiter',' ','newline','pc');
dlmwrite(filename,'ELEMENTS 1','-
append','delimiter','','newline','pc');
% Element information.
memnum=[];
memtype=[];
memnode1=[];
memnode2=[];
memnode3=[];
memnode4=[];
memflag=[];
for i=1:nbs
memnum(i)=i;
memtype(i)=i;
memnode1(i)=i;
memnode2(i)=(i+1);
memnode3(i)=0;
memnode4(i)=0;
memflag(i)=1;
end
for i=(nbs+1):(nbs*2)
memnum(i)=i;
memtype(i)=i;
memnode1(i)=(i+1);
memnode2(i)=(i+2);
memnode3(i)=0;
memnode4(i)=0;
memflag(i)=1;
end
for i=(2*nbs+1):(3*nbs)
memnum(i)=i;
memtype(i)=(2*nbs+1);
memnode1(i)=(i+2);
memnode2(i)=(i+3);
memnode3(i)=0;
memnode4(i)=0;
memflag(i)=1;
end
for i=(3*nbs+1):(4*nbs)
memnum(i)=i;
memtype(i)=(2*nbs+2);
memnode1(i)=(i-(2*nbs-2));
```

```
memnode2(i)=(i-(nbs-3));
memnode3(i)=0;
memnode4(i)=0;
memflag(i)=1;
end
% [N,MT,NODE1,NODE2,NODE3,NODE4,IOUT]
line8b=[memnum',memtype',memnode1',memnode2',memnode3',memnode4',m
emflag'];
dlmwrite(filename,line8b,'-
append','delimiter','\t','newline','pc');
% Member property tables.
dlmwrite(filename,' ','-append','delimiter','','newline','pc');
dlmwrite(filename,'PROPS','-
append','delimiter','','newline','pc');
%Section property information:
for i=1:nbs
secno=int2str(i);
line9b=[secno ,' FRAME '];
dlmwrite(filename,line9b,'-append','delimiter','','newline','pc');
% [ITYPE,IPIN,ICOND,IHYST,ILOS,IDAMG,ICOL,IGA]
line9c=[3,0,0,2,0,0,3,0];
dlmwrite(filename,line9c,'-append','delimiter','
','newline','pc');
% [E,G,A,AS,I,WGT,END1,END2,FJ1,FJ2]
I1=(K(i)*H(i)^3)/(12*(2.1E+11));
line9d=[2.1E+11,8.1E+10,1,1,I1,0,0,0,0,0];
dlmwrite(filename,line9d,'-append','delimiter','
','newline','pc');
% [RA,RF,H1,H2]
%Reference for H1 and H2 - Tagawa [4].
line9e=[0.04,0.04,((H(i)/2)/3),((H(i)/2)/3)];
dlmwrite(filename,line9e,'-append','delimiter','
','newline','pc');
% [PYC,PB,MB,MO,PC,MC,PYT,IEND]
line9f=[-1E+10,-
1E+10,((H(i)*V(i))/2),((H(i)*V(i))/2),1E+10,((H(i)*V(i))/2),1E+10,
0];
dlmwrite(filename,line9f,'-append','delimiter','
','newline','pc');
dlmwrite(filename,' ','-append','delimiter','','newline','pc');
end
for i=(nbs+1):(nbs*2)
secno=int2str(i);
line9b=[secno ,' FRAME '];
dlmwrite(filename,line9b,'-append','delimiter','','newline','pc');
% [ITYPE,IPIN,ICOND,IHYST,ILOS,IDAMG,ICOL,IGA]
line9c=[3,0,0,0,0,0,3,0];
dlmwrite(filename,line9c,'-append','delimiter','
','newline','pc');
% [E,G,A,AS,I,WGT,END1,END2,FJ1,FJ2]
I2=(K((i-nbs))*H((i-nbs))^3*0.2)/(2.1E+11);
line9d=[2.1E+11,8.1E+10,1,1,I2,0,0,0,0,0];
dlmwrite(filename,line9d,'-append','delimiter','
','newline','pc');
dlmwrite(filename,' ','-append','delimiter','','newline','pc');
end
for i=(2*nbs+1);
secno=int2str(i);
line9b=[secno ,' FRAME '];
```

```
dlmwrite(filename,line9b,'-append','delimiter','','newline','pc');
% [ITYPE,IPIN,ICOND,IHYST,ILOS,IDAMG,ICOL,IGA]
line9c=[1,0,0,0,0,0,3,0];
dlmwrite(filename,line9c,'-append','delimiter','
','newline','pc');
% [E,G,A,AS,I,WGT,END1,END2,FJ1,FJ2]
I2=0.00001;
line9d=[2.1E+11,8.1E+10,100,100,I2,0,0,0,0,0];
dlmwrite(filename,line9d,'-append','delimiter','
','newline','pc');
dlmwrite(filename,' ','-append','delimiter','','newline','pc');
end
for i=(2*nbs+2);
secno=int2str(i);
line9b=[secno ,' FRAME '];
dlmwrite(filename,line9b,'-append','delimiter','','newline','pc');
% [ITYPE,IPIN,ICOND,IHYST,ILOS,IDAMG,ICOL,IGA]
line9c=[1,3,0,0,0,0,3,0];
dlmwrite(filename,line9c,'-append','delimiter','
','newline','pc');
% [E,G,A,AS,I,WGT,END1,END2,FJ1,FJ2]
I2=2.1e+11;
line9d=[2.1E+11,8.1E+10,0.01,0.01,I2,0,0,0,0,0];
dlmwrite(filename,line9d,'-append','delimiter','
','newline','pc');
dlmwrite(filename,' ','-append','delimiter','','newline','pc');
end
% Lumped weights at the nodes.
dlmwrite(filename,'WEIGHTS 0','-
append','delimiter','','newline','pc');
nlumpwt(1,1)=1;
nlumpwt(1,2:4)=0;
for i=1:nbs
nlumpwt(i+1,1)=(i+1);
nlumpwt(i+1,2)=(wfl(i))/2;
% nlumpwt(i+1,2)=(wfl(i));
nlumpwt(i+1,3)=0;
nlumpwt(i+1,4)=0;
end
nlumpwt((nbs+2),1)=(nbs+2);
nlumpwt((nbs+2),2:4)=0;
for i=(nbs+3):(nbs*2+2)
nlumpwt(i,1)=i;
nlumpwt(i,2)=(wfl((i-(nbs+2)))/2);
% nlumpwt(i,2)=0;
nlumpwt(i,3)=0;
nlumpwt(i,4)=0;
end
for i=(nbs*2+3):(3*nbs+3)
nlumpwt(i,1)=i;
nlumpwt(i,2)=0;
nlumpwt(i,3)=0;
nlumpwt(i,4)=0;
end
% [N,WX,WY,WM]
dlmwrite(filename,nlumpwt,'-
append','delimiter','\t','newline','pc');
% External (static) nodal loads.
dlmwrite(filename,' ','-append','delimiter','','newline','pc');
```

```
dlmwrite(filename,'LOADS','-
append','delimiter','','newline','pc');
extl(1,1)=1;
extl(1,2:4)=0;
for i=1:(nbs)
extl(i+1,1)=(i+1);
extl(i+1,2)=0;
% extl(i+1,3)=-(wfl(i))/2;
extl(i+1,3)=0;
extl(i+1,4)=0;
end
extl((nbs+2),1)=(nbs+2);
extl((nbs+2),2:4)=0;
for i=(nbs+3):(nbs*2+2)
extl(i,1)=i;
extl(i,2)=0;
extl(i,3)=0;
% extl(i,3)=-(wfl(i-(nbs+2)));
extl(i,4)=0;
end
extl(nbs*2+3,1)=nbs*2+3;
extl(nbs*2+3,2)=0;
extl(nbs*2+3,3)=0;
extl(nbs*2+3,4)=0;
for i=(nbs*2+4):(3*nbs+3)
extl(i,1)=i;
extl(i,2)=0;
extl(i,3)=-(wfl(i-(2*nbs+3)));
extl(i,4)=0;
end
% [N,FX,FY,FM]
dlmwrite(filename,extl,'-append','delimiter','\t','newline','pc');
% Earthquake input control parameters.
dlmwrite(filename,' ','-append','delimiter','','newline','pc');
exctname='EQUAKE ';
extention='.txt';
line12a=[exctname,eqfilelink,extention];
dlmwrite(filename,line12a,'-
append','delimiter','','newline','pc');
% [IBERG,ISTART,DELTAT,ASCALE,END,VEL,DIS,TSCALE]
line12b=[3,1,DELTAT,Dir,-1,0,0,1];
dlmwrite(filename,line12b,'-append','delimiter','
','newline','pc');

%================================ END OF FUNCTION================
```

C.5 Matlab Function to Pull Out Peak Drift

```
%-------------------------------------------------------
% Matlab function to pull out peak Response from JUNK file of
RUAUMOKO
%-------------------------------------------------------
function [PeakDrift]= Pull_out_peak_drift(filename,SH,NoS)
  if NoS<=3
    a=13;
    xy=5;
elseif NoS<=6
    a=13;
    xy=5;
elseif NoS<=9
    a=15;
    xy=5;
elseif NoS<=12
    a=15;
    xy=5;
elseif NoS<=15
    a=16;
    xy=5;
elseif NoS<=18
    a=16;
    xy=5;
end
fid = fopen(filename,'r');
cpt1=0;
PeakResponse=[];
cl=0;
while (1)
    cl=cl+1;
    tline = fgetl(fid);
    if (~ischar(tline))
        break
    elseif (size(tline)==0)
    elseif (strcmp(tline(1),'1')==1)
        if (cpt1==a)
            for i=1:xy
                tline=fgetl(fid)
            end
            cptline=0   ;
            while (strcmp(tline(1),'0')<1)
                DrP=tline(19:27);        %POSITIVE Peak Response
                DrN=tline(50:60) ;       %NEGATIVE Peak Response
                PeakDrift(2*cptline+1)=str2num(DrP);
                PeakDrift(2*cptline+2)=str2num(DrN);
                tline=fgetl(fid);
                cptline=cptline+1;
            end;
            return
        else
            cpt1=cpt1+1;
        end
    end
end
end
```

C.6 Matlab Function to Pull Out Residual Drift

```
% Matlab function to pull out Redisual ISDR from JUNK file of
RUAUMOKO
% Written by Taisuke Masuno
%-------------------------------------------------------
function [residual,DrP]= Pull_out_residual_drift(filename,SH,NoS)
if NoS<=3
    a=11;
    xy=19;
elseif NoS<=6
    a=11;
    xy=28;
elseif NoS<=9
    a=13;
    xy=37;
elseif NoS<=12
    a=13;
    xy=46;
elseif NoS<=15
    a=14;
    xy=55;
elseif NoS<=18
    a=14;
    xy=64;
end
fid = fopen(filename,'r');
cpt1=0;
residual=zeros(1,NoS);
cl=0;
while (1)
    cl=cl+1;
    tline = fgetl(fid);
    if (~ischar(tline))
        break
    elseif (size(tline)==0)
    elseif (strcmp(tline(1),'1')==1)
        if (cpt1==a)
            for i=1:xy
                tline=fgetl(fid);
            end
            cptline=0   ;
            while (strcmp(tline(1),'0')<1)
                DrP=tline(17:27);       %POSITIVE drifts
                residual(cptline+1)=str2num(DrP);    drift ratio
                tline=fgetl(fid);
                cptline=cptline+1;
                if cptline==NoS
                    return
                end
            end
            return
        else
            cpt1=cpt1+1;
        end
    end
end
end
```

Appendix D: Ratcheting Device (*Grip'n'Grab*)

A device to prevent buckling of tension dissipative devices in compression was recently described by Gunning and Weston (2013). The device was inspired by plastic cable ties which can carry tension force, but carry no force in compression as they are pushed through the orifice. It has similar, but opposite, characteristics to a car axle jack which is a compression only device. The tension only device has the behaviour described in Figure D-1 and Figure D-2. The device itself is shown with the teeth in blue. A small lateral compressive force is required to encourage the two parts not to fall away from each other, so that the teeth engage. The dissipate element is shown in brown. Dissipation may occur due to yielding, frictional sliding or other means. Initially the device is loaded elastically in tension (A-B) then yielding/frictional sliding occurs in the dissipative element increasing its length (B-C). When the force is taken off (C-D) there is some elastic shortening of the dissipative element. When compression force is applied, the device carries very little compression but slides (D-E). When tension force is applied again (E-F), the device slips until the teeth are engaged but the dissipative element does not change in length since the axial force in this stage is very small. The maximum possible E-F distance is the tooth pitch. For greater tensions (F-G), displacement increases in the elastic range and then causes dissipation in the dissipative element as before. Preliminary tests of small scale devices indicate excellent behaviour with monotonic dissipation only of the yielding element (Cook et al. 2015).

Such a device has the potential to be used on the outside of rocking walls, in brace, and in other applications requiring energy dissipation. The dissipative element would need to be replaced, and the device reset, after every major event.

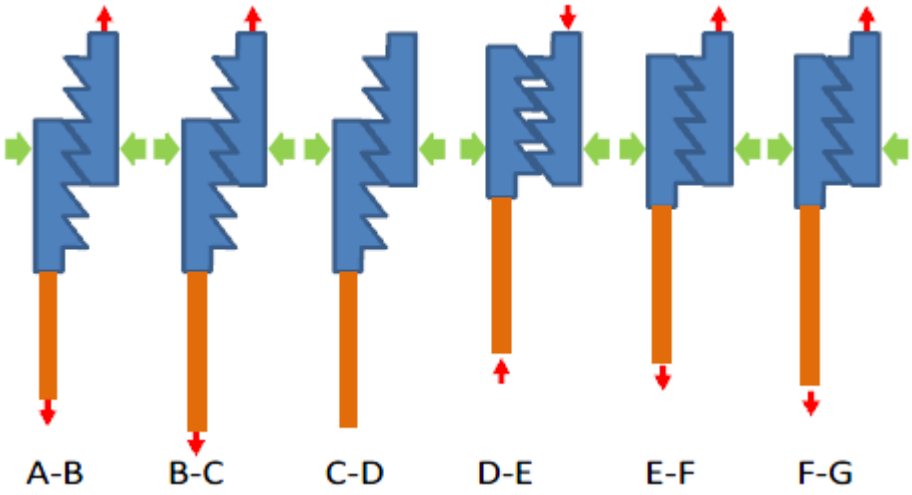

Figure D-1: Ratcheting Device Push-Pull Behaviour

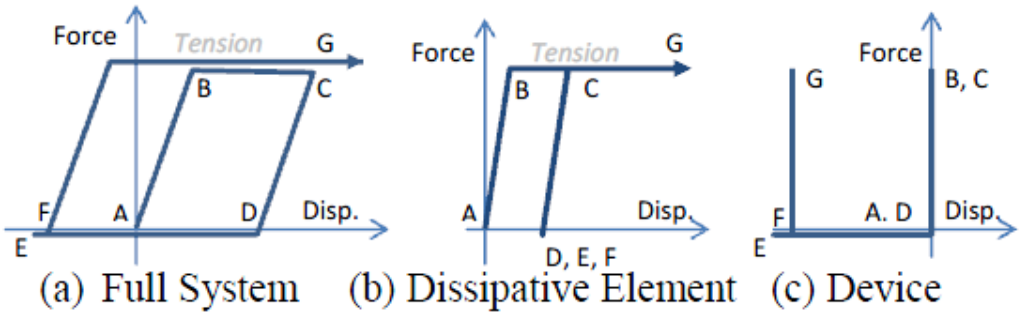

Figure D-2: Ratcheting Device Hysteresis Curve